UNDERSTANDING THE MECHANISMS OF GESTATIONAL EXPOSURE TO ULTRAFINE PARTICULATE MATTER ON PLACENTAL DEVELOPMENT AND DYSFUNCTION IN A MURINE MODEL

A Dissertation

by

JONATHAN CHARLES BEHLEN

Submitted to the Graduate and Professional School of
Texas A&M University
in partial fulfillment of the requirements for the degree of

DOCTOR OF PHILOSOPHY

Chair of Committee,	Natalie Johnson
Committee Members,	Robert Burghardt
	Gregory Johnson
	Shannon Washburn
Head of Department,	Larry Suva

May 2022

Major Subject: Toxicology

Copyright 2022 Jonathan Charles Behlen

ABSTRACT

Particulate matter (PM) air pollution is of growing concern due to increasing evidence of its ability to cause adverse health effects, particularly during development. PM represents a heterogenous mixture of compounds divided into three categories based upon their size (i.e., aerodynamic diameter): coarse (2.5-10 μm), fine (<2.5 μm), and ultrafine (<0.1 μm). Currently, there is no established regulatory limit or guideline for ultrafine particulate (UFP) exposure. Recent data supports the ability of UFPs to impact the placenta directly, via particle translocation, and indirectly, through oxidative stress-related mechanisms. It is well documented that any disruption within the placenta will affect its ability to function, thus potentially negatively impacting crucial windows of fetal growth and development. Given the gap in knowledge concerning the mechanisms of action regarding UFP exposure during pregnancy on placental development, we conducted several *in vivo* studies in a mouse model to investigate the impact of gestational UFP exposure on signaling pathways in placental development. We sought to clarify the role of Nrf2, the master regulator of antioxidant signaling as it relates to UFP exposure. Our findings yield a greater molecular understanding of UFP-driven placental dysfunction. These outcomes confirm how UFP exposure impacts placental development and highlight the importance of the antioxidant response pathway. Ultimately, this research adds to the body of literature that can inform preventive strategies to mitigate maternal exposure and protect fetal health.

DEDICATION

To my friends, family, and loved ones.

ACKNOWLEDGEMENTS

First and foremost, I would like to thank my wife, Dr. Abida Hasan for her love, support, guidance, and encouragement, particularly, when starting veterinary school while trying to finish this body of work. I am beyond grateful for her patience, understanding, and willingness to stay up with me on these long nights. I treasure our relationship more than you know and cannot wait to see what life has in store for us.

I am incredibly thankful for my advisor and committee chair, Dr. Natalie M. Johnson for allowing me the opportunity to join her laboratory in continued pursuit of my doctoral degree. I would have dropped from Texas A&M University's Toxicology program years ago if it had not been for your kindness and trust in me.

I would like to thank my committee members, Dr. Robert C. Burghardt, Dr. Gregory A. Johnson, and Dr. Shannon E. Washburn for their guidance and support throughout the course of my degree. It has been a long journey with many ups and downs so I'm beyond grateful for your continued belief in my journey.

I am deeply indebted to Dr. Jone A. Stanley, as he is not only a significant mentor and driving force in my pursuit of this degree, but one whom I now consider a dear friend and part of my family. Your knowledge, advice, and "coffee times" are greatly appreciated and missed dearly.

My sincere thanks to Dr. Ben Morpurgo, Dr. Andrei Golovko, Dr. Andrew Hillhouse, Dr. Wesley Brashear, Dr. Danila Cuomo, Dr. Joseph Szule, Dr. Rola Barhoumi, and Ms. Chaitali Mukherjee for all their assistance and technical knowledge during my

experiments. The many discussions, guidance, and advice were invaluable throughout the years.

I am grateful for Ms. Kim Daniel and Fawne Toler for their administrative assistance in keeping me on track; Dr. Ivan Rusyn for his input in the Toxicology program and curriculum; and the many professors from whom I had the opportunity to learn both in and outside of the classroom. All faculty and staff within the department made this an incredible experience.

Finally, words cannot express my gratitude towards my loving family, friends, and colleagues Glenn Behlen, Denise Behlen, Bethany Garcia and family, Jeremy Behlen and family, Wesley Hoelscher, Chris Stovall, Benjamin Seufferlein, Erika Berr, Gabriella Valladares, Allie Folcik, Alex Blanchette, Sara Hearon, Krisa Camargo, Kaylie Heiman, Carmen Lau, Drew Pendleton, Toriq Mustapha, Ross Shore, Nick Drury, Navada Harvey, Joshua Freeman, Alen Merdzo, Kirthiram Sivakumar, and many others who were involved in my endeavor including my current attendance of veterinary school. I would not be here without all your support. I cherish the many memories made and hope for more in the future.

Jonathan Charles Behlen

CONTRIBUTORS AND FUNDING SOURCES

Contributors

This work was supported by the dissertation committee consisting of Professors Dr. Natalie N. Johnson (advisor) of the Department of Environmental Health, School of Public Health, Dr. Robert C. Burghardt and Dr. Gregory A. Johnson of the Department of Veterinary Integrative Biosciences, and Dr. Shannon E. Washburn of the Department of Veterinary Physiology and Pharmacology, College of Veterinary Medicine and Biomedical Sciences. Chapter 2 *in vivo* animal experimental work was partly contributed by Dr. Carmen H. Lau. All other work performed for the following dissertation was completed independently by the student.

Funding Sources

This work was supported by the National Institute of Environmental Health Sciences (NIEHS) grant R01ES028866 and P30ES029067.

NOMENCLATURE

8-oxodG	8-Oxo-2’-deoxyguanosine
15-F2t-IsoP	15-F2t-Isoprostane
AhR	Aryl Hydrocarbon Receptor
ARE	Antioxidant Response Element
BC	Black Carbon
CAPs	Concentrated Ambient Particles
CAT	Catalase
CPC	Condensation Particle Counter
CRP	C-Reactive Protein
CYP	Cytochrome P450
DEPM	Diesel Exhaust Particulate Matter
DMA	Differential Mobility Analyzer
DME	Drug Metabolizing Enzyme
DOHaD	Developmental Origins of Health and Disease
E	Embryonic Day
ECs	Electrostatic Classifiers
EPFR	Environmentally Persistent Free Radicals
EVT	Extravillous Trophoblast
GPx	Glutathione Peroxidase
Grx	Glutaredoxin

GSH	Glutathione (reduced)
GSSG	Glutathione (oxidized)
GST	Glutathione S-Transferase
HO-1	Heme-oxygenase 1
HUCAPS	Harvard University Concentrated Ambient Particle System
IARC	International Agency for Research on Cancer
ICM	Inner Cell Mass
IL	Interleukin
IL-1β	Interleukin 1 beta
IUGR	Intrauterine Growth Restriction
Keap1	Kelch-Like ECH-Associated Protein 1
lnRNA	Long Noncoding RNA
LBW	Low Birth Weight
MALAT1	Metastatic Associated Lung Adenocarcinoma Transcript 1
MDA	Malondialdehyde
miRNA/miR	microRNA
mtDNA	Mitochondrial DNA
NAD^+/NADH	Nicotinamide Adenine Dinucleotide
$NADP^+$/NADPH	Nicotinamide Adenine Dinucleotide Phosphate
NAT	N-acetyltransferase
NF-κB	Nuclear Factor Kappa Light Chain Enhancer of Activated B Cells
nm	Nanometer

NP	Nanoparticle
NQO1	NAD(P)H Quinone Oxidoreductase 1
Nrf2	Nuclear Factor Erythroid 2 Related Factor 2
OPC	Optical Particle Counter
PAH	Polycyclic Aromatic Hydrocarbon
piRNA	piwi-interactingRNA
PM	Particulate Matter
PM_{10}	Coarse Particulate Matter (<10 μm)
$PM_{2.5}$	Fine Particulate Matter (<2.5 μm)
PTB	Preterm Birth
Prx	Peroxiredoxin
RNS	Reactive Nitrogen Species
ROS	Reactive Oxygen Species
SAM	S-adenosylmethionine
SFN	Sulforaphane
SOD	Superoxide Dismutase
SULT	Sulfotransferase
SVOC	Semi Volatile Organic Compound
TEM	Transmission Electron Microscopy
TGC	Trophoblast Giant Cell
TNFα	Tumor Necrosis Factor alpha
Trx	Thioredoxin

UCP2	Uncoupling Protein 2
UFP	Ultrafine Particle (<0.1 μm)
$\mu g/m^3$	Microgram Per Cubic Meter
UGT	UDP-glucuronosyltransferase
VACES	Versatile Ambient Particle Concentrator Exposure System
VOC	Volatile Organic Compound

TABLE OF CONTENTS

Page

LIST OF FIGURES

Page

LIST OF TABLES

Page

1. INTRODUCTION

1.1. Air Pollution and Particulate Matter

Air pollution is a serious public health issue and a global contributor to death and diseases [1] with six common or criteria pollutants established by the US EPA Clean Air Act, including carbon monoxide, lead, nitrogen dioxide, ozone, sulfur dioxide, and particulate matter (PM) [2]. Increasing industrialization and urbanization, particularly in developing nations, has resulted in elevated PM levels, and associated adverse health outcomes as collateral damage [1, 3]. PM refers to suspended carbonaceous particles of liquid or solids with associated adsorbed chemicals, metals, or biological components that are not gaseous in nature. PM itself is diverse encompassing several classifications based upon size and is generally expressed as units of particle mass per cubic meter ($\mu g/m^3$) [4]. The three aerodynamically sized categories are coarse (PM_{10} or 10-2.5 μm), fine ($PM_{2.5}$ or <2.5 μm), and ultrafine particles (UFPs, $PM_{0.1}$, or <0.1 μm). UFPs are considered to have almost a negligible mass but a leading contributor to the total number of atmospheric particles [5].

UFPs are defined as particles smaller than 100 nm in size with most produced through combustion processes within urban settings [6]. However, UFPs may also form from aerosols in the atmosphere through active nucleation, condensation, and coagulation processes [7]. Nucleation refers to gaseous molecules forming particles with sizes normally <50 nm [8]. Condensation transfers gaseous molecules into nucleation particles or existing particles [9] while coagulation describes particle collisions forming a single

cluster from two original particles due to Brownian motion [10]. Newly nucleated particles will readily coagulate causing deposition of UFPs observed within the environment [4, 10]. These reactions are especially important in areas of high photochemistry [7] indicating UFPs may have greater spatial and temporal variability compared to other PM fractions. Because UFP generation processes are vastly different and occur at faster rates from coarse and fine PM, UFPs exhibit variable size, shape, charge, surface area, and concentrations [11, 12].

Researchers hypothesize fine and UFPs have increased toxicity due to their small size and increased surface area [13]. Several studies have documented the mortality and morbidity associated with UFP exposure within the respiratory [14] and cardiovascular systems [15, 16]. This toxicity is attributed to UFP's ability to easily transverse and penetrate the pulmonary alveoli [17], which eventually translocate systemically following deposition [18]. Thus, some researchers postulate that UFPs have increased adverse health impacts versus larger PM fractions [19]. Still, there is a lack of data evaluating the effects of UFPs ($PM_{0.1}$) in comparison to PM_{10} and $PM_{2.5}$ with a need for more information regarding the long-term exposure effects. The minimal evidence available indicates associations with UFP exposure to pulmonary and cardiovascular diseases, as well as type 2 diabetes [20] and cancer [21].

Although UFPs are classified upon their size and composition, it is proposed that the PM fraction may contain components bound such as heavy metals [22], polycyclic aromatic hydrocarbons (PAHs) [23], and sulfur and nitrogen oxides that contain the capacity for mutagenic and carcinogenic effects [24-26]. Indeed, there is abundant

information concerning larger PM fractions and their mechanisms of action with associated components, but few studies observe UFP toxicity alone. This knowledge gap is attributed, in part, to the difficulty in measuring UFPs and extrapolating epidemiological data. This dissertation represents an opportunity to close that knowledge gap and help understand mechanisms driving UFP toxicity on the placenta.

1.1.1. Sources and Characteristics of Ultrafine Particles

Particulate matter may be emitted from either natural or anthropogenic sources, which will vary in size and composition. These types of emissions into the atmosphere are primary particles while gaseous transformations [11] and photochemical reactions [27] are secondary particles. Natural primary emissions consist of volcanic eruptions, biological particles, wildfires, marine aerosols, local minerals, and runoff [28-30]. However, most UFP generation is from anthropogenic or man-made sources [6] through hydrocarbon combustion, burning biomass, vehicular emissions, road and agricultural dust, pollutant chemical interactions, industrial emissions, and more [30, 31]. While outside of the scope of this research, cigarette smoke contains many UFPs and their associated chemical components [32]. Additionally, indoor UFP generation, primarily from cooking, is also outside of the scope of this dissertation but should be noted as potential air pollutant and contaminant [33].

Through their generation, UFPs have significant variability within the particles themselves, as well as their spatial concentration [34-37]. This is best observed through seasonal and climate variations [30, 38, 39]. Their small size of <100 nm and almost massless physical properties allow the particles to be suspended in the air longer than

larger sized fractions [38]. Furthermore, this allows UFPs to be affected by meteorological aspects of sunlight, wind, and other weather factors [11, 12, 40]. Weather also contributes to UFP generation (i.e., photochemistry [7]) through condensation and coagulation reactions of sulfate, nitrate, heavy metals, organic and black carbon (BC), and semi- and volatile organic compounds (SVOCs and VOCs) [41]. Additionally, their small size but large surface area allows other compounds to adhere to them after generation potentially altering their physiochemical properties and furthering toxicity [11, 30, 42].

The physiochemical properties of the generated UFPs stem from the emission source, as well as the nature of the core components for secondary particle formation. For example, UFPs emitted from wood combustion can have adhered particles such as PAHs [43]. By contrast, UFPs emitted from motor vehicle combustion center on vehicular maintenance, type of fuel used, vehicle technology, and more [44]. Diesel exhaust particulate matter (DEPM) has an emission range of 20-130 nm while gasoline engines produce exhaust particulate matter between 40-80 nm with varying adherence capacities and toxicities [45].

UFPs within the environment are primarily composed of elemental or BC, organic compounds, nitrates, sulphates, and heavy metals with most mass stemming from carbonaceous sources [46-48]. BC is the primary biproduct of incomplete fossil fuel combustion which is attributed to transportation and industrial activities [38]. BC may serve as the primary core from which sulphates, nitrates, heavy metals, PAHs, and other species may adsorb. PAHs are of particular interest as one of them is listed as known group 1 human carcinogen (benzo[a]pyrene) according to the International Agency for Research

on Cancer (IARC). Additionally, several more PAHs are categorized in group 2A as probably carcinogenic to humans, and even more are listed as possibly carcinogenic to humans in group 2B [49]. While their concentrations on UFPs tend to be low, their toxicity is thought to be higher than the parent compound to which they are bound [50-52]. Overall, anthropogenic sources are the primary contributor to UFP emissions and secondary particle formation within the environment.

1.1.2. Capture and Measurement Technology

While UFPs are traditionally expressed as $\mu g/m^3$, measurements are performed with various technologies. Condensation particle counters (CPCs) and electrostatic classifiers (ECs), which have various size range capabilities, are common technologies used for PM measurement. Additionally, ion mobility air spectrometers are employed to measure particles up to 0.4 nm [19, 53, 54]. **Figure 1.1** demonstrates how popular technologies work in measuring UFPs [30].

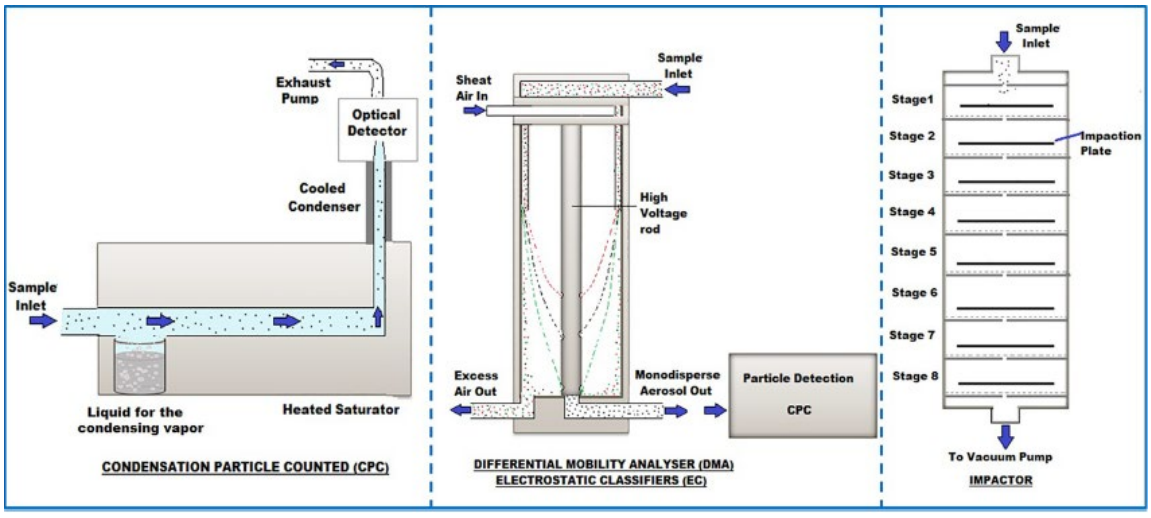

Figure 1.1 Technologies utilized to measure ultrafine particulate matter.*

*Reprinted with permission from Moreno-Ríos, A.L., L.P. Tejeda-Benítez, and C.F. Bustillo-Lecompte, *Sources, characteristics, toxicity, and control of ultrafine particles: An overview.* Geoscience Frontiers, 2022. **13**(1): p. 101-147.

For CPCs, particles undergo a vapor condensation which enlarges them, allowing for optical detection and counting via a laser beam [19]. Since detection is through optics, particle counting is limited to 3 nm in diameter [48]. CPCs can be used in concert with other technologies such as a differential mobility analyzer (DMA) which separates the particles via size before the condensation reactions within the CPCs. This setup strategy of DMA particle separation followed by CPC optical measurement was characterized by Rychlik et al. and was used within our laboratory exposure system [55]. However, CPCs and DMAs have a high cost and limited particle range of approximately 3 to 500 nm [48].

Other technologies for use include portable optical particle counter, laser aerosol spectrometer, low-pressure electric impactors, and aerodynamic particle sizers [30, 56]. Optical particle counter is based on the premise of light scattering; however, this technology is not suitable for UFPs as it cannot accurately measure particles smaller than 300 nm. Low pressure electric impactors and aerodynamic particle sizers are also used but mainly in research settings and not in environmental monitoring equipment due to their high cost. Other methods are utilized when sampling UFPs in a filter, but their use is beyond the scope of this dissertation.

1.2. Ultrafine Particle Toxicity

Ultrafine particulate matter toxicity along with its associated components of BC, heavy metals, PAHs, and other organic compounds, has been linked with several adverse

health outcomes through several underlying biological mechanisms. These include cellular oxidative stress [57, 58], cytotoxicity [39], and mutagenicity [59], which increases the chance of developing a range of diseases later in life.

1.2.1. Toxicokinetics of Ultrafine Particles

PM exerts its adverse health effects primarily via the inhalation route [42, 60, 61]. Several characteristics of UFPs affect the toxicokinetics, including size, shape, charge, concentration, and other physicochemical parameters [38, 62]. Additionally, physiological or general health status is important in determining toxicity (i.e., age, physical activity, and respiratory rate) and ability to recover from insult [19, 63]. To fully appreciate and understand the absorption, metabolism, distribution, and excretion, a brief overview of the human respiratory system is needed. When breathing, air passes through either the nasal or oral cavities then into the pharynx, larynx, and upper trachea which is termed the extra-thoracic area [64]. The trachea enters the thorax where it splits into two bronchi diverging into the right and left lungs. Within the lungs, further branching and dividing into smaller airways eventually end in bronchioles. Attached to the bronchioles are tiny air sacs termed alveoli, which are coated in capillaries allowing for gas exchange to occur between the air and blood.

Inhaled UFPs pass the extra-thoracic area and travel into the bronchioles reaching the terminal alveoli [42]. The smaller the PM, the deeper the particles may travel into the respiratory system. Particles of 100 μm in diameter deposit in the nasopharynx region while those of 10 μm deposit in the primary bronchi [14, 38]. Particles 2.5 μm or smaller will penetrate the alveoli. Early models were used to predict PM fraction deposition by

particle size [65-67]. These models predicted UFP deposition in the terminal bronchioles and alveoli with the highest efficiency, while larger particles were deposited in the upper respiratory airways.

Within the respiratory system, various mechanisms are present to remove the deposited PM. UFPs in the alveoli and terminal bronchioles are primarily removed by alveolar macrophages [68]. If not cleared, particles may accumulate within or translocate through alveolar tissue. Clearance time is slower and less complete than larger UFP particles as demonstrated by Moller and colleagues [69]. The reasons for the slower clearance have been attributed to decreased mucociliary action due to mucus particle penetration or deposition outside and beyond the level of mucus barriers [70]. The slower clearance may lead to accumulation followed by alveolar translocation. Translocation involves particles passing the epithelial barrier and entering the bloodstream [63]. The mechanisms for translocation are not well understood, but evidence suggests endocytosis, exocytosis, and passive diffusion may occur. However, translocation is dependent on particle physiochemical properties [38, 62]. Once in circulation, the inhaled particles are carried throughout the circulatory system and interact with other tissues and organs including the placenta in pregnant women [71].

1.2.1.1. Placental Translocation of Ultrafine Particles

Several human and animal models indicate UFPs are translocated across the placenta and may enter fetal circulation. In 2019, Bové and colleagues were the first research group to identify and visualize up to 9.78 μm BC aggregates on the fetal side of the placenta [71]. The maternal cohort data regarding BC placental aggregates correlated

with their residential BC exposure during pregnancy indicating a dose-response relationship. Additionally, an *ex vivo* human placental model with fluorescently labeled polystyrene beads resulted in 50, 80, and 240 nm size translocation but not 500 nm [72]. This suggests a size effect on placental uptake of UFPs.

In animal models, Valentino and colleagues observed UFPs within the maternal blood lacunae, trophoblast cells and fetal vessels utilizing a rabbit model [73]. In that work, UFPs were generated from DEPM and characterized using transmission electron microscopy (TEM). Veras et al. noted morphological alterations on the maternal side of the placenta within a mouse model [74]. Here, gestational exposure to ambient air pollution from São Paulo resulted in reduced fetal weights and fetoplacental adaptation characterized by smaller maternal blood spaces and increased fetal capillary diffusive conductance. Additionally, in a mouse model with intratracheal administration of nanoparticles (NPs), Paul and colleagues observed their presence within the placenta as well as decreased placental efficiency [75]. Moreover, these alterations correlated to compromised lung development that was observed in adulthood. These highlighted various animal models demonstrate evidence for UFP transport and the potential for direct and indirect effects on placental function and offspring development [76].

1.2.2. General Mechanisms of Ultrafine Particle Toxicity

UFP toxicity is dependent on the physiochemical properties, which include adhered components such as heavy metals, organic compounds, BC, PAHs, and others [52, 77]. Saikia et al associated adsorbed components with adverse health effects [78]. For instance, heavy metals are identified as carcinogenic [79], operating through the

production of reactive oxygen species (ROS) damaging nucleic acids, proteins, and lipids [57, 80]. Oxidative stress and associated inflammation are also linked to several disorders involving the cardiovascular [41], respiratory [14], and neurological systems [81], and cancers [21].

As previously mentioned, PAHs are of particular concern with many compounds classified as either carcinogenic, probably carcinogenic, or possibly carcinogenic to humans [49]. Additionally, they are lipophilic and therefore highly soluble in fatty tissues [51]. While PAHs have known toxicity and are associated with UFPs, Topinka and colleagues argue that more evidence of PAH UFP toxicity is needed due, in part, to PAH reduced numbers and varied chemical properties between compounds [82]. Similarly, BC has been implicated in cardiovascular [21] and respiratory [83] dysfunction. In addition to being an adsorbed component, BC is utilized as the nucleus for UFPs with other compounds and chemicals attached to it including PAHs and VOCs [30]. BC mechanisms of action involve oxidative stress and inflammatory reactions that are often observed within the respiratory system [14].

Finally, *in vitro* studies have demonstrated that UFP exposure can induce epigenetic modifications by increasing oxidative stress through the production of oxidizing species [84]. UFP exposure has been shown to increase DNA methyltransferase expression leading to persistent DNA modifications [26].

1.2.2.1. Biological Mechanisms of Developmental Ultrafine Particle Toxicity

Fine and ultrafine PM are thought to cause adverse effects on fetal development through two general mechanisms: direct and indirect processes. Direct involves

translocation of particles across the placenta and interaction with fetal circulation, whereas indirect operates through modifications of physiological and cellular responses like oxidative stress, inflammation, and epigenetic alterations [85, 86]. Oxidative stress, inflammation, and epigenetics are critical cellular processes that require a delicate balance. Dysregulation has the potential for negative outcomes. These processes and their relationship to nuclear factor erythroid 2-related factor 2 (Nrf2), metastatic associated lung adenocarcinoma transcript 1 (MALAT1), and the phytochemical sulforaphane (SFN) are briefly discussed.

ROS and reactive nitrogen species (RNS) are constantly generated due to normal cellular processes, primarily from mitochondrial metabolism or aerobic respiration [87-89]. Oxidant compounds are used for cell signaling, as well as cellular processes such as inflammation, stress, cell division, and autophagy. While necessary, uncontrolled or deregulated production of oxidant compounds impairs proper cellular function, and leads to diseased and toxic states. Reactive species are counterbalanced by antioxidant systems to maintain proper homeostasis; therefore, oxidative stress is generally defined as an imbalance between pro-oxidants and antioxidant compounds with an overall increase in damaging free radicals.

Several antioxidants and related systems are employed by the cell to maintain homeostasis, such as low molecular weight compounds, non-catalytic proteins, and enzymatic systems [88-90]. Low molecular weight compounds include vitamins C and E, glutathione (GSH), bilirubin, and urate while non-catalytic proteins include thioredoxin (Trx), glutaredoxin (Grx), and metallothioneins. Finally, antioxidant enzymes include

glutathione peroxidase (GPx), superoxide dismutase (SOD), peroxiredoxin (Prx), and catalase (CAT). Redox reduction systems are driven by nicotinamide adenine dinucleotide (NAD^+/NADH) and nicotinamide adenine dinucleotide phosphate ($NADP^+$/NADPH) cycling pairs. Particularly, NADPH is utilized to reduce oxidized glutathione disulfide (GSSG) back into GSH. GSH and GSSG levels and ratio have demonstrated to be effective plasma and tissue markers for oxidative stress [91]. Additionally, cysteine thiol-based regulation are residues which are reactive at low pKa values [88]. Cysteine residues may interact with reactive species to generate other harmful oxidation products. However, the cysteine residue system, like many others, is reversible and serves a function for redox signaling pathways. Modifications of cysteine residues are critical for activation of the Nrf2 antioxidant pathway.

Nrf2 is a basic leucine zipper transcription factor and a member of the cap 'n' collar subfamily which binds to the NFE2-binding motif of the β-globin locus [92]. It was found to regulate the induction of several drug metabolizing enzymes (DMEs), such as glutathione S-transferase (GST), UDP-glucuronosyltransferase (UGT), N-acetyltransferase (NAT), and sulfotransferase (SULT). Additionally, heme oxygenase-1 (HO-1), NAD(P)H quinone oxidoreductase 1 (NQO1), and Trx system are under Nrf2 regulation [93]. Induction of DMEs causes increased cellular detoxification, which occurs through Nrf2 binding to the antioxidant response element (ARE). ARE binding follows activation through cysteine thiol redox signaling, allowing for repressor kelch-like ECH-associated protein 1 (Keap1) dissociation and Nrf2 nuclear translocation. With Keap1 bound, Nrf2 is polyubiquitinated and rapidly degraded under basal conditions. Nrf2

regulation is further enhanced by the long noncoding RNA (lnRNA) MALAT1 in a positive and/or negative association under oxidative stress conditions. Overexpression of MALAT1 was shown to lower Keap1 which results in increased activated Nrf2 [94]. Conversely, MALAT1 was shown to interact with Nrf2 prior to binding to the ARE decreasing activation overall indicating Nrf2/MALAT1/ARE as a pathway of oxidative stress interest [95].

While modulation of Nrf2 is a critical and tightly regulated process, several chemical classes are known to induce ARE genes through Nrf2 activation. These chemicals include phytochemicals (i.e., SFN), therapeutics (i.e., oltipraz), endogenous chemicals (i.e., nitric oxide), nitro-fatty acids, and environmental compounds (i.e., paraquat) to list a few [96, 97]. Although diverse, these chemicals operate through their ability to modify the thiol groups correlated with NQO1 gene expression. Modifications of Nrf2 are thought to alter Nrf2/Keap1 structure allowing for dissociation following ubiquitination inhibition. SFN is a known potent plant molecule that acts as an inducer to Nrf2 activation [98, 99]. Many cruciferous vegetables like broccoli and brussels sprouts contain the precursor molecule glucoraphanin. The enzyme myrosinase cleaves glucoraphanin into SFN during mastication or through plant damage. Within a neutral or alkaline pH environment, SFN will transform into an electrophile group increasing bioactivity. Arguably, most regions throughout the world lack the ability to access the latest molecular targeted pharmaceuticals. Therefore, foodstuff containing bioavailable chemicals for disease prevention is a potential suitable and realistic solution to combat oxidative stress damages within these environments.

As previously described, heavy metals, PAHs, VOCs, and other components are present creating an oxidative stress environment through either direct or indirect mechanisms which alter redox signaling [100, 101]. The generated reactive species can induce macromolecular damage to DNA, proteins, and lipids while shifting sensitive cysteine thiol systems to activate [85]. Adsorbed compounds have demonstrated the capacity to generate mitochondrial damage, which in turn leads to excess NADPH oxidase and superoxide production [102, 103]. PAHs activate a superfamily of enzymes called cytochrome P450 (CYP) that function as monooxygenases. CYP transcription is known to occur through the aryl hydrocarbon receptor (AhR). Stejskalova and Pavek have described CYP1A1 as the most important xenobiotic metabolizing enzyme within the placenta, with its dysregulation/dysfunction attributed to several pregnancy complications [104]. Crosstalk among Nrf2 and AhR could potentially be of interest as both have shown to induce expression of each other in response to PM exposure [105].

With the indirect source of reactive species production, there is an increase in Nrf2, often regarded as the master regulator of the antioxidant response [106]. Through increased oxidative stress, nuclear factor kappa-light-chain-enhancer of activated B cells (NF-κB) is activated leading to an inflammatory response through pro-inflammatory cytokine production [107]. NF-κB activation is associated with increased interleukin (IL) 1 beta (IL-1β) and tumor necrosis factor alpha (TNFα). This inflammatory reaction intricately links Nrf2 and NF-κB, as lack of Nrf2 activity has demonstrated to exacerbate NF-κB signaling [108, 109].

1.2.2.1.1. Placental Oxidative Stress and Inflammation

It is well established that fine and UFPs have the capacity to generate reactive oxygen species [110]. Ambroz et al., measured oxidative biomarkers, urinary 8-oxo-7,8-dihydro-2-deoxyguanosine (8-oxodG) and plasma 15-F2t-isoprostane (15-F2t-IsoP), in mothers and infants living in a polluted region of the Czech Republic [111]. $PM_{2.5}$ and benzo[a]pyrene ambient concentrations correlated with 8-oxodG and 15-F2t-IsoP levels, respectively. Furthermore, in a cohort from Durban, South Africa, pregnant women exposed to air pollution demonstrated high circulating lymphocytes [112]. Lymphocytes are markers reflective of oxidative stress. Women in a more industrialized area demonstrated higher counts compared to women living in a less industrialized area with lower pollution. Additionally, Nrf2 and GSH expressions were decreased while malondialdehyde (MDA), SOD, and uncoupling protein 2 (UCP2) gene expression were all increased. Increased MDA, SOD, and UCP2 are indications of maternal systemic oxidative stress.

Plasma homocysteine, an established marker for a risk of cardiovascular disease, has been correlated with increased $PM_{2.5}$ exposure [113]. Homocysteine is a thiol-containing amino acid produced by intracellular demethylation of methionine and is normally rapidly metabolized, keeping plasma levels low. Homocysteine levels in umbilical cord blood were found to be increased in direct linear correlation with PM exposure in a human cohort study; investigators confirmed an 8.1% increase in cord blood homocysteine concentration for every 5 $\mu g/m^3$ increase in $PM_{2.5}$ [114]. Increased $PM_{2.5}$ and BC exposure during pregnancy were also correlated with placental nitrosative stress, measured via 3-nitrotyrosine concentrations [115]. Exposure to $PM_{2.5}$ during gestation has

also been associated with markers of mitochondrial damage in mothers and newborns in the form of alterations in mitochondrial DNA (mtDNA). Finding alterations in mtDNA is representative of dysfunction of mitochondrial repair systems due to cumulative oxidative stress. Mitochondrial DNA content in umbilical cord leukocytes was reduced with increased $PM_{2.5}$ exposure during pregnancy [116]. This association between increased prenatal $PM_{2.5}$ exposure and decreased cord blood mtDNA was confirmed by Brunst et al. [117]. Markers of mtDNA damage in maternal blood were seen in positive association with $PM_{2.5}$ exposure during pregnancy by Grevendonk et al. [118].

Another measure of oxidative stress is telomere length, wherein biological aging has been related to shortened length. A decrease in telomere length in cord blood as well as in the placenta has been associated with increased $PM_{2.5}$ exposure in several human studies [119]. While this finding was not consistent in a study by Rosa et al. [120], specific windows of $PM_{2.5}$ exposure during a pregnancy and neonatal sex identified two factors that contributed to varying telomere length. The multifactorial nature of oxidative stress is further supported by other studies that assess oxidative stress arising from various insults during pregnancy. For example, maternal trauma has been shown to result in increased placental mtDNA copy number [117]. The pathways of oxidative stress in PM exposure are similar to the pathways for development of oxidative stress due to psychosocial stress, diet/nutrition, and maternal exposure to smoke [121]. Independent from findings of oxidative stress, $PM_{2.5}$ exposure during pregnancy has also been found to trigger inflammation both systemically and in the placenta [122]. C-reactive protein (CRP), a biomarker of systemic inflammation that is often elevated in pre-eclampsia, [123]

has also been demonstrated to increase with $PM_{2.5}$ exposure during pregnancy [124]. Intrauterine inflammation and oxidative damage have been demonstrated in murine models using fine and ultrafine PM exposure during pregnancy to support this relationship [125, 126].

Animal models that have delved into the mechanistic pathways of oxidative stress and inflammation highlight the deleterious effects of PM exposure on pregnancies. DEPM exposure during gestation in a mouse model resulted in an increase in placental immunomodulatory cytokines IL-2, IL-5, IL-12, and granulocyte monocyte colony stimulating factor in one study, [127] and multiple inflammatory cytokines, especially IL-5 and IL-6 in another [128]. Ye et al. [129] observed an increase oxidative stress marker superoxide dismutase in response to fine PM exposure during pregnancy. De Melo et al. [130] reported increased IL-4 expression in the placenta after $PM_{2.5}$ exposure to rats pre-pregnancy and antenatally. While oxidative stress and inflammation states are induced by $PM_{2.5}$ exposure in most studies evaluating these pathways, the literature is less consistent regarding which markers are consistently affected. While IL-2, IL-6, IL-8, and TNFα, biomarkers of systemic inflammation, were increased in ICR mouse serum after $PM_{2.5}$ pregnancy exposure, markers of oxidative stress were less consistent. CAT decreased and HO-1 increased, which indicates an oxidative stress effect, but there were no differences noted in GSH [131]. Endotracheal instillation of low dose $PM_{2.5}$ to pregnant rats on gestational days 10 and 18 demonstrated inflammatory marker IL-6 in maternal blood but failed to elucidate a difference in GSH-Px and MDA in placenta homogenate, indicating oxidative stress was less important in this model [132]. Another marker of oxidative stress,

15-F2t-IsoP, was associated with structural changes in the umbilical cord vessels, which were thinner after exposure to polluted ambient air in a mouse model; this "busy street" air exposure was associated with increased lipid peroxidation in umbilical cords and decreased fetal weights [133]. Increased 8-isoprostanes were demonstrated by Wang et al. [134] in UFP-exposed dam plasma. Increased 8-OHdG in mouse placentas represented increased PAH-biotransforming enzymes, intrauterine inflammation, and oxidative damage after UFP exposure [126]. In sum, oxidative stress/redox signaling imbalances and pro-inflammatory responses have been implicated as mechanisms of action for adverse outcomes resulting from $PM_{2.5}$ and UFP exposure in a breadth of both human and animal studies.

1.2.2.1.2. Placental Epigenetic Alterations

First described by Conrad Waddington in 1940, epigenetics refers to changes in gene expression without a change in DNA sequence that are mitotically or meiotically heritable [135-137]. This discussion will focus on epigenetic changes associated with $PM_{2.5}$ exposure given the well documented changes associated and the myriad of effects throughout lifespan [138]. Chemical changes to DNA via DNA methylation and non-coding RNA have been linked to modulation of gene expression via a complex regulatory network that comes into play upon pregnancy associated $PM_{2.5}$ exposure that ultimately contributes to altered molecular cell signaling pathways and systemic oxidative stress. While these findings have been demonstrated by multiple human cohort studies, the exact mechanisms of how PM results in epigenetic alterations remain to be evaluated.

The link between $PM_{2.5}$ exposure during pregnancy and adverse offspring outcomes is thought to be in part due to DNA methylation [139]. Global hypomethylation in placental tissue and other altered DNA methylation, including gene specific alterations, have been reported following $PM_{2.5}$ exposure during pregnancy [140]. DNA hypomethylation and hypermethylation have both been associated with abnormalities. While global hypomethylation may lead to genomic instability [141, 142], hypermethylation has been associated with Down's syndrome and gestational diabetes [143, 144]. As an example, lower mean placental LINE-1 methylation, and specifically seven CpG sites, were associated with lower birthweight and maternal residence near a major highway in a study by Kingsley et al. [145]. Gene expression of S-adenosylmethionine (SAM), which is a key substrate involved in methyl group transfers, [146] and a decrease in placental tissue global DNA methylation were associated with first trimester fine PM exposure in one cohort study [140]. In another study, fine PM exposure was associated with DNA methylation in the promoter region of the leptin gene, an energy-regulating hormone involved in fetal growth and development [147]. DNA methylation was linked to oxidative stress by SOD2 promoter methylation levels in umbilical cord blood in an air pollution cohort study by Zhou et al. [148]. In another study, several genes, of which some have been associated with long-term cardiopulmonary outcomes, altered promoter region DNA methylation in newborn blood after fine PM exposure during pregnancy [149]. An increase in the DNA mutation rate in the placenta related to $PM_{2.5}$ exposure has been implied by an increase in *Alu* rate [150], which indicates increased global methylation, as well as altered DNA methylation in *APEX1, ERCC4, DAPK,* and

PARP1, key tumor suppressor and DNA mismatch repair genes [151, 152]. Because these DNA mismatch repair and tumor suppressor genes play a role in adult cancer risk and development, these findings link early life (fetal and neonatal) PM exposure with cancer risks later in life.

Independent of nuclear DNA, mtDNA epigenetic modification has also been associated with long-term risks for disorders and diseases such as cancer, obesity, cardiovascular disease, and diabetes [153]. Placental mtDNA has been shown to undergo epigenetic modification in correlation with $PM_{2.5}$ exposure. For example, *in utero* exposure to $PM_{2.5}$ was causally implicated in a decrease in mtDNA content, as well as MT-RNR1 region methylation alterations [154].

Exposure to fine PM has not only been found to alter DNA and mtDNA, but also non-coding RNAs, which are not translated into protein. These include piwi-interacting RNA (piRNA), microRNA (miRNA; miR), and long noncoding RNA (lnRNA), which have been found to interact with key regulatory proteins and transcription factors to ultimately regulate some biological processes despite their noncoding role [155-157]. Following human second trimester $PM_{2.5}$ exposure, Tsamou et al. [158] found a significant decrease in the expression of miR-21, miR-146a, and miR-222 in the placental tissues, and increased miR-20a and miR-21 expression after $PM_{2.5}$ exposure during the first trimester. DEPM and metal-rich PM exposure in adults was found to significantly increase miR-21, a key regulator in apoptosis and vascular cell proliferation [159, 160]. The role of epigenetics has been established in the development of disease but understanding the

role of fine and ultrafine PM exposure to pregnancies in altering DNA, mtDNA, and noncoding RNA requires further research to assess long-term effects.

1.3. Placenta Development

The placenta is a transient reproductive organ utilized by viviparous animals for successful reproduction [161]. It acts as the interface between maternal and fetal blood for nutrient, gas, and waste exchange [162]. In addition, it produces hormones necessary for proper fetal physiologic function and growth and development while forming the barrier necessary from the maternal immune system [163]. The organ is comprised of several different cell types, but is primarily of trophoblast lineage. These incredible cells have the ability to alter maternal anatomy and physiology, inherently controlling placental efficiency [164]. Several species have developed different placentation methods, which demonstrate varied sizes, shapes, cell types, and fetal-maternal interactions, allowing for species-specific maximal reproductive efficiency. Many of these contrasting placenta types and potential animal models are further discussed in varying detail.

As the interface between mother and fetus, the placenta is quite variable among the animals. Several attributes such as shape, maternal-fetal interface, cellular interdigitation, and vascular arrangement can be used to differentiate one species from another [165, 166]. Bloodstream arrangement has not been described extensively as the other characteristics but indicates the physiological diffusion potential and efficiency between mother and fetus. Placental shape (discoid, zonary, cotyledonary, and diffuse) illustrates how the placenta contacts the uterine wall. The maternal-fetal interface (epitheliochorial, synepitheliochorial, endotheliochorial, and hemochorial), describes the

barrier type between origin cells [167]. Finally, cellular interdigitation (labyrinth, villous, trabecular, lamellar, and folded) reveals how intertwined maternal vasculature is with trophoblast cells.

1.3.1. Application of Animal Models to Investigate Placental Development

Due to the wide variation of placenta among mammals, challenges arise when selecting the proper model. Several laboratory models are fairly well-established owning to various criteria including short gestational periods, large litters, genomic manipulations, and cost efficiency [168]. However, larger animals tend to be utilized for fetal physiology. Ethical concerns arise with any animal studies, but are highlighted with larger sized models, particularly non-human primates. Non-human primates have the closest relationship to humans making them the most ideal candidate, but due to ethics as well as cost, single progeny, and long gestational time, feasibility of using them for study becomes limited.

Mouse placenta models are utilized extensively within the literature. Mice have several advantages including short gestational periods, large litter size, relatively low housing, and upkeep costs, and well establish genomics with mutational lines available. Molecular phylogenetics associates rodents with primates in that both exhibit hemochorial placentation even though they evolved separately [169]. The mouse and human placenta similarities and differences are well documented, with mouse placental developmental genes or cells having analogs to humans [170, 171]. While the mouse is widely used due to previously discussed advantages, several disadvantages must be considered. Trophoblast invasion is shallow within the mouse placenta compared to humans [164].

This is best demonstrated by the fact that mouse decidual blood vessels are lined by endothelium whereas human endothelial lining of decidual blood vessels is replaced with trophoblasts that exhibit endothelial-like qualities [172]. Mouse uterine natural killer cells are implicated in uterine artery remodeling in contrast to trophoblasts in humans [173, 174]. Given the shallow trophoblast invasion in mice, pathologies associated with uterine artery remodeling may be best served in another animal model.

Placental endocrine functions vary between mice and humans as well [175]. During mouse gestation, ovarian functions produce progesterone, while the corpus luteum is maintained by pituitary prolactin followed by placental lactogens from trophoblast giant cells (TGCs). In contrast, human chorionic gonadotrophin is produced by the trophoblasts to maintain the corpus luteum for progesterone production in the beginning of pregnancy, after which progesterone production is taken over by the newly formed syncytiotrophoblast layer about eight weeks into gestation. Additionally, human placental endocrine hormones include chorionic somatomammotropin and placental growth hormone.

Further disparities between mice and humans include interstitial implantation, timing of the functional yolk sac, placental nutrient exchange areas, number of trophoblast layers in the hemochorial type, and the presence of trophospongium [168, 170]. Moreover, gestational length needs to be addressed further. The mouse gestational period is approximately three weeks compared to nine to ten months in humans. Much of the fetal development observed in humans occurs post-parturition in mice. Humans have more developed offspring due to their longer gestation, despite the need for parental care

following birth. It should be noted that, similar to mice, rats also have essentially the same placental characteristics: pituitary prolactin maternal recognition of pregnancy; hemochorial, discoid placental structure with labyrinth zone interface; corpus luteum as the primary production source of pregnancy hormones; three-week gestational length; and large litter size [176]. However, unlike mice, rats have deep trophoblast decidual artery modeling like humans. Given this difference, rats could be considered an advantageous model in investigating the spiral artery remodeling mechanism of placentation.

The guinea pig is another promising and established model for placenta studies utilized in nutrient transfer research [177, 178]. Contrasting to mouse and human-like placentas, guinea pigs are hemomonochorial but contain a sub-placenta structure without an analog to humans [179, 180]. Additionally, guinea pigs demonstrate deep and extensive trophoblast invasion with spiral artery remodeling as observed in humans [181]. However, guinea pigs also have several disparities with humans, as mice do, such as yolk sac retention [180].

Sheep have been utilized for fetal growth and development research [182, 183]. Fetal physiology is well-studied within the sheep model, but several disadvantages exist [165]. Sheep have different placentation than humans [184]. Sheep exhibit an epitheliochorial type maternal-fetal interface. Epitheliochorial interfaces lack cellular invasion and erosion of the uterine epithelium, and display cotyledonary attachments. While they may be useful in studying fetal aspects of pregnancy, sheep as candidates for studying transplacental substrate exchange need further evaluation given other potential models available.

Humans are primates which include Old and New World monkeys and the great apes. The most common species utilized in primate studies of placentation are macaques and baboons [168]. These primates have been used for studying reproductive biology and pathologies [185, 186]. Old World monkeys have strikingly similar characteristics to humans. They demonstrate extensive trophoblast invasion followed by spiral artery remodeling [187], villous placenta structure [188], and maternal-fetal interface [189]. However, some of the differences between Old World monkeys and humans relate to implantation. Old World monkeys demonstrate superficial implantation of the blastocyst, where part of the blastocyst remains in the uterine cavity [189, 190]. Following superficial implantation, cytotrophoblasts spread in a dramatically delineated and thick trophoblastic shell from the anchoring villi [189, 191, 192]. The human placenta trophoblast shell is less uniform and streams into the surrounding endometrium with extravillous trophoblasts (EVTs) invading the decidua for vascular remodeling [193]. Therefore, Old World monkeys have a scarcity of interstitial trophoblast compared to humans. Unfortunately, some of the main challenges with using primates include ethical concerns as well as cost for colony maintenance.

Other animal models exist outside of the previously discussed, but mouse models are the popular model for research. The mouse has stark differences compared to humans in implantation, yolk sac use, hormone production, and shallow trophoblast invasion. However, when considering not only functional anatomy and physiology, but also other reproductive factors, laboratory costs, and available genomic manipulations, the mouse

becomes a viable option despite the imperfect correlation with human anatomy and physiology.

1.3.2. Mouse Placenta

The mouse placenta is a single discoid, hemochorial placenta, similar to humans but with significant differences [170]. The mouse placenta is divided into two major "zones," each with distinct morphological and functional differences. The junctional zone has an endocrine and energy reserve function, while the labyrinth zone serves as the primary location for nutrient and waste exchange between the maternal-fetal circulation [194]. The junctional zone contains two primary cell types: spongiotrophoblasts and glycogen cells. Spongiotrophoblasts have large quantities of rough endoplasmic reticulum correlating with significant secretory function of placental lactogens [175, 195]. Additionally, TGCs which line the venous channels [196] within the junctional zone are believed to have endocrine function [197]. Their function may have the capacity for maternal crosstalk with the developing conceptus. The second primary cell type are the glycogen cells, which as their name implies, amass significant amounts of glycogen, which may serve as energy reserves. Interestingly, the glycogen cell population is scarce before embryonic day (E) 14.5, but multiply till E 18.5 before declining again [198].

The labyrinth zone trophoblasts form extensively branched villi with three distinct layers. There are two layers of syncytiotrophoblast cells with vast gap junctions linking them [199] and a fetal endothelial layer [170]. Though hemochorial in nature, the layered arrangement is referred to as hemotrichorial [200].

1.3.2.1. Mouse Placenta Development

Even though mouse placentas differ from human placentas in gross morphology, both species utilize hemochorial type placentation, therefore, their structures and mechanisms are thought to be similar [162, 171]. For this reason, mice are used as a popular model for studying various aspects of development as previously discussed. Following fertilization, extraembryonic cellular lineages begin at E 3.5 depicted in **Figure 1.2** [201, 202]. The trophectoderm forms a type of shell around the blastocyst in which the inner cell mass (ICM) that generates the embryo resides. The trophectoderm will differentiate into trophoblast cells that ultimately generate the placenta. The trophoblast cell is the defining cell type of the placenta with pluripotency which comprises most of the placenta with one exception: the fetal vasculature. Endothelial cells from the extraembryonic mesoderm populate the vasculature which ultimately forms the allantois and umbilical cord [171, 203]. The trophectoderm allows the formation of the blastocoelic cavity as fluid accumulation enlarges the blastocyst. Additionally, the trophectoderm cells on the edge and away from the ICM stop proliferating and begin endoreduplicative cellular cycles forming primary TGCs. By E 4.5, implantation of the uterine epithelium, aided by TGCs, is quickly followed by several cellular proliferation events [162, 170, 196, 202, 204]. The ICM further differentiates into epiblast and primitive endoderm cell lineages. The trophectoderm is split into a polar area surrounding the ICM and mural area surrounding the blastocoel. The polar trophectoderm continues to proliferate in response to fibroblast growth factor 4 produced by the epiblast. As the polar trophectoderm differentiates, proliferation generates the extraembryonic ectoderm around E 6.5. Further proliferation of the extraembryonic ectoderm occurs where cells farthest away from the

epiblast differentiate into the ectoplacental cone. Marginal cells of the ectoplacental cone differentiate into secondary TGCs which contain the invasive qualities needed to penetrate the endometrium for spiral artery remodeling. The height of trophoblast cell invasion is between E 7.5 to 9.5 [203] which involves TGCs to erode the maternal smooth muscle and endothelial vessels of the spiral arteries. This remodeling allows for increased maternal blood flow where vasoconstrictive activity is controlled by the conceptus [205].

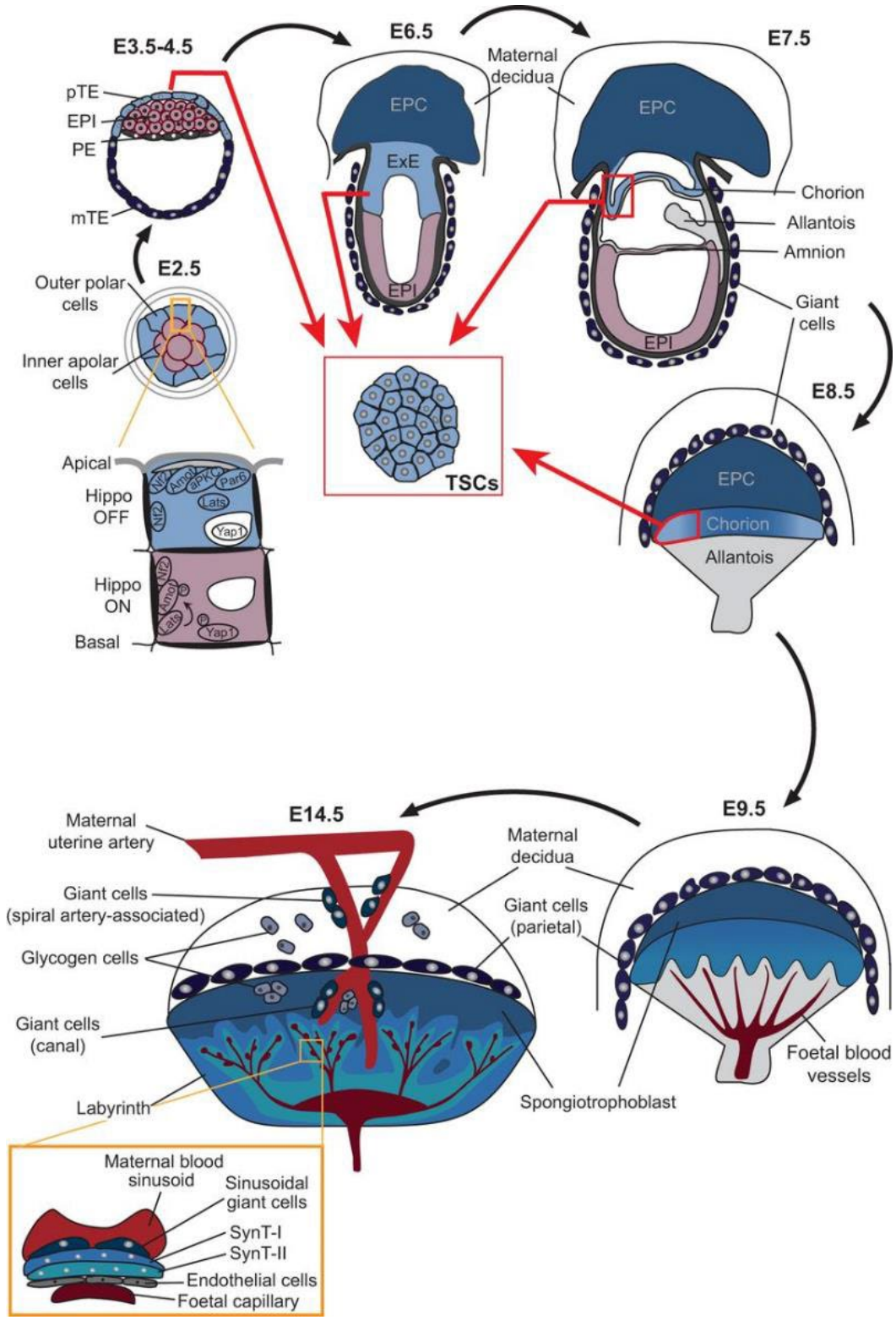

Figure 1.2 Embryonic days depicting major events during placental development.*

*Reprinted with permission from Latos, P.A. and M. Hemberger, From the stem of the placental tree: trophoblast stem cells and their progeny. *Development*, 2016. **143**(20): p. 3650-3660.

Early mouse embryogenesis and placental development, like in humans, likely occurs in a hypoxic environment [206]. While the polar trophectoderm differentiates and proliferates, this causes an avascular zone around the conceptus where nutrition is derived from glandular histotroph [207]. The yolk sac absorbs the histotroph, growing rapidly and eventually surrounding the conceptus except for the ectoplacental cone, due to its distance. Initially, the yolk sac is comprised of two layers: an outer parietal and inner vascularized visceral layer [208]. Histotrophic nutrients diffuse across the layers but as pregnancy progresses, the outer avascular layer disintegrates with TGC migration leaving the vascular inner visceral layer exposed, directly forming an inverted yolk sac. As previously mentioned, the continuity and functionality of the yolk is a key difference between rodents and humans.

As the ectoplacental cone and overall trophoblast cell invasion occurs, the extraembryonic ectoderm differentiates and expands to form the chorionic ectoderm. The chorionic epithelium is lined with mesothelial cells which ultimately form the labyrinth [162, 171, 204]. Simultaneously, the allantois derives from the mesoderm at the posterior end of the embryo at E 8.5 which contacts the chorionic ectoderm. Chorioallantois apposition is critical for pregnancy progression, with failure resulting in lethality [171, 203]. Chorioallantois fusion allows for direct contact with the chorionic ectoderm signaling for invagination to begin through Gcm1 transcription factor [209, 210]. The

invaginations signal for further differentiation causing cell fusion to form syncytiotrophoblasts. This pseudo-multinucleated layer will act as a barrier between fetal and maternal vasculature. As the invaginations deepen, blood sinusoids form which is funneled from the erosion of spiral arteries. Within the mouse, the maternal-fetal barrier is comprised of three layers, hemotrichorial: two layers of syncytiotrophoblasts of fetal derived blood vessels and one fetal endothelial layer derived from extraembryonic mesoderm [170, 171]. The maternal aspect forms a fenestrated layer, but given its sizeable gaps, is not considered continuous [203]. Around E 10.5 the invaginations result in the establishment of the labyrinth zone which grows continuously over the next several days. The continued growth and development of the labyrinth zone drastically increases surface area to further maternal-fetal nutrient and waste exchange occurring through a counter-current manner of blood flow [172]. Issues arising with labyrinth formation results in impaired placental perfusion with reduced nutrient and waste exchange [211].

During labyrinth zone development, the spongiotrophoblastic junctional zone, resides between the labyrinth and outer TGC-maternal decidua layer boundary. The junctional zone originates from the continuity of ectoplacental cone cells expressing trophoblast specific protein alpha [196, 212]. Again, it contains primarily three different cell types: spongiotrophoblasts, glycogen cells, and an out layer of TGCs bordering the maternal decidua. Glycogen cells are believed to be energy reserves while spongiotrophoblasts act in an endocrine capacity due to their production of growth factors and hormones [164, 195, 213].

1.3.3. Human Placenta

The human placenta is a single discoid, hemochorial type [214] comprised of highly branched villus trees rather than the labyrinth formation observed in the mouse [215]. The fetal villi originate from the chorionic plate within in each lobule [208]. The basal plate, which abuts the maternal decidua, folds forming septae helping to create the lobule which contain branched villus trees. The maternal blood flows from the spiral arteries and into the intervillous space bathing the villi eventually draining into the uterine veins. The villi are covered in a single layer of syncytiotrophoblast cells formed from the underlying cytotrophoblast layer which acts a stem cell reserve. Maternal-fetal circulation begins in the second trimester until parturition.

1.3.3.1. Human Placenta Development

Similar to mice, the morula and blastocyst stages begin placental development. An outer band of trophoblast cells surround the embryo and blastocoel cavity creating the first cell lineage [216] approximately E 4-5. Around E 6-7, the blastocyst hatches from the zona pellucida allowing for uterine epithelium attachment and placental development to begin [217]. The outer trophoblast cell layer opposed to the ICM, polar trophectoderm, functions for implantation. Upon implantation, trophectodermal cells differentiate and fuse forming syncytiotrophoblast [208]. Newly differentiated and fused syncytiotrophoblasts invade the endometrium by E 11. Under the layer of syncytiotrophoblasts, a layer of cytotrophoblasts expand and surround the newly implanted blastocyst. As previously noted, this helps cause a hypoxic environment similar to mice and a possible trigger for proper additional proliferation and later invasion [206]. Syncytiotrophoblasts continue to expand, eroding small capillaries and endometrial

glands, creating the precursors to the intervillous space [208]. The glandular histotroph provides nutrition needed during the early stages of placental and fetal development [218, 219].

The underlying cytotrophoblasts are in direct contact with the villous basal membrane. Surrounding the blastocyst, the cytotrophoblast fuse at the implantation site to form an additional second layer of syncytiotrophoblasts [220, 221]. The secondary layer of syncytiotrophoblast cells creates the inner epithelial border towards the intervillous space. With increasing fusion, syncytiotrophoblast knots form [222] causing cytoplasmic protrusions which indicate high cellular turnover. Within the first trimester, cytotrophoblasts move through the syncytiotrophoblasts to reach the maternal layer. At E 14 this column of interstitial cytotrophoblast will anchor the placenta to the uterine wall [223] by invading the underlying maternal decidua [224]. These interstitial invading cells are now termed EVTs because they accumulate around the spiral arteries invading them. Human EVT penetration is deep, reaching the inner third of the myometrium of the uterine wall [193]. This causes smooth muscle loss around the spiral arteries where EVTs slowly replace the endothelium. Interestingly, endothelial loss through apoptosis with subsequent replacement occurs through Fas/FASL interactions [225]. Once replaced, the EVTs will alter their phenotypes to mimic the endothelial cells they replaced. Subsequently, more EVTs will obstruct the spiral artery lumen effectively creating a plug [224]. This has been hypothesized to protect the developing conceptus from free radical mediated stress while creating a hypoxic environment until late first trimester [193, 226]. Around 14 weeks, the arterial plugs disintegrate increasing oxygen concentration [193]. Spiral artery remodeling

occurs between gestational week 20 to 22 [223]. It should be noted that insufficient or failure to remodel has been associated with several pathologies including preeclampsia and intrauterine growth restriction [211, 227].

Approximately two weeks after conception, finger-like projections begin to protrude into the intervillous space from the chorion [228]. These chorionic villi are the functional unit of the human placenta. Within a week, mesenchymal derived cells from the embryoblast invade the villi transforming them into the secondary chorionic villi. By the end of the third week, mesenchymal cells differentiate into blood cells and vessels forming tertiary villi in a process termed vasculogenesis. These villi eventually contain a connective tissue core. During the second trimester, the human placenta experiences significant growth for proper conceptus development [227, 229, 230].

1.3.4. General Placental Functions

It is essential to discuss placental functions given the context of this dissertation. Placental function has considerable impact on fetal development and programming which is further discussed in the following section. Therefore, the focus of placental functions will be broken down into several, albeit not entirely inclusive, categories which seemingly have the greatest impact: nutritional and waste transportation, endocrine activity, and protective/barrier role.

1.3.4.1. Nutrition and Waste Transportation

As previously discussed, several different types of placentation are present. Regardless of how intricate and elaborate the maternal-fetal interactions, transport across the membranes occurs and thus warrants a categorical discussion. The primary

mechanisms observed within the placenta are simple diffusion, protein transporters, and endocytosis [208]. Simple diffusion is the passage of molecules across the lipid bilayer without the expenditure of energy. Hydrophobic molecules transverse the lipid bilayer more readily driven by a concentration gradient, while hydrophilic molecules will cross more slowly. Factors affecting the concentration gradient will subsequently affect the rate of diffusion. This is best characterized with alterations in maternal-fetal blood flow [231].

Protein transport methods rely on carrier proteins for the passage of lipophobic and large compounds. This process is key to several nutrients such as sugars, lipids/fatty acids, and amino acids. For instance, the simple sugar glucose is transported in the solute carrier family of genes while also showing spatial concentrations differences noted between apical and basal surfaces [232, 233]. Glut1 and Glut3 proteins are seemingly the predominate isoforms, but expression of others is present [234]. Additionally, amino acid diffusion is slow while most uptake occurs through a family of transporters [235].

Lipids and fatty acids are equally important for fetal development [236]. Triglycerides, ester bonded fatty acids bound to glycerol, cannot transverse the placenta but do so through binding to lipoproteins. Lipoproteins are protein complexes which bind and transport fats and lipid components in the blood [237]. Several receptors have been identified spatially for lipoproteins along the syncytiotrophoblasts including very-low-density [238], low-density [239], and high-density [240] receptors within the human placenta. As gestation increases, very-low-density and low-density receptor expression increases but is suppressed when complicated by intrauterine growth restriction (IUGR)

and preeclampsia [238, 241, 242]. Altogether, maternal-fetal cholesterol transfer is important and occurs through placental lipoprotein uptake [237].

While triglycerides cannot cross the placenta, they can be degraded into their monomeric fatty acid forms. Syncytiotrophoblast cells have been noted to express lipases and lipoprotein lipases [243]. Interestingly, IUGR placentas have decreased expression of endothelial cell lipase. In a review by Duttaroy in 2009, three lipid systems have been implicated for free fatty acid transfer within the human placenta outside of simple diffusion [244]. Fatty acid transport proteins transport medium and long-chained fatty acids. Additionally, fatty acid binding protein appears to preferentially bind long-chained fatty acids. Finally, fatty acid translocase is expressed in syncytiotrophoblasts. Further nutrient availability activates several transcription factors downstream (i.e., FXR, PPAR, LXR, PXR, and SREBP-1) which regulate their expression.

Endocytosis and exocytosis are the third major component of placental transport. This is best characterized by immunoglobulins, large proteins, and even cholesterol uptake [208]. Uptake of immunoglobulin G occurs through nonspecific endocytosis in the human placenta [245] as well as other maternal proteins in syncytiotrophoblasts [246]. Rodents display endocytosis during early organogenesis [247]. The placenta demonstrates various methods for nutrient transport depending on the size, shape, and classification of molecule. With a degree of certainty, we can assume that disruption within any of these transport mechanisms and following pathways may lead to placental and fetal dysfunction.

1.3.4.2. Endocrine Activity

A wide range of hormones, most of which have physiological effects on the mother, are secreted from the placenta regardless of the animal model. The variety of hormones include steroid hormones, neuroactive hormones, and prolactin and growth hormone family [248]. Prolactin and growth hormone family include placental lactogens, prolactin, growth hormone and more [249], however, species variations occur in placental gene expression [195, 250, 251]. Prolactin and growth hormonal family has been associated with maternal metabolic alterations with pregnancy including maternal insulin and glucose metabolism [252] as well as lactation and maternal behavior [253].

Steroid hormones include the classical estrogens and progesterone [254]. In humans, the placenta serves as the primary source, while in mice, the corpus luteum within the ovary contribute much of the hormone production [254, 255]. These two steroid hormones have several functions throughout pregnancy in shaping maternal physiology. Elevated concentrations have been associated with gestational diabetes [256] while reduced concentrations are seen in preeclamptic women [257]. Additionally, both have been implicated in regulating insulin and glucose homeostasis [258, 259] and appetite and lipid regulation through neuropeptide Y [260] and leptin [261] production during pregnancy. Before parturition, progesterone levels decline in several mammalian species including rodents [262] and humans [263]. Progesterone inhibits prostaglandin production along with gap junction, ion channel, and oxytocin receptor gene expression within the myometrium [255]. These actions in concert decrease uterine contractility until term where estrogen levels rise causing parturition associated gene expression [264]. Finally, these hormones are implicated in mammary gland development [265] as well as post-

partum maternal behavior [266]. Thus, the placental derived steroid hormones are critical for proper growth and development as well as altering maternal physiology and behavior. Neuroactive hormones are produced by the placenta in several mammalian species which include melatonin and serotonin enzyme biosynthesis as expressed in the human [267] and serotonin in mice [268] along with human kisspeptin [269] and thyrotropin releasing hormone [270]. Additional hormones produced by the placenta include parathyroid hormone-related protein, leptin, activins (members of transforming growth factor β family), and chorionic gonadotropin [248].

1.3.4.3. Protective Barrier

In addition to nutrient transport and endocrine activity, the placenta has several protective functions. While the placenta is arguably incredibly good at fetal protection, it is not impervious [71]. Several chemicals/compounds have been shown to cross the placenta and cause abnormalities, especially chemicals labeled as teratogens through various molecular mechanisms [271]. Regardless, the placenta does serve as a physical barrier as the syncytiotrophoblasts have been noted to inhibit pathogen entry. This is best characterized in demonstration that *Listeria* is inhibited by normal syncytiotrophoblasts but penetrates the maternal-fetal interface at damaged or absent sites [272].

The human placenta expresses several classes of efflux transporters like organic anion and cation transporters, multidrug resistance protein family and more [273, 274]. These transporters are believed to provide protection for the developing fetus hindering the possibility for xenobiotic insults. Additionally, the placenta possesses detoxifying capabilities should xenobiotic insults occur. A particularly effective family of proteins are

the CYP enzymes [275]. These enzymes are critical for defense measures for proper fetal development. Altogether, the placenta employs several methods (i.e., physical barrier, transporters, and detoxifying enzymes) to protect the developing fetus from adverse stimuli.

1.4. Developmental Origins of Health and Disease

Correct intrauterine growth and development is paramount for proper life-long health. Perturbations within this period may affect appropriate body planning and overall development which is known as developmental programming [276]. Developmental programing with future health implications have been studied, [277] but the placenta's role and its function is the focus of this dissertation. Due to its functional roles that were previously discussed, it stands to reason that the placenta may have a drastic impact on the overall future health of the developing fetus. David Barker and colleagues highlighted this phenomenon in 1989 when they correlated ischemic heart disease with birth weight [278]. Ultimately, the group concluded that intrauterine development had been compromised before birth rendering individuals more susceptible to later diseases in life. Several countries have confirmed the results with their own follow-up studies [279-281].

Mechanistic data was lacking until links were made between IUGR fetuses and decreased renal nephrons [282], less pancreatic β-cells [283], fewer cardiomyocytes [284], altered brain [285], liver [286], and lung [287] development, and more. These developmental outcomes have been associated, in part, to improper placental function as well as intrauterine hypoxia [288], maternal stressors [289], and arguably environmental contaminants [290]. Thus, more research is needed to address the placenta's critical role

in later health highlighting the role of Developmental Origins of Health and Disease (DOHaD) as observed in human epidemiological studies.

1.5. Epidemiological Particulate Matter Exposure Studies

Limited data exists concerning UFP exposure with reported detection techniques in human epidemiological data. Due to the heterogenous nature of air pollution and PM, it is difficult to specifically quantify UFP exposure only in epidemiological studies. Therefore, the best exposure data resides in $PM_{2.5}$ as indicators for potential UFP toxicity for human health outcomes. Human epidemiological data has demonstrated an association between $PM_{2.5}$ exposure and adverse pregnancy outcomes such a preterm birth (PTB), low birth weight (LBW), and stillbirth. Risks of both PTB and LBW have been associated with $PM_{2.5}$ exposure during pregnancy as demonstrated in several systematic reviews with meta-analyses [291-294]. Reductions in birth weight from −15.9 to −23.4 g have been noted in a dose-dependent fashion for every 10 $\mu g/m^3$ increase in $PM_{2.5}$ exposure. Moreover, exposure during the third trimester has been implicated with an increased risk of both PTB and LBW [295, 296]. Further supporting the association between LBW and exposure to air pollution, a reverse observation during the 2008 Beijing Olympics revealed that infants who were exposed to less air pollution during the 8^{th} month of gestation weighed 23 grams more than infants born one year prior or after the Olympics [297]. While fetal growth and gestational age at delivery are commonly linked to variables of exposure during the latter portion of pregnancy, early exposure may affect fetal development rather than growth, altering anatomic or cognitive outcomes. Further

research breaking down pregnancy exposures by week may illuminate some of these potential effects.

One cohort study demonstrated an increased risk of stillbirth by 42% for pregnancies exposed to "high" levels of $PM_{2.5}$ during the third trimester. This association was not noted if pregnancies were exposed during the whole duration, or during the first or second trimesters [298]. The association with increased risk of stillbirth with exposure to $PM_{2.5}$ has not been consistent, however. Two meta-analyses failed to demonstrate a relationship between $PM_{2.5}$ exposure and stillbirth, even though ambient air pollution was associated with increase stillbirth risk [292, 299]. Future research may work to elucidate these risks, as well as potential causal associations.

1.6. Animal Particulate Matter Exposure Models

The transient nature, delicacy, and ethics surrounding pregnancy pose a challenge in designing and conducting studies to assess human pregnancy-related outcomes in a controlled way, especially as it relates to exposure to PM. As previously discussed, animal models can serve as a surrogate for human pregnancy not only to assess pregnancy and related outcomes, but with an increased degree of exposure control. Dose, timing, duration, mechanisms of action, modality of exposure, and specific uteroplacental, maternal, and fetal outcomes are qualities that can be assessed when animals are used for pregnancy-related research. Murine models are well documented in assessing these effects.

The use of animal models allows researchers to expose gravid females to PM in graduated doses which can simulate human environments wherein 'not all pollution is

equal'. Further, timing of exposure can be controlled to target specific "trimesters," periods of effect during pregnancy, weeks, and even duration of exposure in a given day. Evaluating effects by trimester may reveal more categorical data while breaking down results by the "week" during pregnancy may result in continuous data that can help pinpoint critical windows of toxicity. Limiting the duration of exposure in a given day can mimic actual human exposure where women may be subjected to higher levels of or specific types of pollution for only short durations of time during daily life.

To address the issue that 'not all pollution is equal,' Chen and Lippmann [300] described methods for regulating and characterizing the dose and size of PM for inhalation toxicology models. PM can be reduced to separate components as well as it can be parsed out by particle size into fine and ultrafine PM mixtures. Additionally, modality of PM exposure can be controlled using whole-body versus nose-only exposure, or even intranasal or intratracheal instillation, with each option carrying its own advantages and disadvantages. Nose-only chambers or intratracheal particle instillation introduce additional variables that must be accounted for including stress and anesthetic effects. By contrast, exposure of murine models to ambient pollution using traffic or polluted urban air, while increasing variables and limiting reproducibility, potentially improves upon the ability to extrapolate results to human life. Different environments vary from areas with low-level pollution to areas with high levels of pollution such as Beijing, previously mentioned in discussion of human data [301, 302].

Delivery of fine and ultrafine PM to pregnant murine models has been achieved via concentrated ambient particles (CAPs) by some investigators [300]. The Harvard

University Concentrated Ambient Particle System (HUCAPS), for example, has been used to select for UFPs in several studies. HUCAPS can concentrate ultrafine PM without concentrating ambient aerosol tenfold in comparison to ambient air PM concentration to reflect US urban pollution [303-308]. Comparable systems, such as the New York University Versatile Ambient Particle Concentrator Exposure System (VACES) [309-311] and the Ohio State University OASIS-1 aerosol concentration system [312-314] have been used similarly. The HUCAPS achieves a similar degree of concentration but condenses PM with a shift towards slightly smaller fine and ultrafine particle size in comparison to the VACES system. Using the VACES system, Klocke et al. [309] achieved an average concentration of 92.69 ± 19.16 $\mu g/m^3$. Studies arising from the Columbus, OH region reported similar concentrations of PM [312-314].

Aside from PM concentration, another aspect of PM delivery that must be considered is composition. Our own laboratory has produced and described a mixture of aerosolized ultrafine PM that simulates actual urban pollution [315] by atomizing a diluted solution composed of sulfates, organics, nitrates, chloride, ammonium, and DEPM [55]. Our system produced PM with a particle size peak diameter of 50 nm, ranging from 20 to 220 nm, with an average mass concentration of 101.94 $\mu g/m^3$, which amounts to a 24 hour mean daily dose of 25 $\mu g/m^3$. Similarly, Wu et al. [316] sought to replicate the chemical composition, size, hygroscopicity, and acidity observed during pollution-related haze events in India and China [317] by using the same atomizer method to investigate the impact of ultrafine ammonium sulfate particles (peak diameter of 10-20 nm) with an average mass concentration of 153 $\mu g/m^3$ on offspring development. These average mass

concentrations and mean daily doses stand comparably with the U.S. EPA's standards which do not account for UFPs.

Adding a layer of complexity, Cormier and colleagues have sought to replicate airborne PM found at abandoned hazardous waste facilities known as Superfund sites [318]. This airborne PM includes combustion-generated environmentally persistent free radicals (EPFR) [319] and represents integrated pollutant-particle systems consisting of phenoxy- and semiquinone-type radicals formed and stabilized by transition metal oxide–containing particles. Cormier et al. employed EPFR that have been adsorbed to UFPs in several exposure models [320-324] at environmentally relevant doses to achieve alveolar deposition dose to murine neonates equivalent to deposition in human infant pulmonary tissue [321].

Fossil fuel combustibles, such as vehicle-derived PM [325-327] and aerosolized residual oil fly ash [328] have also been studied for their potential toxicities especially relating to pregnancy. A high-volume UFP sampler [325, 326] was used to collect nano-scale PM from a heavy traffic site around the Los Angeles I-110 Freeway by Morgan and colleagues. DEPM has also been studied using re-aerosolized engine-produced particles with *in vivo* inhalation models [329]. As an alternative to re-aerosolization of PM, direct exposure to freshly generated diesel exhaust has been extensively studied in animal models [330]. Rodents have been exposed to both particulate and gaseous components associated with traffic-related air pollution with diesel exhaust concentrations ranging from 90 to 300 $\mu g/m^3$ $PM_{2.5}$ [331-334].

As previously mentioned, inhalation is only one mode of PM or DEPM delivery that has been employed. Intranasal application [125, 335], oropharyngeal administration [336], intratracheal instillation [337, 338], oral gavage [339], and intraperitoneal injection of particles [340] are alternative delivery routes that have been used to assess PM and/or DEPM exposure in prenatal models. While outcomes from these various modes of exposure can result in differing pathological consequences [341], translocation of PM into maternal systemic circulation may be of greater consequence to fetal development when assessing *in utero* exposure, even though systemic administration of particles does not represent a physiologic route of exposure [342].

In summary, several methods can and have been used to assess toxicologic effects of air pollution using murine models, each with advantages and disadvantages to focus on different aspects of pregnancy-related outcomes. These modalities of focused exploration of pollution and PM exposure using animal models allows for a deeper understanding of the underlying biological mechanisms that explain findings from human epidemiological studies.

1.6.1. Adverse Birth Outcomes in Animal Models

Exposure to PM has been inconsistently correlated with adverse birth outcomes in murine models. While there is a consensus that PM induces an initial growth restriction, various models have demonstrated differences in long-term outcomes, and some have reported that growth restriction, abortion, stillbirth, and birth weight are unaffected. In the haze event recreation study by Wu et al. [316], rat models demonstrated a significantly shorter gestational duration, fewer live offspring at delivery per pregnancy, and smaller

average birth weight. Pregnant females were exposed to ammonium sulfate particulate representing specific UFP properties observed in Asian urban settings. The lower neonatal body weight persisted until after the offspring were weaned, which coincides with significantly reduced concentrations of plasma triacylglycerol. Subsequent postnatal weight by day 105 demonstrated an absence of difference in body weight between prenatal exposure groups regardless of consumption of a low- or high-fat diet. In another study featuring gestational *in utero* exposure to concentrated ambient $PM_{2.5}$ with continued exposure until weaning at 3 weeks of age [312], Gorr and colleagues observed significantly reduced birth weights in FVB mice. In comparison to control mice, exposed offspring demonstrated slightly higher weights at 3 months of age, with increased absolute heart weight, which correlated with significant adulthood cardiovascular dysfunction. Additionally, Liu et al. [132] observed fetal weight to be significantly decreased with a rat maternal exposure to $PM_{2.5}$ from gestational days 10 to 18. An increase in absorbed blastocysts and abnormal placental pathology was also noted following this segmented exposure.

DEPM exposure to pregnant C57Bl/6 mice resulted in significantly lower birthweight offspring with persistently reduced body weight at 4 weeks of age in a study by Manners et al. [335]. Prenatal diesel exhaust exposure has been simulated by other studies, confirming reduced fetal birthweight [327]. While the early finding of reduced fetal birthweight was not reproduced by Chen et al. [338], when C57Bl/6 mice were exposed to DEPM antenatally, offspring did not appropriately gain weight from postnatal week two until the end of observation at 20-22 weeks of life, which correlated with poor

food intake. The poor food intake and poor weight gain corresponded with increased epididymal adipose tissue mass. The effect of *in utero* exposure on weight gain later in life was underscored by increased offspring weight gain despite similar food intake noted in a second exposure group, in which control offspring were fostered by $PM_{2.5}$-exposed dams during lactation and into adulthood.

A separate phenomenon of "catch-up" growth, wherein a growth-restricted neonate rapidly gains weight after delivery, has been demonstrated in multiple studies. The effect of periconception PM exposure has also been investigated. C57Bl/6 mice were either exposed to ambient $PM_{2.5}$ preconceptually, during pregnancy, and through lactation or during pregnancy and lactation alone by Chen et al. [314]. Here the authors demonstrated decreased birthweight followed by a period of accelerated growth during lactation. A sexual dimorphic effect was observed between females and males where female offspring growth trajectory was accelerated until seven weeks. Males continued along this accelerated growth trajectory until 18 weeks when the observation period was over. Gorr and colleagues [312] demonstrated similar findings with a "catch-up" phase. These rodent models mirror epidemiological data supporting the "thrifty phenotype" hypothesis [343]. However, Tsukue et al. [344], also assessed preconception DEPM exposure but demonstrated a continued growth lag rather than a "catch-up" phase at eight weeks of age in a C57Bl/6 mouse model. Regardless of continued growth restriction or postnatal growth acceleration, these observations indicate that offspring may suffer the effects of maternal preconceptual PM exposure with potential lifelong consequences according to DOHaD.

1.7. Central Hypothesis and Specific Aims

Rationale: There is growing epidemiological evidence that supports exposure to PM_{10} and $PM_{2.5}$ leads to IUGR, PTB, stillbirth, and other adverse pre and postnatal outcomes [345-347]. But significant uncertainties exist concerning UFPs. Currently, there are no regulations toward UFP exposure but are thought to have greater toxicity than PM_{10} and $PM_{2.5}$ [348]. The increased toxicity should be of concern based on DOHaD which *in utero* environments contribute to short and long-term health effects on the conceptus indicating pregnant women as a vulnerable population [349-351].

Central Hypothesis: The central hypothesis of the current study is that "*in utero* exposure to UFPs cause adverse health outcomes through placenta dysfunction that is modified by the ability to respond to UFP-induced oxidative stress". The objectives are to (i) determine UFPs role in causing placenta dysfunction through the identification of novel pathways utilizing RNA sequencing; (ii) characterize the role of Nrf2 in antioxidant response in the placenta from UFP exposure; and (iii) identify if dietary activation of Nrf2 via sulforaphane supplementation mitigates UFP exposure and developmental outcomes.

Specific Aim 1: Determine the effects of gestational exposure to UFPs on the placenta.

Our working hypothesis is that UFP exposure leads to an oxidative imbalance and inflammatory physiological state within the placenta which results in adverse developmental outcomes. The objective of this aim is to ascertain the adverse effects of gestational exposure to environmentally relevant doses of UFPs on the placenta. This is important as limited *in vivo* data exists concerning this classification of PM. Moreover,

the data has the potential to be utilized for the implementation of federal regulations concerning pregnant women especially within the work force.

Specific Aim 2: Evaluate how genetic modulation of Nrf2 alters key pathways in response to gestational UFP exposure. The working hypothesis of this aim is that lack of Nrf2 (*Nfe2l2*$^{-/-}$) increases susceptibility. Thus, these factors interact and help regulate oxidative stress altering perinatal outcomes. Our objective is to identify the modulatory role of master antioxidant regulator, Nrf2, on UFP derived placental dysfunction.

Specific Aim 3: Determine how dietary activation of Nrf2 with the phytochemical sulforaphane may protect oxidative stress following gestational UFP exposure. The working hypothesis is that gestational supplementation with sulforaphane will counter UFP exposure and protect against adverse developmental outcomes. The objective is to establish the proof-of-principle that Nrf2 activation through sulforaphane administration mitigates the oxidative stress induced by gestational UFP exposure.

Overall, findings should demonstrate the vulnerability of offspring exposed to UFPs during pregnancy, highlighting the importance of mitigating UFP exposure to prevent adverse health outcomes.

2. GESTATIONAL EXPOSURE TO ULTRAFINE PARTICLES REVEALS SEX- AND DOSE-SPECIFIC CHANGES IN OFFSPRING BIRTH OUTCOMES, PLACENTAL MORPHOLOGY, AND GENE NETWORKS*

2.1. Overview

Particulate matter (PM) causes adverse developmental outcomes following prenatal exposure, but the underlying biological mechanisms remain uncertain. Here we elucidate the effects of diesel exhaust ultrafine particle (UFP) exposure during pregnancy on placental and fetal development. Time-mated C57Bl/6n mice were gestationally exposed to UFPs at a low dose (LD, 100 μg/m3) or high dose (HD, 500 μg/m3) for 6 hours daily. Phenotypic effects on fetuses and placental morphology at gestational day (GD) of 18.5 were evaluated, and RNA sequencing was characterized for transcriptomic changes in placental tissue from male and female offspring. A significant decrease in average placental weights and crown to rump lengths was observed in female offspring in the LD exposure group. Gestational UFP exposure altered placental morphology in a dose and sex-specific manner. Average female decidua areas were significantly greater in the LD and HD groups. Maternal lacunae mean areas were increased in the female LD group, whereas fetal blood vessel mean areas were significantly greater in the male LD and HD groups. RNA sequencing indicated several disturbed cellular functions related to lipid

---

*Reprinted with permission from Behlen JC, Lau CH, Li Y, Dhagat P, Stanley JA, Rodrigues Hoffman A, Golding MC, Zhang R, Johnson NM. *Toxicol Sci*. 2021 Nov 24;184(2):204-213. doi: 10.1093/toxsci/kfab118.

metabolism, which were most pronounced in the LD group and especially in female placental tissue. Our findings demonstrate the vulnerability of offspring exposed to UFPs during pregnancy, highlighting sex-specific effects and emphasizing the importance of mitigating PM exposure to prevent adverse health outcomes.

2.2. Introduction

Air pollution represents a major environmental cause of morbidity and mortality worldwide [352]. According to the most recent State of Global Air Report, approximately 6.67 million deaths were attributable to air pollution exposure in 2019, ranking fourth after high blood pressure, tobacco, and dietary risks [353]. For the first time, the impact of exposure on infant health and survival was included in this latest analysis. Strikingly, air pollution accounted for 20% of newborn deaths worldwide, mostly related to complications of low birth weight and preterm birth. Understanding the importance of timing of exposure (i.e., during placental and fetal development periods) and biological pathways affected are critical for the assessment and ultimate mitigation of the adverse health effects of air pollution.

Ambient particulate matter (PM) is a heterogeneous mixture classified based upon their size (i.e., aerodynamic diameter), including coarse (≤10 μm or PM_{10}), fine (≤2.5 μm or $PM_{2.5}$), and ultrafine (≤0.1 μm or $PM_{0.1}$) fractions. The levels of $PM_{2.5}$ and ultrafine particles (UFPs) are significantly elevated under typical urban environments [315], because of primary emissions [354] and new particle formation [355]. Both PM_{10} and $PM_{2.5}$ are an important driver of adverse birth outcomes. Increases in both have been consistently linked with significantly elevated risks for infant low birth weight (LBW) and

preterm birth (PTB) [291-294]. Rodent models evaluating $PM_{2.5}$ generated from various sources confirm effects on adverse pregnancy outcomes. There is broad consensus on initial pollutant-induced fetal growth restriction, with more variation in the long-term effects of altered offspring growth trajectories that may be driven by differences in exposure models [312, 335, 356]. Evidence is also emerging on the adverse developmental outcomes in response to exposure to UFPs during pregnancy [316]. Importantly, UFPs are not currently regulated by the U.S. National Ambient Air Quality Standards while PM_{10} and $PM_{2.5}$ are regulated [2]. Moreover, in addition to indirect mechanisms of action driven through systemic maternal oxidative stress and inflammation [85], placental translocation of UFPs may elicit marked effects via direct mechanisms of action. Evidence from *in vivo* animal exposure models [73], *ex vivo* human placental models [72], and recent direct evidence from human placentae [71] demonstrate transport of UFPs across the placental barrier indicating potential direct effects on placental function and offspring health.

Adverse perinatal outcomes are traditionally regarded as an indicator of improper placental function [357]. Based on the Developmental Origins of Health and Disease (DOHaD) hypothesis, *in utero* environments contribute to the short and long-term health of the developing conceptus [349-351]. Human epidemiologic studies have supported an impact of *in utero* PM exposure on placental function [121, 358]. However, investigations have yet to determine specific particle size effects and related mechanisms of action. Currently, there exist considerable uncertainties concerning the biological mechanisms underlying the adverse health effects relevant to prenatal PM exposure [359, 360].

In this study, we applied our murine inhalation exposure model [55] to assess the impact of UFP exposure on the placenta. Phenotypic effects and transcriptomic changes were evaluated via RNA sequencing with qRT-PCR validation to address this knowledge gap and further understand the molecular mechanisms involved with exposure to UFPs during pregnancy.

2.3. Materials and Methods

2.3.1. Animals and Particulate Matter Exposure

Male and female C57Bl/6n 8- to 10-week-old mice (Jackson Laboratory, Bar Harbor, ME) were kept in a 12-hour light dark cycle and time-mated in an AAALAC approved facility at Texas A&M Institute for Genomic Medicine (TIGM). Following a one-week acclimation period and upon identification of a vaginal plug or sperm present on vaginal cytology (GD 0.5), females were weighed and randomly assigned to one of three exposure groups: filtered air (FA), low dose (LD) 100 $\mu g/m^3$ UFP, or high dose (HD) 500 $\mu g/m^3$ UFP. Whole body exposure occurred in a controlled system for 6 hours per day from GD 0.5 to 18.5 (Figure 2.6). Average 24-hour exposures for LD and HD equaled 25 $\mu g/m^3$ and 125 $\mu g/m^3$, respectively. This equivalent dose of 25 $\mu g/m^3$ is the acceptable level set by the World Health Organization guidelines for $PM_{2.5}$ but under the 35 $\mu g/m^3$ limit for $PM_{2.5}$ set by the U.S. EPA. Currently, there are no set guidelines for UFP exposure. Expanding upon this, this is why th current study included an additional level of 500 $\mu g/m^3$ (~125 $\mu g/m^3$ in 24-hours) to evaluate gestational exposure maternal/fetal dose responses.

The exposure system was modified from our previous study [55]. Briefly, exposure chambers consisted of a 27 X 19 X 13" stainless steel, air-tight box wherein mice were individually housed in 1.5 X 4.5" cylindrical air-flow chambers. High-efficiency particulate air (HEPA) filtered air was continuously pumped into each chamber via a separate pump allowing for either filtered air control or dilution air for particulate matter (Figure 2.7). As previously described in detail by Rychlik et al., we employed a multicomponent aerosol mixture representative of PM chemical composition under typically polluted urban environments consisting of ammonium nitrate, ammonium sulfate, diesel exhaust PM (NIST, SRM 2975), and potassium chloride, with the mass fractions of 44, 39, 10, and 7%, respectively. UFP generation and characterization followed the same principles and standards as previously described [361, 362]. During exposures, we continuously monitored particle mass concentration using a tandem differential mobility analyzer (DMA) and condensation particle counter (CPC) to ensure consistent particle concentrations within chambers throughout the exposure duration. We monitored particle size and further verified size and morphology using transmission electron microscopy (TEM), described below.

Exposures occurred between 0800 and 1400 hours from September through December 2019. Mice had access to standard chow, 19% protein extruded rodent diet (Teklad Global Diets), and water *ad libitum* except during exposure timeframes. Weights were measured daily before exposure to assess any alterations to maternal weight gain during gestation. By GD 14.5, successful dam pregnancies were assessed via tracked weight gain and obvious gravidity. At the end of exposure on GD 18.5, which correlates

with an optimally grown placenta but before spontaneous birth, pregnant dams were humanely euthanized using a mixture of pentobarbital sodium and phenytoin sodium. Placental and fetal tissue samples were sex-separated visually using a dissecting microscope and pooled per dam. All approved protocols were followed according to the Texas A&M University Institutional Animal Care and Use Committee #2019-0025.

2.3.2. Transmission Electron Microscopy (TEM)

UFP morphology of our representative PM solution was verified at Texas A&M Image Analysis Laboratory (IAL) using a FEI Morgagni 268 TEM with a MegaView III CCD camera while operating at an accelerating voltage of 60kV. Briefly, the PM suspensions were incubated on glow discharge grids and stained with uranyl acetate. Excess uranyl acetate was blotted followed by two brief ultrapure water rinse steps and allowed to air dry. Bound PM solution was then imaged.

2.3.3. Tissue Preparation, Staining, and Analysis

Following euthanasia, GD 18.5 placentas (from 3 dams per exposure group) were extracted and whole tissues fixed in 10% neutral buffered formalin for 24-48 hours on a plate shaker. Tissues were transversely trimmed and transferred to 70% ethanol for storage until processing and paraffin embedding. Embedded tissues were serially sectioned at 5 μm where the first and fifth slide were used for hematoxylin and eosin (H&E) staining.

H&E-stained slide analysis was performed by a board-certified veterinary anatomic pathologist. All stained slides were blinded to minimize bias. Slides were observed using light microscopy on an Olympus BX53 microscope equipped with an Olympus SC180 camera operating Olympus cellSens 2.3 software. Based on H&E-stained

slides, placenta morphology of the decidua, spongiotrophoblast, and labyrinth zones were calculated via pixels [363]. For each H&E-stained section, approximately ten 40X random labyrinth zone images were captured depicting maternal lacunae and fetal vessels that were averaged by sex and treatment doses.

2.3.4. RNA Isolation and Sequencing

Total RNA was isolated from sex-separated pooled GD 18.5 placenta using TRIzol reagent according to the manufacturer's instructions. RNA was quantified using a Nanodrop Spectrophotometer/Fluorometer (DeNovix DS-11 FX+ V3.35) with 260/280 absorbance values of ≥1.8 and bioanalyzer integrity number ≥7.0. Samples were submitted for RNA sequencing library preparation at the Texas A&M Institute for Genome Sciences and Society (TIGSS). Libraries were created using TruSeq® Stranded Total RNA library prep kit on an Illumina® NextSeq 500 according to manufacturer's protocol. FASTQ files were analyzed using Basepair software (https://www.basepairtech.com/) with a RNA Sequencing pipeline that included the following steps: reads were aligned to the transcriptome derived from UCSC genome assembly (mm39) using STAR [364] with default parameters; read counts for each transcript were calculated using featureCounts [365]; differentially expressed genes were determined using DESeq2 [366] and a cut-off of 0.05 on adjusted p value (corrected for multiple hypotheses testing) was used for creating lists and heatmaps, unless otherwise stated. Gene set enrichment analysis (GSEA) was performed on normalized gene expression counts, using gene permutations for calculating p value. Further up and downstream cluster analysis was identified by Ingenuity Pathway Analysis (IPA) software (https://digitalinsights.qiagen.com/) [367].

2.3.5. Experimental Validation by qRT-PCR

To validate the expression of differentially expressed genes, 20 genes were selected from antioxidant, inflammatory, and lipid transport functions including *Nfe2l2, Keap1, Hmox, Gpx1, Txn1, Ahr, Pparg, Il1b, Il6, Nfkb1, Tnf, Ptgs2, Tgfb1, Smad3, Hnf4a, Nr1h4, Apoa1, Apob, Apoe*, and *Pfkfb1*. Total RNA was extracted using TRIzol reagent according to manufacturer's protocol where RNA quantification occurred using a Nanodrop Spectrophotometer with ≥1.8 260/280 nm absorbance values. Following purification, cDNA was reverse transcribed (Qiagen QuantiTect® Reverse Transcription), and transcription levels analyzed using SYBR Green qRT-PCR (Applied Biosystems™ *Power* SYBR™ Green PCR Master Mix) on a Roche LightCycler® 96 System according to manufacturer's recommendations. Primer sequences of selected genes are shown in supplementary information table 1 (Table 2.1). Gene transcription levels were calculated using $2^{-\Delta\Delta CT}$ with *Gapdh* as the reference gene.

2.3.6. Statistics

Statistical analysis was performed using GraphPad Prism (V 9.0.2) to assess differences between treatment groups. Statistics were conducted separately by sex. Ordinary one-way analysis of variance (ANOVA) with Dunnett's multiple comparisons tests were conducted on all phenotypic analyses. Adjusted p values of <0.05 from both tests were considered statistically significant.

2.4. Results

2.4.1. Particulate Matter Characterization

Transmission electron microscopy (TEM) was used to help verify the size of our particles. Fig. 1A depicts PM solution pre-atomization. PM appearance is primarily spherical from the 2975 SRM diesel soot constituent. Fig. 1B shows the post-atomization of our PM solution (i.e., what is pumped into the chambers for exposure). Particle size range was 0.02 to 0.5 μm as indicated in Fig. 1C and 1D for both LD and HD chambers. The peak particle diameter was 0.049 and 0.066 μm (or 49 and 66 nm) for LD and HD, respectively, over the entire exposure period within the UFP range. The mean PM mass concentration for the LD and HD exposures over the time course of each exposed pregnant dam averaged 101.40 ± 10.08 (mean ± SD) and 492.47 ± 33.14 $\mu g/m^3$ as determined by the real-time mass concentration system (Figure 2.8).

2.4.2. Perinatal Outcomes

UFP exposure was not overtly toxic to pregnant dams as indicated by daily maternal weight gain (Fig. 2A), fetal weight (Fig. 2B), or placenta to fetal weight ratios (Fig. 2E). Moreover, there was no significant variation in litter size (data not shown). However, significant reductions in female LD groups for placental weight, p=0.0258 (Fig. 2C) and fetal crown to rump length, p=0.0161 (Fig. 2D) was observed in comparison to female FA controls. Overall, average fetal weights and crown to rump lengths for both males and females demonstrated a decreasing trend in LD and HD groups as compared to FA while placenta to fetal weight ratios exhibited an upward trend.

2.4.3. Histological Analysis of Placental Tissue

Histological analysis was performed on H&E-stained slides to evaluate morphological alterations of exposed placenta to varying UFP concentrations. As shown

in Fig. 3A, female decidua layer indicated a significant increase in size for both LD ($p=0.0084$) and HD ($p=0.0208$) exposure groups as compared to FA controls. The total placental area for both males and females were not significantly altered in response to exposure. Fig 3B and 3C are representative images of a female FA GD 18.5 placenta with its associated 40X labyrinth zone. Within the labyrinth zone images (Fig. 3C), dotted outlines indicate maternal lacunae while arrows label fetal vessels. Fig. 3D and 3E show the average areas measured for the maternal lacunae and fetal vessels, respectively. The average maternal lacunae area was significantly increased in the female LD group ($p=0.0072$) compared to the FA control group. Alternatively, the mean area of fetal blood vessels was significantly greater in the male LD ($p=<0.0001$) and HD ($p=0.0313$) groups versus FA controls.

2.4.4. RNA Sequencing Analysis

The effect of UFP exposure during pregnancy on GD 18.5 placentas was further assessed through RNA sequencing and subsequent pathway analysis clustering. The results indicated several hundred differentially expressed genes in both male and female placentas exposed to the LD or HD as compared to FA control. Volcano plots were constructed using Fold Change Log_2: [-1.0 to 1.0] with a p value of <0.05 as cutoffs. Four plots are depicted: male LD vs. FA (Fig. 4A), female LD vs. FA (Fig. 4B), male HD vs. FA (Fig. 4C), and female HD vs. FA (Fig. 4D). Statistically significant differentially expressed genes from all four groups ranged from 10 to 876 genes.

To further identify the transcriptomic pathways affected, IPA software identified lipid transport and metabolism primarily through farnesoid X receptor (FXR), liver X

receptor (LXR), and retinoid X receptor (RXR) cell signaling. Fig. 5 reveals the top analysis pathways from IPA where Table 2.2 indicates the top up-regulated genes from each exposure group by sex.

2.4.5. qRT-PCR Validation

qRT-PCR was performed on a set of 20 genes selected based on IPA results, as well as gene identified as related to oxidative stress or inflammation with *Gapdh* as the internal reference. Generally, as depicted in Figure 2.9, the gene expression levels between RNA sequencing and qRT-PCR match with the 20 selected genes for inflammatory, antioxidant, and lipid transportation pathways. Overall, RNA sequencing was validated according to the selected genes.

2.5. Discussion

We previously developed an exposure system to replicate urban UFP exposure [55]. Urban PM is primarily composed of organics, sulfates, nitrates, ammonium, black carbon, and chloride [315]. The nitrate constituent is attributable to vehicle emissions and industrial sources, the sulfate is due to the burning of sulfur-containing fuels or coal burning from power plants, and black carbon is produced mainly by diesel vehicles. Previous research demonstrated *in utero* UFP exposure led to an immunosuppressive environment in the lung of prenatally exposed offspring [55]. This effect was more pronounced in C57Bl/6 compared to BALB/c mice. Additionally, in a multiplex model employing paternal alcohol exposure in C57Bl/6 mice, gestational co-exposure to UFPs using the same model system exacerbated offspring growth inhibition measured out to 1 month [368]. Male and female offspring co-exposed to paternal alcohol/maternal UFPs

displayed an average ~20% and ~30% respective reduction in body weight, compared to control groups. In both studies, these effects were observed at 100 $\mu g/m^3$, our low dose level. The objective of this study was to determine UFP effects at varying doses on perinatal outcomes and the placenta.

Average maternal exposure concentrations were consistent (Figure 2.8) and only slightly more variable in the high dose (HD), as compared to the low dose (LD) exposure group. The HD mean particle diameter (66 nm) was also slightly higher than the LD average peak particle diameter (49 nm). This reflects the relationship between particle diameter and PM mass concentration, wherein higher mass concentrations yield higher particle diameters due to aerosol nucleation and growth [317]. Thus, while it is difficult to compare varying mass concentrations with the exact same PM size, our study closely matches PM size at these two separate exposure levels.

Following gestational UFP exposure, we observed significant decreases in female placental weights and fetal crown to rump lengths, pronounced in the LD group (Fig. 2). Several studies have implicated malnourishment or lack of oxygen leading to decreased placenta size is associated with adverse perinatal conditions and later chronic diseases such as asthma, coronary heart disease, and lymphoma [369-373]. We did not observe any significant differences between exposure groups regarding maternal weight gain, fetal weight, or placenta to fetal weight ratios. While differences in fetal weight were not significant, decreasing weight with increasing exposure trends were observed for both sexes. In a similar exposure model employing UFPs generated from ammonium sulfate throughout gestation, rat offspring in the exposed group had increased rates of stillbirth,

decreased birth weight, and were small for gestational age compared to filtered air controls [316]. In a model employing concentrated ambient particles in the UFP range, Gorr [312] and Chen et al. [314] both noted decreased offspring birth weights.

The placenta barrier between the mother and fetus regulates growth, transportation of nutrients, wastes, and gases as well as immunogenicity. While the barrier was once thought to be impervious, we now know that several chemicals and compounds may cross including UFPs [71]. Several studies have indicated that PM2.5 and UFPs affect placental morphology and function [74, 132]. In our study, gestational UFP exposure, mainly at the LD level affected placental morphology, mimicking phenotypic data. We observed increased placenta decidua areas (LD and HD) and maternal lacunae size (LD) in females, whereas we observed increased placenta fetal vessel size (LD and HD) in males (Fig. 3). Veras and colleagues demonstrated decreased fetal weights and altered maternal side of the placenta hinting at a fetal capillary adaptation [74]. A similar adaptation may be occurring in our model in males, wherein increased fetal vessel size aims to expand oxygen and nutrient delivery to the fetus. Additionally, adaptations may be occurring due to other mechanisms in female offspring that showed marked effects on maternal blood spaces. Glycogen cells (GCs) in the spongiotrophoblast layer (i.e., junctional zone) often associate with maternal blood spaces in contact with the decidua zone [203]. GCs serve as an energy store to provide additional nutrition to the placenta. Effects on maternal vessel size and decidua areas may alter normal placenta physiology, relating back to growth restriction.

To further identify the effect of UFPs on the placenta, RNA sequencing was conducted and showed marked gene expression differences varying by sex and dose (Fig.

4). Following, qRT-PCR confirmed altered gene expression levels of several prominent antioxidant, inflammatory, and lipid transportation pathways (Figure 2.9). Interestingly, we observed greater placental gene disruption within the LD group compared to the HD, and in females compared to males. Upon further investigation, we observed an increase in antioxidant and inflammatory genes in both doses and sexes. Many models indicated oxidative stress and inflammatory pathways as potential causes of pathology. In prior studies, pregnant mice exposed to diesel exhaust PM had increased expression of IL-2, IL-5, IL-12, and granulocyte monocyte colony stimulating factor in the placenta [128]. In 2015, de Melo and colleagues associated $PM_{2.5}$ with increased IL-4 on the fetal portion of the placenta in Wistar rats [130].

A top canonical pathway identified by Ingenuity Pathway Analysis (Fig. 5) implicate the role of FXR/RXR activation in response to UFP exposure. FXR is activated in part by oxysterol ligands and heterodimerizes with RXR to mediate lipid metabolism and inflammation [374]. LXR belongs to the same sub-cluster of metabolic transcription factors, which have similar activation and binding properties [375]. In the placenta, activation of LXR by oxysterols have been shown to inhibit trophoblast differentiation and survival [376]. Oxysterols, which are cholesterol oxidation products, can accumulate under oxidative stress conditions and disrupt placental function. Further review of our qRT-PCR data support alterations in this pathway (Figure 2.9) as shown by significant fold changes in exposed versus control groups in *Nr1h4* (FXR), several of the apolipoprotein genes, and *Hnf4a*. Hnf4a, hepatocyte nuclear factor 4 alpha, is a transcription factor controlling the regulation of several hepatic genes and may play a role

in liver, kidney, and intestinal development [377, 378]. Loss of function mutations are associated with Maturity Onset Diabetes of the Young (MODY) characterized by decreased insulin production in early life due to β-cell pancreatic dysfunction [379]. Given whole body *Hnf4a*$^{-/-}$ is embryonic lethal [380], liver-specific *Hnf4a*$^{-/-}$ demonstrate decreased plasma triglyceride and cholesterol levels with an increase in plasma bile salts [381]. Furthermore, it was proposed the observed hypotriglyceridemia resulted from decreased apolipoprotein B expression. Moreover, Hnf4a has known cross-talk with several nuclear receptors [382]. Fxr and Hnf4a may act as agonists or antagonists toward each other's activity maintaining cellular homeostasis in either a cooperative or obstructive manner. The regulation patterning of *Hnf4a* aligns with our current model. We observed an increase of *Hnf4a* with apolipoprotein expression due to UFP exposure with crosstalk namely through *Fxr* and *Lxr*. It is known that increased apolipoprotein B is associated with the beginning of atherosclerotic events [383]. Lipid metabolism is increased in pre-eclampsia shifting the balance of lipid removal mechanisms [384]. Therefore, exposure to UFPs could be associated with increased risk of pre-eclampsia and other adverse perinatal outcomes through antioxidant, inflammatory, and lipid transportation/metabolism pathways. One limitation of our study is sequencing of whole placental tissue, which includes numerous cell types. Therefore, data should be interpreted in this context and future studies applying single cell sequencing may shed light on the role of cellular alterations in response to UFPs.

The sex-specific effects observed in our model correspond with other studies showing differential male and female placental responses following prenatal exposures

[385]. For instance, a model employing maternal high-fat, high-cholesterol diet led to differentially expressed lipid pathway genes in placentae of females compared with males [386]. LXR expression was more abundant in female placentas. Likewise, Braun et al. demonstrated while male offspring were severely impacted by prenatal inflammatory insult, females exhibited a unique set of placental vulnerabilities and developmental consequences not present in males [387]. Despite observed differences, the exact mechanisms associated with sexual dimorphism requires additional insight, which recent studies are beginning to address using multiple -omics techniques. For example, using a metabolomics approach, Saoi et al. highlighted sex-specific differences in normal C57Bl/6J placental mitochondrial function that may differentially protect fetuses against oxidative stress [388].

In summary, our work demonstrates that UFP exposure during gestation affects the placental weight, fetal crown to rump length, placental maternal lacunae, and fetal vessel size in a sexual dimorphic manner. Additionally, RNA sequencing reveals multiple placental signaling pathways mainly affecting lipid metabolism through *Fxr/Lxr* and *Hnf4a* activation.

2.6. Figures

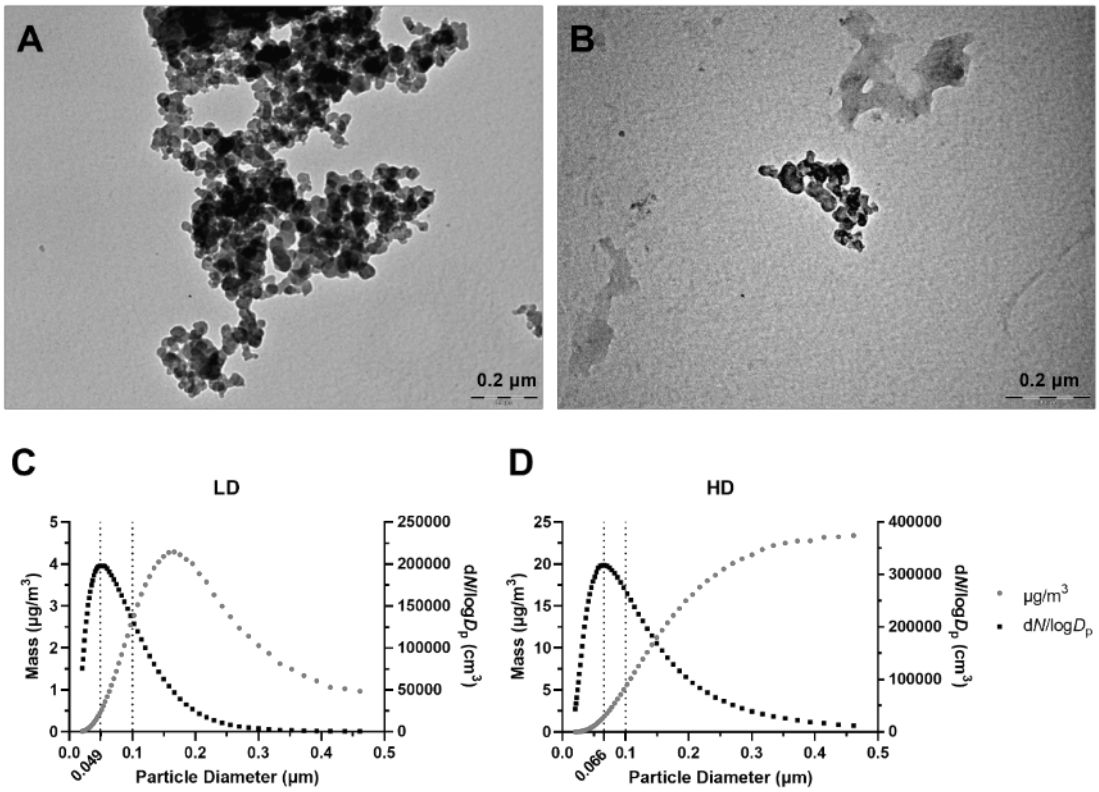

Figure 2.1 Ultrafine particle characterization with size and concentration distribution.

(A) TEM of the pre-atomized PM solution. (B) TEM of post-atomized PM solution. Scale 0.2 µm = 200 nm. (C) Low dose (LD) PM particle size (black) and concentration (gray) distribution, with the peak particle diameter of 0.049 µm (49 nm). (D) High dose (HD) PM particle size (black) and concentration (gray) distribution, with the peak particle diameter of 0.066 µm (66 nm).

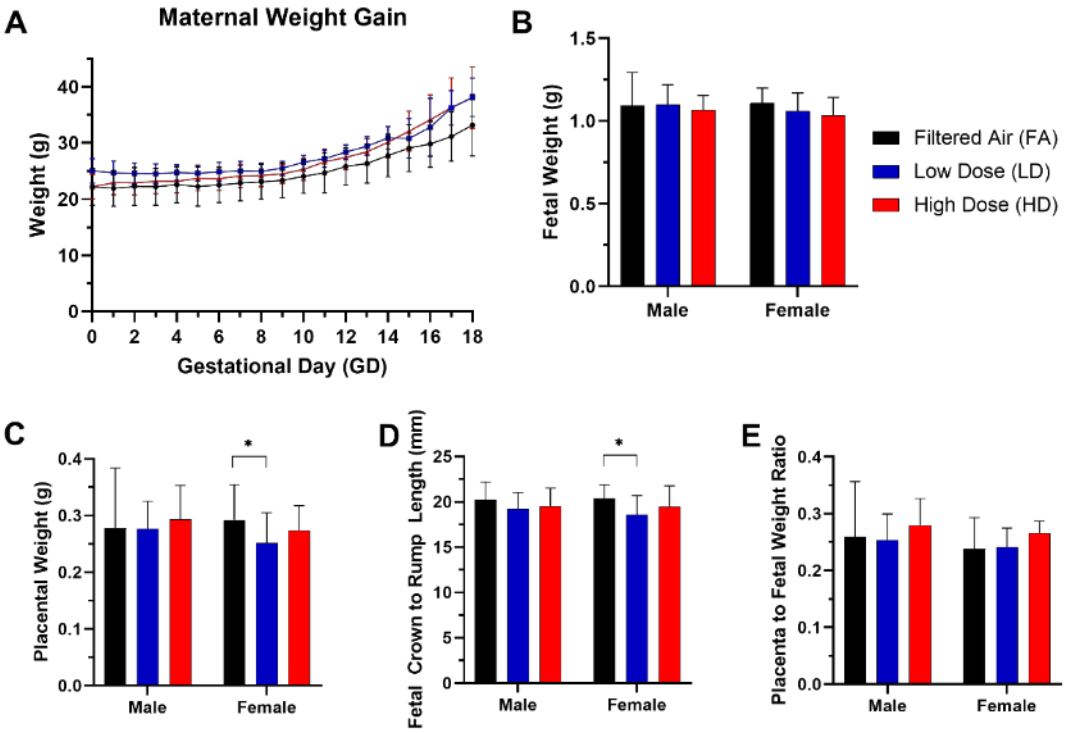

Figure 2.2 Gestational exposure to UFPs impacts fetal development.

(A) Average maternal weight gain ± SD across exposure groups. Groups include filtered air (FA) control (n= 6; black line), low dose (n=6; LD) 100 µg/m3 (blue line), and high dose (n=5; HD) 500 µg/m3 (red line). No significant differences were observed across groups. (B) Fetal weights at GD 18.5 averaged by sex did not differ significantly across exposure groups. (C) Average placental weights at GD 18.5 show a significant decrease in the LD female group compared to FA control. (D) Average crown to rump lengths at GD 18.5 also show a decrease in the LD female group versus FA control. (E) Placenta to fetal weight ratios at GD 18.5 did not vary significantly across exposure groups. Offspring sample sizes include FA male (n = 13), LD male (n = 22), HD male (n = 20), FA female (n = 18), LD female (n = 25), and HD female (n = 24). Error bars represent SD. Data

analyzed separately by sex using one-way ANOVA with Dunnett's multiple comparison test. *p<0.05.

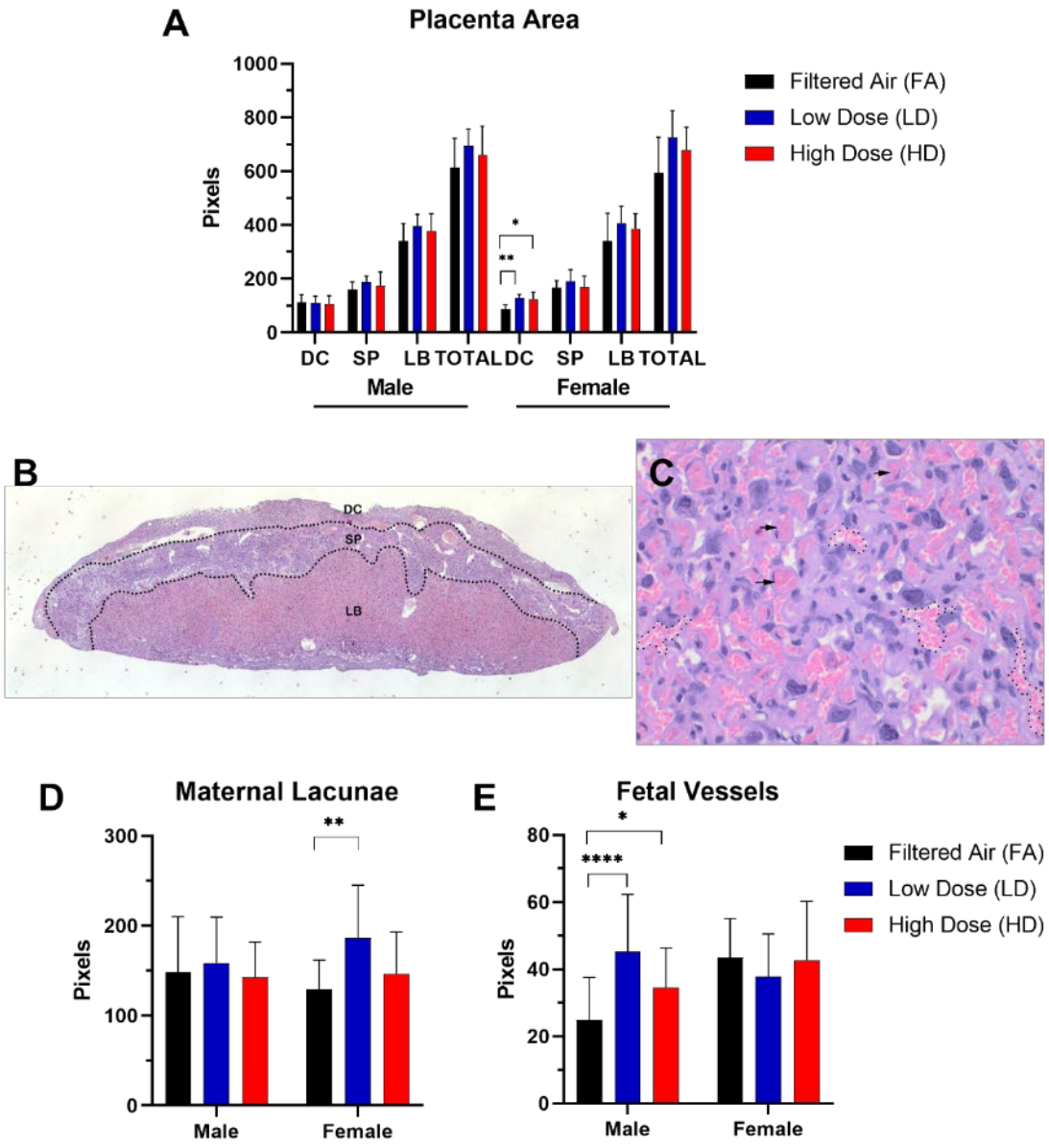

Figure 2.3 Gestational exposure to UFPs alters placenta morphology.

(A) Individual (DC, decidua, SP, spongiotrophoblast, and LB, labyrinth) and total area of placenta layers within each exposure group by offspring sex at GD 18.5. Average female decidua area was significantly greater in the LD and HD groups vs. FA control. (B) Representative H&E-stained GD 18.5 placenta showing separation by layers. (C) Representative H&E-stained GD 18.5 placenta highlighting the labyrinth zone (40x). Arrows indicate fetal vessels while dotted outlines indicate maternal lacunae. (D) Mean area of maternal lacunae show increase in the female LD group compared to FA control. (E) Mean area of fetal blood vessels was significantly greater in the male LD and HD groups vs. FA control. Error bars represent SD. Data analyzed separately by sex using one-way ANOVA with Dunnett's multiple comparison test. *$p<0.05$; **$p<0.01$; ****$p<0.0001$.

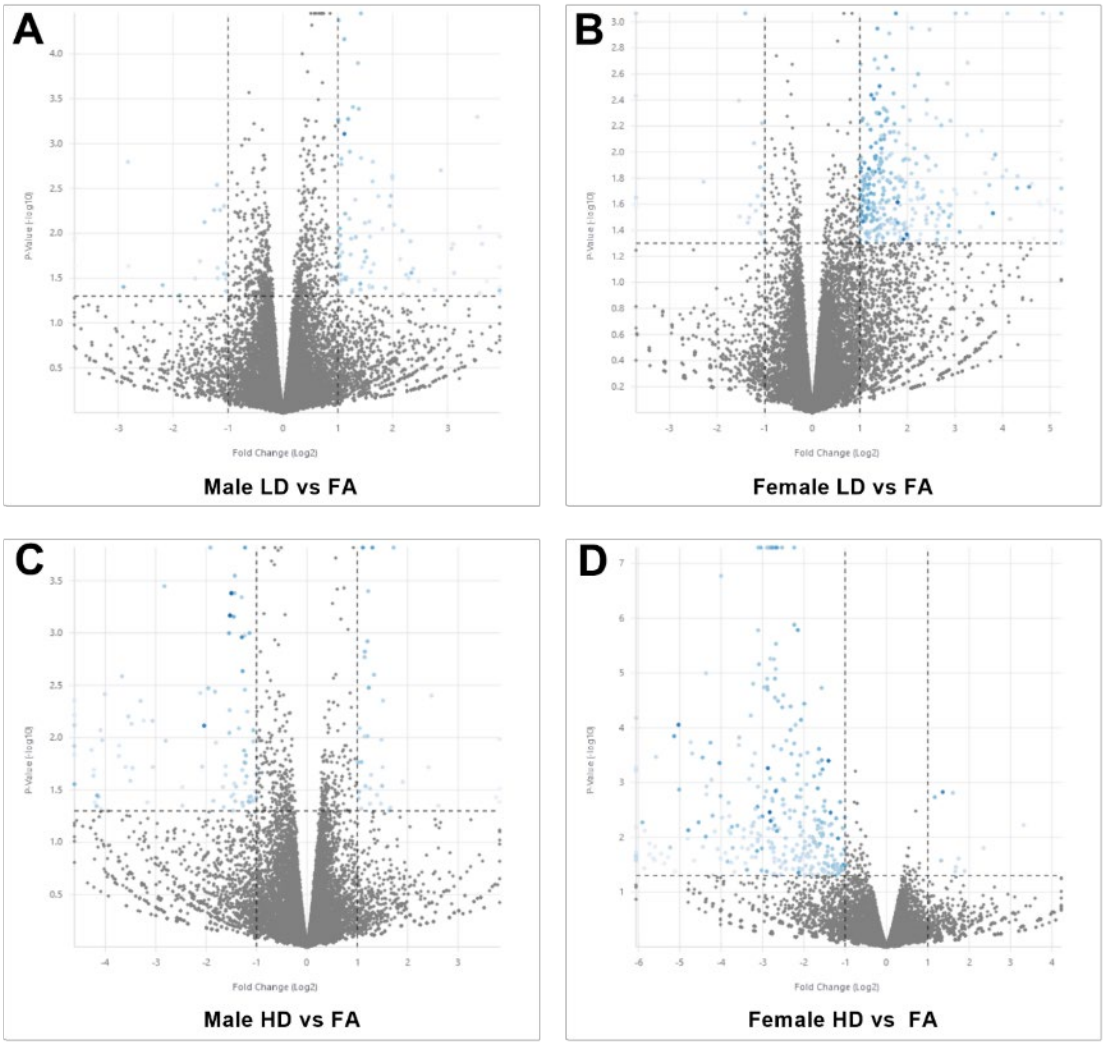

Figure 2.4 Volcano plots identifying differentially expressed genes in placenta in response to UFP exposure.

Each dot represents an individual gene that each display variance in respect to p value and fold change. The four plots indicate the exposure groups by sex, including (A) Male LD vs. FA, (B) Female LD vs. FA, (C) Male HD vs. FA, and (D) Female HD vs. FA.

Figure 2.5 Top canonical pathways as identified by ingenuity pathways analysis (IPA).

The four plots indicate the exposure groups by sex, including (A) Male LD vs. FA, (B) Female LD vs. FA, (C) Male HD vs. FA, and (D) Female HD vs. FA.

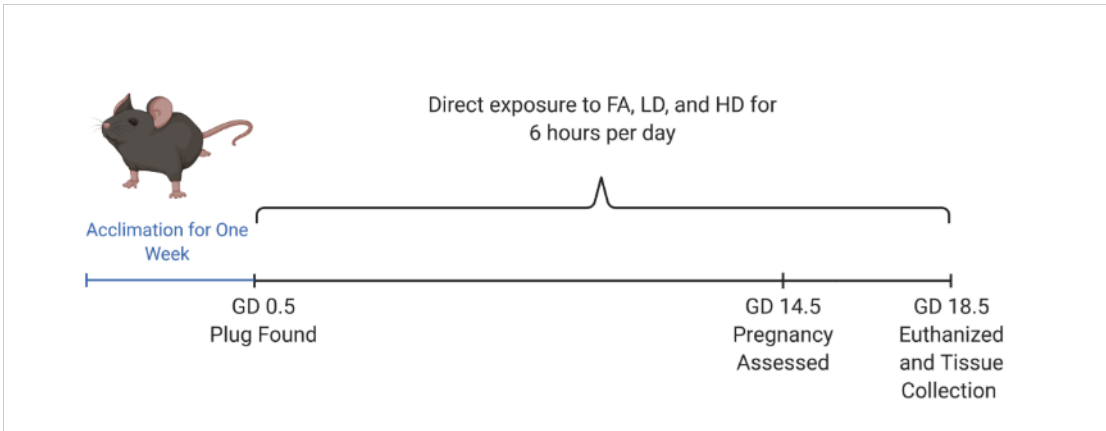

Figure 2.6 Illustration indicating exposure timeline.

Each dam had a one-week acclimation period to exposure system (without PM) before time-mating. Upon the presence of plug or vaginal cytology with sperm (termed GD 0.5), dams were randomized into an exposure group and exposed throughout gestation until GD 18.5. Created with BioRender.com.

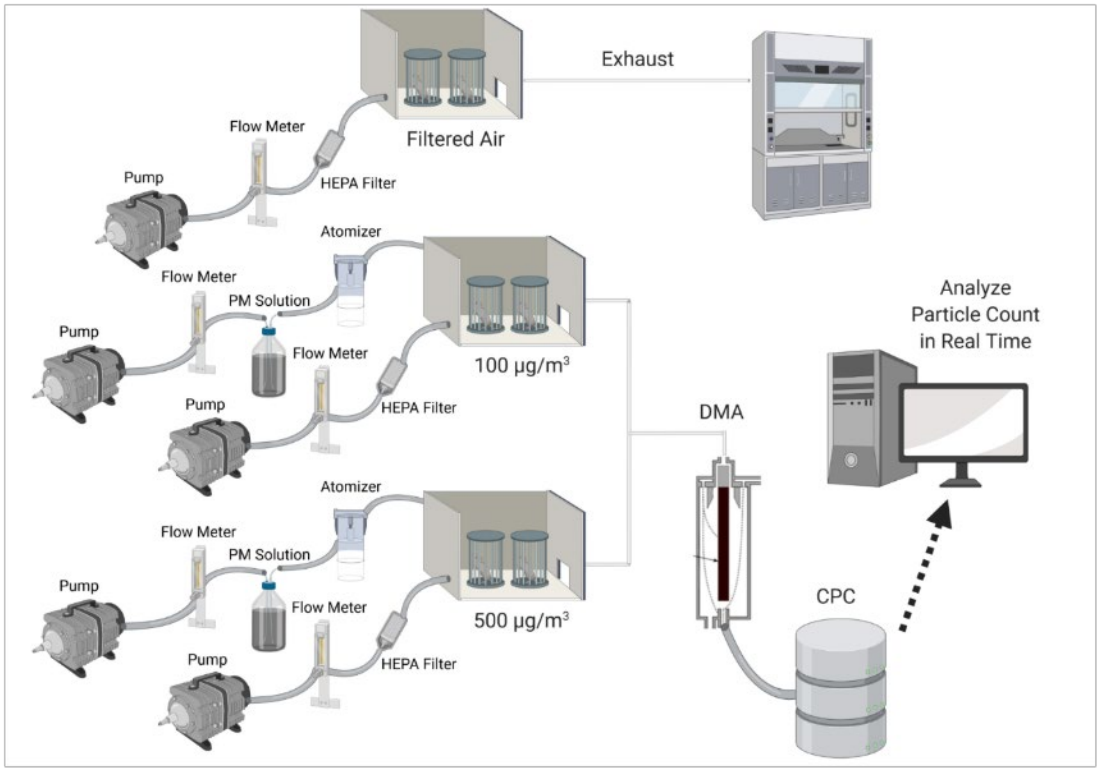

Figure 2.7 Illustration depicting exposure system design and setup.

Three chambers with individually housed pregnant dams were separated into filtered air (FA), low dose (LD, 100 µg/m^3), or high dose (HD, 500 µg/m^3). Each had a HEPA filtered air pump where the LD and HD chambers had an additional PM solution pump. Real-time mass concentration analysis was performed using a tandem differential mobility analyzer (DMA) and condensation particle counter (CPC) to ensure consistent particle concentrations within chambers throughout the exposure duration. Created with BioRender.com.

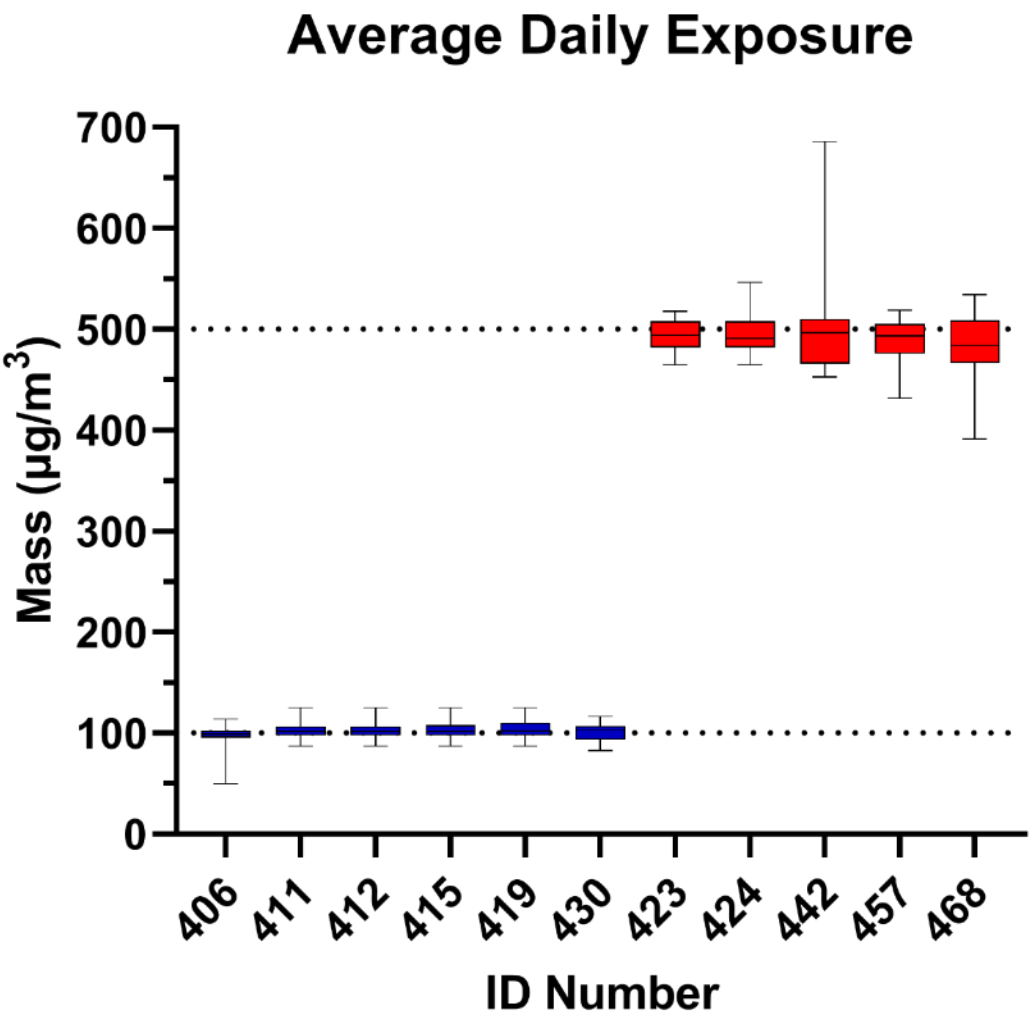

Figure 2.8 Individual dams shown by ID number with corresponding average daily PM mass concentrations ± SD from GD 0.5 to 18.5.

The overall average mass concentration for the low dose (LD) group shown in blue (n=6 dams) was 101.40 ± 10.08. The overall average mass concentration for the high dose (HD) group was slightly more variable with 492.47 ± 33.14 as indicated in red (n=5 dams).

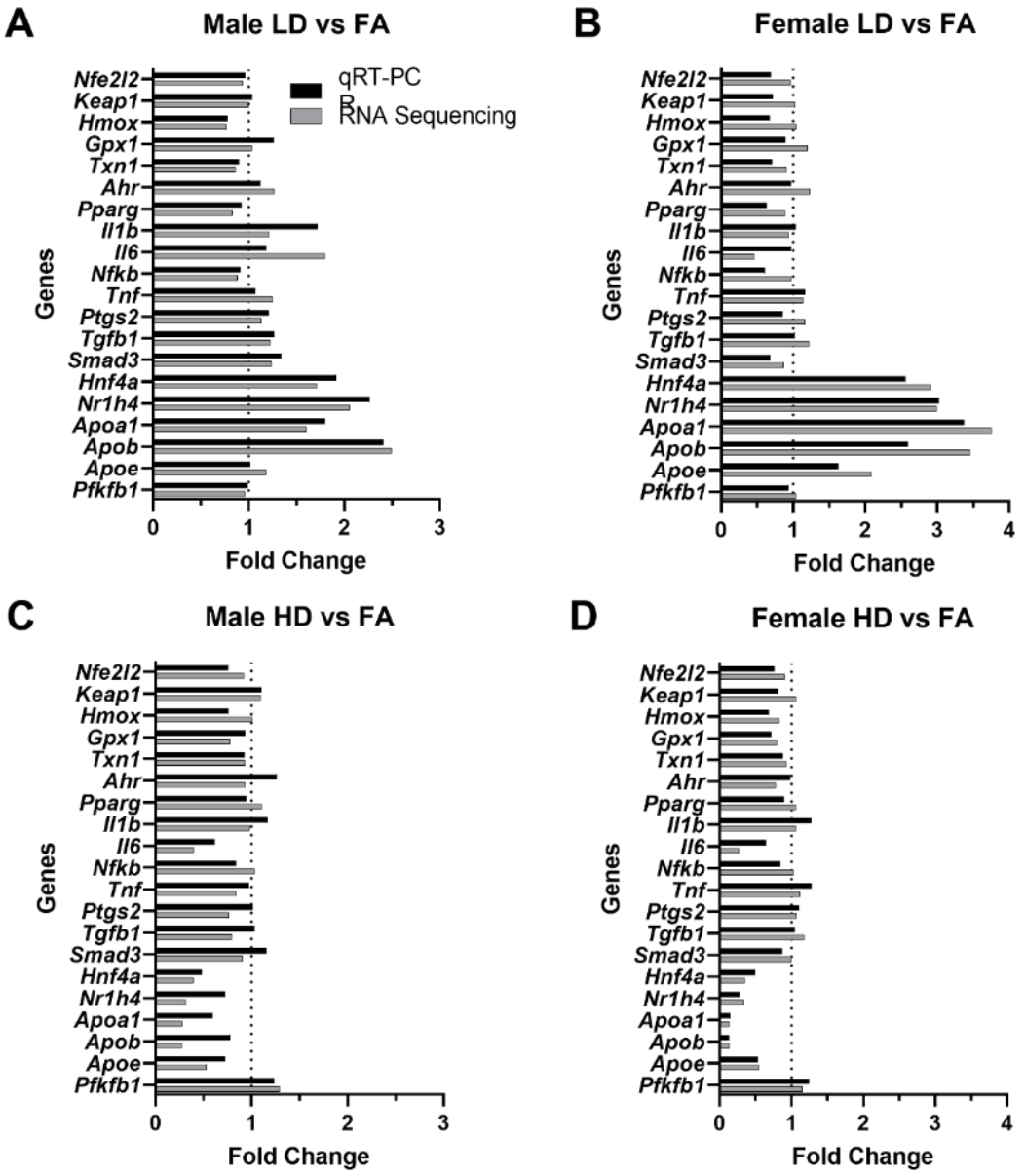

Figure 2.9 qRT-PCR validation of RNA sequencing gene expression data.

Twenty differentially expressed genes were validated by qRT-PCR compared to RNA sequencing analysis. Gene expression data show a high degree of similarity. X-axis indicates fold change and Y-axis illustrates gene symbols. Black bars represent qRT-PCR

while grey counterpart depict RNA sequencing fold change. The four plots indicate the exposure groups by sex, including (A) Male LD vs. FA, (B) Female LD vs. FA, (C) Male HD vs. FA, and (D) Female HD vs. FA.

Table 2.1 List of primer sequences 5' to 3'.

Gene	Forward Sequence (5' → 3')	Reverse Sequence (5' → 3')	T_m (°C)
Nfe2l2	CTTTAGTCAGCGACAGAAGGAC	AGGCATCTTGTTTGGGAATGTG	59.09
Keap1	TCGAAGGCATCCACCCTAAG	CTCGAACCACGCTGTCAATCT	59.92
Hmox	ATGGCGTCACTTCGTCAGAG	AAGCTGAGAGTGAGGACCCA	60.15
Gpx1	CAGTCCACCGTGTATGCCTT	TTGCCATTCTGGTGTCCGAA	59.97
Txn1	GCTTGTCGTGGTGGACTTCT	AACTCCCCCACCTTTTGACC	60.03
Ahr	TGTGCAGAATCCCACATCCG	AATCAAGCGTGCATTGGACTG	60.10
Pparg	GGAAGACCACTCGCATTCCTT	GTAATCAGCAACCATTGGGTCA	59.63
Il1b	GCCACCTTTTGACAGTGATGAG	AAGGTCCACGGGAAAGACAC	59.83
Il6	ACGATGATGCACTTGCAGAAAA	GGAAATTGGGGTAGGAAGGACT	59.44
Nfkb1	GAAATTCCTGATCCAGACAAAAAC	ATCACTTCAATGGCCTCTGTGTAG	58.68
Tnf	CCCACGTCGTAGCAAACCA	GGCAGAGAGGAGGTTGACTT	59.66
Ptgs2	TGCTGGTGGAAAAACCTCGT	AAAACCCACTTCGCCTCCAA	60.11
Tgfb1	CAAGGGCTACCATGCCAACT	GTACTGTGTGTCCAGGCTCCAA	61.26
Smad3	CACGCAGAACGTGAACACC	GGCAGTAGATAACGTGAGGGA	59.35
Hnf4a	GGTTTAGCCGACAATGTGTGG	TCCCGCTCATTTTGGACAGC	60.38
Nr1h4	GCTTGATGTGCTACAAAAGCTG	CGTGGTGATGGTTGAATGTCC	59.15
Apoa1	GCTCAAGAGCAACCCTACCTT	GCTTTCTCGCCAAGTGTCTTC	59.90
Apob	AAGCACCTCCGAAAGTACGTG	CTCCAGCTCTACCTTACAGTTGA	59.92
Apoe	GACCCAGCAAATACGCCTG	CATGTCTTCCACTATTGGCTCG	59.02
Pfkfb1	GAAGGTCACGTTGCGGTTTTT	GCCGAGTTTCACTTGCTTGAT	59.81

Table 2.2 List of differentially expressed genes in placenta in response to UFP exposure.

The top 10 differentially expressed genes as identified by RNA sequencing are shown for each exposure group by sex.

Male LDvsFA

Gene Symbol	Gene Name	Log2Fold Change	P-Value
Ano5	anoctamin 5	4.52	1.09E-02
Gm10220	predicted gene 10220	4.27	3.97E-02
Cyp4a14	cytochrome P450, family 4, subfamily a, polypeptide 14	4.26	4.03E-02
Calm5	calmodulin 5	4.18	4.69E-02
Fads2b	fatty acid desaturase 2B	4.16	2.37E-02
Oxtr	oxytocin receptor	4.15	4.34E-02
Fbxo40	F-box protein 40	3.71	3.43E-02
Wfdc18	WAP four-disulfide core domain 18	3.63	1.32E-02
Fut4-ps1	fucosyltransferase 4, pseudogene 1	3.59	4.60E-02
Krt83	keratin 83	3.59	8.49E-03

Male HDvsFA

Gene Symbol	Gene Name	Log2Fold Change	P-Value
4931406H21Rik	RIKEN cDNA 4931406H21 gene	3.34	2.00E-02
Pzp	PZP, alpha-2-macroglobulin like	3.29	1.32E-02
Pak5 Pak7	p21 (RAC1) activated kinase 5	2.37	3.02E-02
Rgn	regucalcin	1.66	3.75E-02
Dazl	deleted in azoospermia-like	1.57	5.09E-03
9030625G05Rik	RIKEN cDNA 9030625G05 gene	1.54	4.89E-02
Ccdc172	coiled-coil domain containing 172	1.33	2.18E-02
Rd3	retinal degeneration 3	1.21	2.57E-02
Lrrc38	leucine rich repeat containing 38	1.07	4.40E-03
Tcf15	transcription factor 15	1.05	2.34E-02

Female LDvsFA

Gene Symbol	Gene Name	Log2Fold Change	P-Value
Cfd	complement factor D	10.34	1.90E-02
Cyp2e1	cytochrome P450, family 2, subfamily e, polypeptide 1	6.57	4.03E-02
Slc16a14	solute carrier family 16 (monocarboxylic acid transporters), member 14	6.11	2.90E-02
Sprr2a1	small proline-rich protein 2A1	5.72	5.78E-03
Sprr2a2	small proline-rich protein 2A2	5.72	5.78E-03
Ptpn5	protein tyrosine phosphatase, non-receptor type	5.57	6.14E-05
Serpina3k	serine (or cysteine) peptidase inhibitor, clade A, member 3K	5.24	4.97E-02
2010016I18Rik	RIKEN cDNA 2010016I18 gene	5.24	1.14E-02
Tceg1l	transcription elongation regulator 1-like	5.09	2.75E-02
Magea3	MAGE family member A3	4.97	2.34E-02

Female HDvsFA

Gene Symbol	Gene Name	Log2Fold Change	P-Value
Efhc2	EF-hand domain (C-terminal) containing 2	3.32	6.00E-03
Snora52	small nucleolar RNA, H/ACA box 52	2.34	1.57E-02
Sult6b2	sulfotransferase family 6B, member 2	1.89	4.14E-02
Ngf	nerve growth factor	1.74	2.44E-02
Mir27a	microRNA 27a	1.68	3.50E-02
Cldn18	claudin 18	1.66	4.19E-02
Ctse	claudin 18	1.60	1.54E-03
Tfrc	transferrin receptor	1.36	1.49E-03
Klk7	kallikrein related-peptidase 7	1.32	2.66E-02
Klk4	kallikrein related-peptidase 4	1.17	1.85E-03

3. ROLE OF NRF2 IN PLACENTAL INFLAMMATION AND BILE ACID METABOLISM DYSREGULATION FOLLOWING GESTATIONAL EXPOSURE TO ULTRAFINE PARTICLES*

3.1. Overview

Exposure to ultrafine particles (UFPs, $PM_{0.1}$) during pregnancy triggers placental oxidative stress and inflammation, similar to fine PM ($PM_{2.5}$). The *Nrf2* gene encodes a redox-sensitive transcription factor that is a major regulator of antioxidant and anti-inflammatory responses. Disruption of NRF2 is known to substantially enhance $PM_{2.5}$-driven oxidant and inflammatory responses; however, specific responses to UFP exposure, especially during critical windows of susceptibility such as pregnancy, are not fully characterized; To investigate the role of NRF2 in regulating maternal antioxidant defenses and placental responses to UFP exposure, wildtype (WT) and *Nrf2*$^{-/-}$ pregnant mice were exposed to either low dose (LD, 100 μg/m^3) or high dose (HD, 500 μg/m^3) UFP mixture or filtered air (FA, control) throughout gestation; *Nrf2*$^{-/-}$ HD-exposed female offspring exhibited significantly reduced fetal and placental weights. Placental morphology changes appeared most pronounced in *Nrf2*$^{-/-}$ LD-exposed offspring of both sexes. Glutathione (GSH) redox analysis revealed significant increases in the GSH/GSSG ratio (reduced/oxidized) in WT female placental tissue exposed to HD in comparison with

---

*Reprinted with permission from Behlen JC, Lau CH, Pendleton D, Li Y, Hoffmann AR, Golding MC, Zhang R, Johnson NM. *Antioxidants (Basel)*. 2022 Feb 10;11(2):352. doi: 10.3390/antiox11020352.

Nrf2$^{-/-}$ HD-exposed mice. The expression of inflammatory cytokine genes (*Il1β, Tnfα*) was significantly increased in *Nrf2*$^{-/-}$ placentas from male and female offspring across all exposure groups. Genes related to bile acid metabolism and transport were differentially altered in *Nrf2*$^{-/-}$ mice across sex and exposure groups. Notably, the group with the most marked phenotypic effects (*Nrf2*$^{-/-}$ HD-exposed females) corresponded to significantly higher placental *Apoa1 and Apob* expression suggesting a link between placental lipid transport and NRF2 in response to high dose UFP exposure; Disruption of NRF2 exacerbates adverse developmental outcomes in response to high dose UFP exposure in female offspring. Morphological effects in placenta from male and female offspring exposed to low dose UFPs also signify the importance of NRF2 in maternal–fetal response to UFPs.

3.2. Introduction

Ambient particulate matter (PM) represents a significant hazardous element of air pollution [2]. PM is classified as coarse (PM_{10}), fine ($PM_{2.5}$), and ultrafine particles (UFPs; $PM_{0.1}$) based on their size [315, 317, 389]. The fine and ultrafine fractions can penetrate deeper in the airways in comparison with coarse particles, leading to numerous adverse health effects, particularly when exposure occurs during periods of rapid growth and development, such as the prenatal period [359]. Evidence from epidemiological studies links PM exposure, mainly $PM_{2.5}$, during pregnancy with several adverse perinatal outcomes, including preterm birth, infant low birth weight, and placental growth [291, 293, 294, 359, 390-392].

The placenta is a transient reproductive organ serving as the interface between mother and fetus. There are several functions for the placenta, including nutrient, gas, and waste exchange, which are critical for proper intrauterine growth and development [162-164]. Improper placental function can lead to adverse perinatal outcomes [357]. PM exposure affects placental function in many ways, mainly through maternal systemic and placental oxidative stress and inflammation [121]. Additionally, findings from animal exposure models, ex vivo human placental models, and evidence from human placentae demonstrate UFPs can translocate across the placenta, indicating direct exposure [71-73, 133]. For instance, Wick et al. demonstrated the size-dependent transport of fluorescently labeled particles with diameters of 50, 80, and 240 nm (but not 500 nm) across human placental explants into the fetal circuit [72]. Evidence is emerging on the maternal and fetal-health-related effects specific to UFPs (<100 nm).

UFPs typically exist in high concentrations from traffic sources because of direct emissions and new particle formation [355, 393]. Emerging results from our in vivo models demonstrate that UFPs represent an important toxic component driving adverse pregnancy and neonatal pulmonary health outcomes [55, 316]. Findings from our research also show that gestational exposure to UFPs alters placental morphology and signaling pathways related to lipid processing, particularly in female offspring [394]. Additionally, other mouse models demonstrate the role of placental oxidative stress in adverse outcomes. For instance, Morales-Rubio et al. verified that gestational UFP exposure increased intrauterine inflammation and oxidative damage, displayed by increased 8-OHdG in mouse placentae [126]. Wang et al. [134] showed increased plasma 8-

isoprostane levels, a marker of oxidative stress, in pregnant mice exposed to UFPs. In that model, offspring pulmonary immune maturation was inhibited, playing a role in neonatal respiratory infection risk [322]. Interestingly, findings from a birth cohort study demonstrating increased susceptibility of lower respiratory tract infections in infants prenatally exposed to $PM_{2.5}$ was significantly modified by polymorphisms in the maternal *Nrf2* gene [395].

Nuclear factor E2-related factor 2 (NRF2) is a transcription factor central in response to oxidative stress [93, 106]. Under oxidative stress conditions, reactive oxygen species (ROS) promote the dissociation of NRF2 from its repressor protein KEAP1, which typically keeps NRF2 tethered to a ubiquitin ligase complex for degradation [396]. Disassociation from KEAP1 allows NRF2 cytoplasmic accumulation and subsequent binding to antioxidant response elements (AREs) for the transcription of numerous downstream genes. NRF2 binding regulates antioxidant genes such as NAD(P)H quinone oxidoreductase 1 (*Nqo1*), heme-oxygenase 1 (*Ho-1*), superoxide dismutase (*Sod*), catalase (*Cat*), and glutathione peroxidase 1 (*Gpx-1*) [397]. Disruption of NRF2 has been shown to enhance disease susceptibility following a wide range of environmental exposures, including allergic airway inflammatory responses induced by chronic exposure to diesel exhaust PM in an adult mouse model [398]. To date, results from gestational PM exposure models, and specific responses to UFPs relevant to placental and fetal effects are lacking. Therefore, in this study, we investigated the role of NRF2 in maternal systemic and placental responses to gestational UFP exposure. We employed a knockout model

(*Nrf2*$^{-/-}$) in our established gestational UFP inhalation model [55, 394] to further elucidate the underlying mechanisms of UFP toxicity related to developmental endpoints.

3.3. Materials and Methods

3.3.1. Animals and Ultrafine Particle Exposure

All procedures were approved by the Institutional Animal Care and Use Committee of Texas A&M University #2019-0025. *Nrf2*-deficient mice (*Nrf2*$^{-/-}$) on C57Bl/6J background were obtained from Dr. Tom Kensler. Genotyping for homozygous wildtype (*Nrf2*$^{+/+}$) and null (*Nrf2*$^{-/-}$) mice was carried out as previously described [399] (details in supplemental information). Mice were kept under standard housing conditions including 12 h light–dark cycle, 22–24 °C, and 40–60% humidity. Standard 19% protein extruded rodent chow (Teklad Global Diets) and water were given ad libitum, except during exposure timeframes.

To study the role of NRF2 in response to gestational UFP exposure, 8- to 10-week-old female mice were acclimated to filtered air for one-week in exposure chambers. Following acclimation, time-mating, and identification of a vaginal plug, termed gestational day (GD 0.5), wildtype (WT) and *Nrf2*$^{-/-}$ pregnant mice were randomly assigned to filtered air (FA) control, low dose (LD; 100 μg/m^3), or high dose (HD; 500 μg/m^3) UFP. Particle generation and gestational exposures were conducted as previously described [394]. Gestational exposures occurred for 6 h daily from GD 0.5 to 18.5. Average exposures for LD (100 μg/m^3) and HD (500 μg/m^3) equated to a 24 h average of 25 and 125 μg/m^3, respectively (Figure 3.8). UFP peak diameter ranged from 71 to 79 nm. Following exposure on GD 18.5, dams were euthanized, and maternal tissues collected

and processed. Sex-separated placental and fetal tissues were collected using a dissecting microscope and pooled per litter. Illustration of exposure timeline shown in Figure 3.9.

3.3.2. Sample Collection and Processing

Post-euthanasia, tissues utilized for histological assessment were fixed in 10% neutral buffered formalin for 24–48 h. Following, tissues were stored in 70% ethanol until trimming, processing, and paraffin embedding. Serial 5 μm cross-sections were obtained where every first and fifth slide were used for hematoxylin and eosin (H&E) staining as observed in Figures 3.2 and 3.3. Histological analysis [363] of blinded slides was performed by a board-certified veterinary anatomic pathologist using an Olympus BX53 microscope with an Olympus SC180 camera operating Olympus cellSens 2.3 software. Placenta area of the decidua, spongiotrophoblast, and labyrinth zones were calculated via pixels. For each H&E-stained section, approximately ten 40X random labyrinth zone images were captured to measure fetal vessels and maternal lacunae.

Additionally, tissues were snap-frozen in liquid nitrogen and stored in −80 °C until analysis. Blood and placental collection for redox determination followed Jones and Liang [91]. Briefly, whole blood was added to a borate buffer stock solution containing γ-glutamylglutamate (γ-GluGlut) as an internal standard and centrifuged. The supernatant was transferred to a perchloric/boric acid solution and snap frozen. Samples were thawed and centrifuged to precipitate proteins in preparation for high performance liquid chromatography (HPLC) analysis. Potassium hydroxide/tetraborate solution was used to adjust the pH to 9.0. Dansyl chloride solution was added and placed in the dark for 20–24 h. Finally, chloroform was added, and the perchlorate/chloroform layer was centrifuged

where the upper (aqueous) layer was transferred and frozen at −80 °C. Placental tissue homogenates bypassed the first step of borate buffer stock solution and were directly added to the perchloric/boric acid solution. Subsequent processing and analysis steps were the same.

3.3.3. HPLC Run Conditions, Protocol, and Redox Analysis

HPLC run conditions and redox analysis followed Jones and Liang with slight modifications [91]. Briefly, thawed derivatized samples were centrifuged before transfer and 35 µL injection into an UltiMate 3000 HPLC (Thermo Fisher Scientific) autosampler onto a SUPELCOSIL™ LC-NH2 HPLC Column (Supelco 5µm, 4.6 mm × 250 mm) at 35 °C. Fluorescence excitation and emission detection were set at 335.0 and 515.0, respectively, including 48 °C constant temperature. HPLC mobile phases included solvent A (80% v/v methanol/water) and solvent B (acetate-buffered methanol). Flow rate was kept constant at 1 mL per min. Typical mobile phase gradients were as follows: initial conditions of 80% A, 20% B for 10 min; linear gradient change from 10 min to 30 min to 20% A, 80% B; from 35 to 38 min, linear gradient returned to 80% A, 20% B and held until 42 min total run. Approximate elution time frames of compounds of interest were as follows: cystine (CySS) from 9 to 9.5 min; cysteine (Cys) from 10 to 10.5 min; γ-GluGlut from 12 to 13 min; glutathione (GSH) from 19 to 19.5; and glutathione disulfide (GSSG) from 23.5 to 24 min.

3.3.4. RNA Isolation and qRT-PCR

TRIzol reagent was used to extract total RNA from sex-separated, pooled GD 18.5 placentas according to manufacturer's instructions (Invitrogen, Thermo Fisher Scientific).

RNA quantity and purity were assessed using a Nanodrop Spectrophotometer/Fluorometer (DeNovix DS-11 FX+ V3.35) with 260/280 absorbance values ≥1.8. Total RNA was then reverse transcribed into cDNA using Qiagen QuantiTect® Reverse Transcription kit (Cat # 205311). Quantitative real-time PCR was performed with Applied Biosystems™ Power SYBR™ Green PCR Master Mix (Cat # 4367659) on a Roche LightCycler® 96. The reaction conditions were as follows: 50 °C for 2 min; 95 °C for 10 min; and 45 cycles of 94 °C for 15 sec, 60 °C for 30 sec, and 72 °C for 30 sec. Gene transcription levels were analyzed using $2^{-\Delta\Delta CT}$ method. *Gapdh* was used as the reference gene. Primer sequences are in Table S1.

3.3.5. Statistics

All statistical analyses were performed using GraphPad Prism (V 9.2.0) and expressed using mean ± SD. Phenotypic analyses among groups were tested using two-way analysis of variance (ANOVA) with Tukey's multiple comparisons test. Tests were considered statistically significant with a p value < 0.05.

3.4. Results

3.4.1. Exposure and Particulate Matter Characterization

Our whole-body inhalation exposure system was designed to mimic representative urban UFPs, composed of ammonium sulfate, ammonium nitrate, diesel soot (NIST, SRM 2975), and potassium chloride [55]. A dose response to 6 h daily exposure to 100 and 500 $\mu g/m^3$ UFPs was previously employed by Behlen et al. [394]. This system utilized a differential mobility analyzer coupled with a condensation particle counter, which allowed us to control PM mass concentration in real-time, yielding stable concentrations inside

exposure chambers. Figure 3.8A depicts the average daily exposure by mouse identification number. The randomly assigned pregnant mice were separated into three exposure groups within each genotype: FA, LD, or HD. The average PM mass concentration over the entire exposure time course was 98.14 ± 13.24 (mean ± SD) and 497.68 ± 34.77 μg/m^3 for LD and HD chambers, respectively. Particle diameters ranged from 0.02 μm to 0.5 μm with 0.071 and 0.079 μm (71 and 79 nm) peak particle diameters for LD and HD chambers, respectively, over the course of gestational exposures (Figure 3.8C-D). Maternal weight gain was tracked for individual dams, and is shown in Figure 3.8B for dams with viable pregnancies on GD18.5. These include wildtype (WT) filtered air (FA) control (n= 6), WT low dose (LD) (n = 6), WT high dose (HD) (n = 5), *Nrf2*$^{-/-}$ FA (n = 3), *Nrf2*$^{-/-}$ LD (n = 3), and *Nrf2*$^{-/-}$ HD (n = 5). There were no significant differences in average maternal weight across groups throughout the gestational exposure.

3.4.2. Phenotypic Outcomes Highlight Fetal Weight Impact in Nrf2$^{-/-}$ female HD-Exposed Offspring

Following exposure on GD 18.5, sex-separated placental and fetal tissues were collected, and phenotypic outcomes assessed. Significant decreases were observed in placental weight in the *Nrf2*$^{-/-}$ mice exposed to HD, in comparison with the WT FA group (Figure 3.1A). The average fetal weight in female *Nrf2*$^{-/-}$ offspring was significantly decreased in comparison with the WT FA group and the matched WT HD group (Figure 3.1B). Interestingly, the only difference noted in fetal crown to rump lengths was in the WT female LD-exposed group (Figure 3.1C). Offspring sample sizes range from 12–25 per group, collected from 3–6 dams (as indicated in Figure 3.8 and Figure 3.1 legends).

3.4.3. Histological Analysis of Placental Tissues Show Impact in Nrf2$^{-/-}$ male and female LD-Exposed Offspring

Representative placental images are shown for placentas collected from male (Figure 3.2) and female (Figure 3.3) offspring in wildtype (WT) and *Nrf2*$^{-/-}$ mice exposed to FA, LD, and HD. No gross histological changes were observed across the different groups. Differences between area measurements within different layers of the placenta (decidua, spongiotrophoblast, and labyrinth zones), as well as diameters for the maternal and fetal blood vessels were observed across the different groups (Figure 3.4). Area measurements for the decidua were significantly reduced in female *Nrf2*$^{-/-}$ offspring exposed to LD (4A). For the spongiotrophoblast (4B) and labyrinth (4C) regions, areas were significantly reduced in both male and female *Nrf2*$^{-/-}$ offspring exposed to LD. Overall, the total placental areas (4D) were also significantly reduced in these same groups (*Nrf2*$^{-/-}$ LD-exposed male and female offspring). Fetal vessel area measurements revealed differing effects of genotype and exposure in placentae collected from male offspring. Fetal vessel areas were greater in the FA-exposed *Nrf2*$^{-/-}$ group compared with FA-exposed WT, wherein the LD-exposed *Nrf2*$^{-/-}$ group had significantly reduced fetal vessel size as compared with LD-exposed WT (4E). No differences in maternal lacunae sizes were observed between groups (4F).

3.4.4. Oxidative Stress Biomarkers Demonstrate Differential Effect of HD Exposure on GSH and Cys Ratios

Levels of glutathione (GSH), glutathione disulfide (GSSG), cysteine (Cys), and cystine (CySS) were determined in maternal serum and placenta. Average levels for individual species are shown in Table S2. The ratios of reduced/oxidized species are depicted in Figure 3.5. GSH is a critical thiol antioxidant that in reduced form (GSH) can donate an electron to detoxify ROS, thus forming the oxidized form (GSSG). A higher ratio of GSH/GSSG indicates a greater percent of reduced GSH available (i.e., enhanced antioxidant capacity). Overall, the GSH/GSSG ratio for female placentas was significantly higher in the WT group exposed to HD, as compared with the HD-exposed *Nrf2*$^{-/-}$ group (Figure 3.5C). Cys is a precursor to GSH synthesis, which forms CySS under oxidative conditions. Interestingly, the Cys/CySS ratio in maternal serum was significantly higher in HD-exposed *Nrf2*$^{-/-}$ dams in comparison with HD-exposed WT dams (Figure 3.5D).

3.4.5. Placental Gene Expression Emphasizes Role of Genotypes, Exposure and Sex

Expression of several genes related to oxidative stress and inflammatory cytokines were assessed in offspring placentas using quantitative real-time PCR. Expression levels of *Nqo1* (Figure 3.6A) were significantly decreased in *Nrf2*$^{-/-}$ FA- and LD-exposed males and females, as expected. We also evaluated *Ahr* (Figure 3.6B) and found levels were significantly elevated in all *Nrf2*$^{-/-}$ groups, except for male LD. The expression of *Cyp1b1* was significantly increased in FA- and LD-exposed *Nrf2*$^{-/-}$ groups for both male and female Figure 3.6C). Strikingly, the expression of inflammatory cytokines *Il1β* and *Tnfα* (Figure 3.6D and 6F) was significantly increased in all *Nrf2*$^{-/-}$ groups, excluding the female HD group for *Il1β*. *Il6* (Figure 3.6E) did not demonstrate any significant changes among groups.

In our recent work, RNA sequencing of whole placental tissues collected from WT mice exposed to FA, LD, or HD, revealed altered bile acid metabolism [394]. These changes were sex- and dose-specific, with significantly increased expression of several genes in placenta, including *Tgfβ1*, *Smad3*, *Hnf4α*, *Nr1h4* (Farnesoid X Receptor-FXR), *Apoa1*, and *Apob.* To investigate changes in these genes by genotype within each exposure group, we evaluated expression in placental tissues from WT and *Nrf2*$^{-/-}$ mice exposed to FA, LD, or HD (Figure 3.7). *Tgfβ1* expression was significantly increased in *Nrf2*$^{-/-}$ mice exposed to FA and HD in male and female placentas, in comparison with WT FA and WT HD, respectively (7A). Similarly, significant increases in *Smad3* across all dose groups were observed in *Nrf2*$^{-/-}$ mice for all female groups and FA-exposed *Nrf2*$^{-/-}$ males (7B). Expression of *Hnf4α* was also significantly increased in *Nrf2*$^{-/-}$ mice in FA- and HD-exposed males, as well as HD-exposed females (7C). *Nr1h4* (FXR) expression was significantly reduced in FA- and LD-exposed *Nrf2*$^{-/-}$ females (7D). Expression of *Apoa1* was significantly decreased in female *Nrf2*$^{-/-}$ mice exposed to FA and LD, yet increased in *Nrf2*$^{-/-}$ HD-exposed females (7E). Likewise, *Apob* expression was significantly increased in *Nrf2*$^{-/-}$ HD-exposed females (7D).

3.5. Discussion

Gestational PM exposure is associated with numerous adverse birth outcomes [359]. These include premature birth, fetal growth restriction, and infant low birth weight, all of which are significant risk factors for neonatal morbidity and mortality [291-294, 400]. Although not currently regulated by air quality standards, UFPs may exert enhanced maternal–fetal toxicity due to increased oxidative capacity and their ability to cross the

placental barrier, as evidenced in experimental models and human placentae [71-73, 133]. Findings from experimental models confirm UFP-specific effects on adverse pregnancy outcomes, including reduced gestational length and decreased offspring birth weights and lengths [316, 401].

Our previous gestational UFP inhalation model employing either a low dose (LD, 100 μg/m^3) or high dose (HD, 500 μg/m^3) throughout gestation demonstrated sex- and dose-specific effects on placental morphology and signaling pathways related to lipid metabolism [394]. In that study, a significant decrease in average placental weights and crown-to-rump lengths was observed in female offspring in the LD exposure group. Moreover, transcriptomic analysis indicated several disturbed cellular functions related to lipid metabolism, which were most pronounced in the LD group, especially in female placental tissue. Building from these findings in WT mice, the main objective of this study was to assess the role of *Nrf2* in placental responses to gestational UFP exposure. Accordingly, we exposed WT or *Nrf2*$^{-/-}$ pregnant mice to FA, LD, or HD from GD 0.5 to 18.5. Daily exposure levels were consistently stable. Phenotypic data showed significantly lower fetal crown to rump lengths in WT LD-exposed females, yet placental weights in this group, significantly reduced in our previous model [394], failed to reach statistical significance in this analysis. Our main finding from phenotypic measurements in this study was significantly decreased fetal weights in *Nrf2*$^{-/-}$ HD-exposed female offspring. NRF2 signaling is essential in normal placental development and fetal growth, and dysregulation has been implicated in intrauterine growth restriction, preeclampsia, and preterm birth [402]. Mouse models also demonstrate a role of *Nrf2* in trophoblast function

in normal placentation and angiogenesis [403]. In our model, *Nrf2*$^{-/-}$ mice in the control group, exposed to FA, did not exhibit significantly different phenotypic measures in comparison with the WT FA-exposed group. Likewise, upon challenge with the LD, significant differences were not observed between mice of different genetic backgrounds. The most susceptible group, in terms of effects on fetal weight, was the *Nrf2*$^{-/-}$ female mice exposed to the HD. These findings suggest the inability of mice lacking functional NRF2 to respond to an environmental challenge, but only at a high enough dose. The failure of susceptibly to manifest in reduced fetal lengths in this group is unexpected, as only the female WT, LD-exposed group showed significantly lower fetal lengths. However, this may reflect other measures of growth that influence length and are not directly impacted by UFPs in a linear dose–response mechanism. These nuances in different growth measures require further consideration.

In our previous work, WT mice exposed to UFPs throughout gestation exhibited morphological changes in placenta that varied by sex and dose [394]. An increase in placental decidua area, the outer layer on the maternal side, was observed in placenta from female offspring exposed to LD and HD. In our current investigation, we observed decreased decidua areas placenta from female *Nrf2*$^{-/-}$ offspring exposed to LD. Moreover, in both sexes of *Nrf2*$^{-/-}$ offspring exposed to LD, we observed decreased areas within the spongiotrophoblast and labyrinth layers, intermediary and fetal sides, respectively, as well as overall. These findings suggest placental insufficiency in offspring lacking functional NRF2 largely in both sexes exposed to LD. Indeed, previous studies demonstrate significant reductions in both total and labyrinth volume in placenta of *Nrf2*$^{-/-}$ mice [403].

Collectively, these findings highlight the NRF2 deficient signaling may affect nutrient transfer capacity. Additionally, our data demonstrate differential effects of *Nrf2* status and exposure on fetal vessel size. Previously, we reported LD exposure increased fetal vessel size in female placenta, perhaps as a compensatory mechanism. In this study, we saw the lack of *Nrf2* in our FA control group resulted in increased measurement of fetal vessel size in male placenta. Interestingly, male *Nrf2* null mice exposed to LD had decreased fetal vessel size. There were no effects on maternal "vessels,", i.e., lacunae in *Nrf2* null mice across exposure groups. In our model, as described above, fetal growth effects were most pronounced in HD-exposed female offspring lacking *Nrf2*. The lack of morphological effects in HD-exposed placenta points out the complexity of placental exchange capacity. Future functional measurements may better inform placental nutrient transfer capacity, especially as related to fetal growth restriction.

To further tease apart the effects of UFP exposure in WT and $Nrf2^{-/-}$ mice, we evaluated oxidative stress biomarkers in maternal serum and placental tissues. Oxidative stress is known to underlie PM-induced adverse pregnancy outcomes [112]. Redox states of GSH/GSSG and Cys/CySS have been applied in many assessments of disease pathologies and environmental exposures [100]. Diesel exhaust particle exposure has been shown to alter Cys redox state in a mouse model of HDM-induced asthma [404]. Likewise, GSH redox was demonstrated to be skewed toward oxidative stress (i.e., decreased GSH/GSSG ratio) in lung cells and neonatal mice exposed to combustion-generated PM with a high free radical content. In our model, we observed a significant increase in the GSH/GSSG ratio in WT, HD-exposed female placenta in comparison with the $Nrf2^{-/-}$ HD

female group. Since several genes related to GSH synthesis have antioxidant response elements (ARE) in their promoter regions, a lack of NRF2 signaling would result in presumably less GSH production [106]. Contrary to other reports showing that PM decreased GSH/GSSG ratios, we noted that HD exposure increased the GSH/GSSG ratio in the female WT HD group. This may indicate HD exposure, which is high at 500 $\mu g/m^3$, triggers NRF2 in response to chronic gestational exposure (GD 0.5 to 18.5) resulting in enhanced GSH production. In this case, *Nrf2*$^{-/-}$ female mice exposed to HD fail to mount the same response. Alternatively, in the maternal serum we observed changes in the Cys/CySS ratio, wherein *Nrf2*$^{-/-}$ dams exposed to HD had significantly higher ratios compared with WT, HD-exposed dams. GSH and Cys redox states are not in equilibrium, and other models have shown PM-induced oxidative stress impacts Cys redox differently than GSH [404]. Additionally, it is important to note the levels in different compartments, maternal serum versus placental tissue, can reflect unique redox signatures. Additionally, increased maternal Cys levels in plasma have been associated with preeclampsia and adverse pregnancy complications, including premature delivery and low birth weight [405, 406]. PM exposure is associated with several of these outcomes. Our data suggest increased CyS/CySS in response to HD PM depends on maternal NRF2 status. Additional measures of oxidative stress, also at varying time points, may further inform our model.

Based on known impacts of UFPs on oxidative stress and inflammatory pathways, as well as recent findings from our gestational UFP exposure model showing how UFPs affect placental bile acid metabolism [394], we evaluated several genes involved in these pathways to investigate the role of NRF2. We observed significantly decreased placental

expression of *Nqo1* in *Nrf2*$^{-/-}$ male and female FA- and LD-exposed groups, indicating less constitutive activation in *Nrf2*, and failure to elicit response to LD exposure. *Nqo1* is one of two major quinone reductases in mammalian systems and is a prototypical *Nrf2* target gene. Thus, it is expected that we would not see its induction mice lacking *Nrf2*. Other pathways, including the aryl hydrocarbon receptor (AhR) pathway, can influence *Nqo1* transcription. The AhR pathway plays a major role in xenobiotic metabolism, with downstream targets including cytochrome P450s such as CYP1A1 and CYP1B1. PAHs (polycyclic aromatic hydrocarbons) are PM-associated toxicants and known AhR ligands. In our model, all *Nrf2*$^{-/-}$ groups, with the exception of LD males, showed increased *Ahr* placental expression. Its downstream target *Cyp1a1* was not detected in any groups (data not shown), and interestingly, *Cyp1b1* expression was significantly increased in *Nrf2*$^{-/-}$ FA- and LD-exposed male and female placentae, but not HD groups.

Nrf2 signaling also plays an anti-inflammatory role via crosstalk with the NF-κB pathway, decreasing IκBα degradation, thereby blocking NF-κB-driven inflammation [407]. Moreover, the induction of heme oxygenase-1 (HO-1) can also inhibit NF-κB signaling and proinflammatory cytokines IL6 and TNFα. Although we did not see differences in *Il6* expression in our model, we did see significantly increased expression of *Tnfα* in all *Nrf2*$^{-/-}$ groups, ranging from 4–6-fold, and *Il1β*, ranging from 2–4-fold, in all *Nrf2*$^{-/-}$ group, excluding female HD. TNFα is an inflammatory cytokine produced by macrophages/monocytes responsible for a range of signaling events within cells. IL1β is also a potent inflammatory cytokine, and both TNFα and IL1β can drive systemic inflammation. Lack of Nrf2 activity can exacerbate NF-κB signaling, leading to increased

cytokine production [108, 109]. This trend was somewhat similarly observed for *Tgfβ1* expression. *Tgfβ1* is a multifunctional cytokine, and in our model, expression was significantly increased in male and female *Nrf2*$^{-/-}$ placentas in the FA and HD groups. Interestingly, its downstream target, *Smad3*, was increased in all female *Nrf2*$^{-/-}$ groups, and only increased in FA male *Nrf2*$^{-/-}$ placentas. Collectivity, these data support NRF2 important anti-inflammatory role, basally and in response to an environmental challenge. The lack of functional NRF2 signaling leads to a pro-inflammatory environment in the placenta.

Since gestational UFP exposure was previously shown to impact bile acid metabolism in our mouse model using WT mice [394], particularly in female placentae, we carried out gene expression analysis on keys genes significantly upregulated in our WT exposure model. These included nuclear receptors *Hnf4α* and *Nr1h4* (FXR) and apolipoproteins *Apoa1* and *Apob*, the primary protein components of HDL and LDL, respectively. *Hnf4α* was increased in male *Nrf2*$^{-/-}$ FA- and HD-exposed groups, and was also increased in female *Nrf2*$^{-/-}$ HD-exposed mice. *Nr1h4* (FXR) gene expression was decreased in female *Nrf2*$^{-/-}$ FA and LD groups. Likewise, *Apoa1* was decreased in these groups (female *Nrf2*$^{-/-}$ FA and LD). Alternatively, *Apoa1* and *Apob* was significantly increased female *Nrf2*$^{-/-}$ HD-exposed mice. Overall, the group with the most marked phenotypic effects (*Nrf2*$^{-/-}$ HD-exposed females) corresponded to significantly higher placental *Apoa1* and *Apob* expression suggesting a link between placental lipid dysregulation and placental growth in response to high dose UFP exposure. Our sex-specific findings require additional investigation on the underlying mechanisms, including

confirmation of protein expression and functional effects. A previous study assessing *Nrf2* in *Drosophila* flies showed *Nrf2*/Cap-n-collar protein binding occurs in different genetic loci, Hr4 (DHR4) locus versus Hnf4 (dHNF4) locus for females vs. males, respectively [408]. The evidence of female susceptibility in our mammalian model and translation to exposed human populations necessitates further mechanistic study.

3.6. Conclusions

In summary, the disruption of NRF2 directly impacts inflammatory cytokine signaling in placental tissue. The lack of NRF2 exacerbates adverse developmental outcomes in response to UFP exposure, particularly in female offspring exposed to a high dose of UFPs, possibly via oxidative stress and the dysregulation of lipid transport. Other subtle effects of a low dose of UFPs on placental morphology necessitate further study.

3.7. Figures

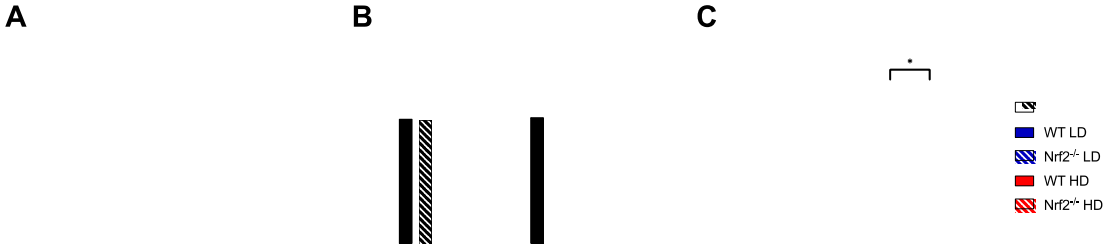

Figure 3.1 Phenotypic effects of UFPs.

(A) Average placental weights at GD 18.5 show a significant decrease in the *Nrf2*$^{-/-}$ HD female group compared with WT FA control female group. (B) Fetal weights at GD 18.5 averaged by sex demonstrates a significant decrease in *Nrf2*$^{-/-}$ HD compared with WT HD and WT FA in females. (C) Average crown to rump lengths at GD 18.5 show a decrease

in the LD versus FA control for WT females. Offspring sample sizes include WT FA male (n = 13), WT LD male (n = 22), WT HD male (n = 20), WT FA female (n = 18), WT LD female (n = 25), WT HD female (n = 24), *Nrf2*$^{-/-}$ FA male (n = 13), *Nrf2*$^{-/-}$ LD male (n = 16), *Nrf2*$^{-/-}$ HD male (n = 23), *Nrf2*$^{-/-}$ FA female (n = 11), *Nrf2*$^{-/-}$ LD female (n = 12), and *Nrf2*$^{-/-}$ HD female (n = 20). Data analyzed using two-way ANOVA with Tukey's multiple comparison test (* $p < 0.05$; *** $p < 0.001$; **** $p < 0.0001$).

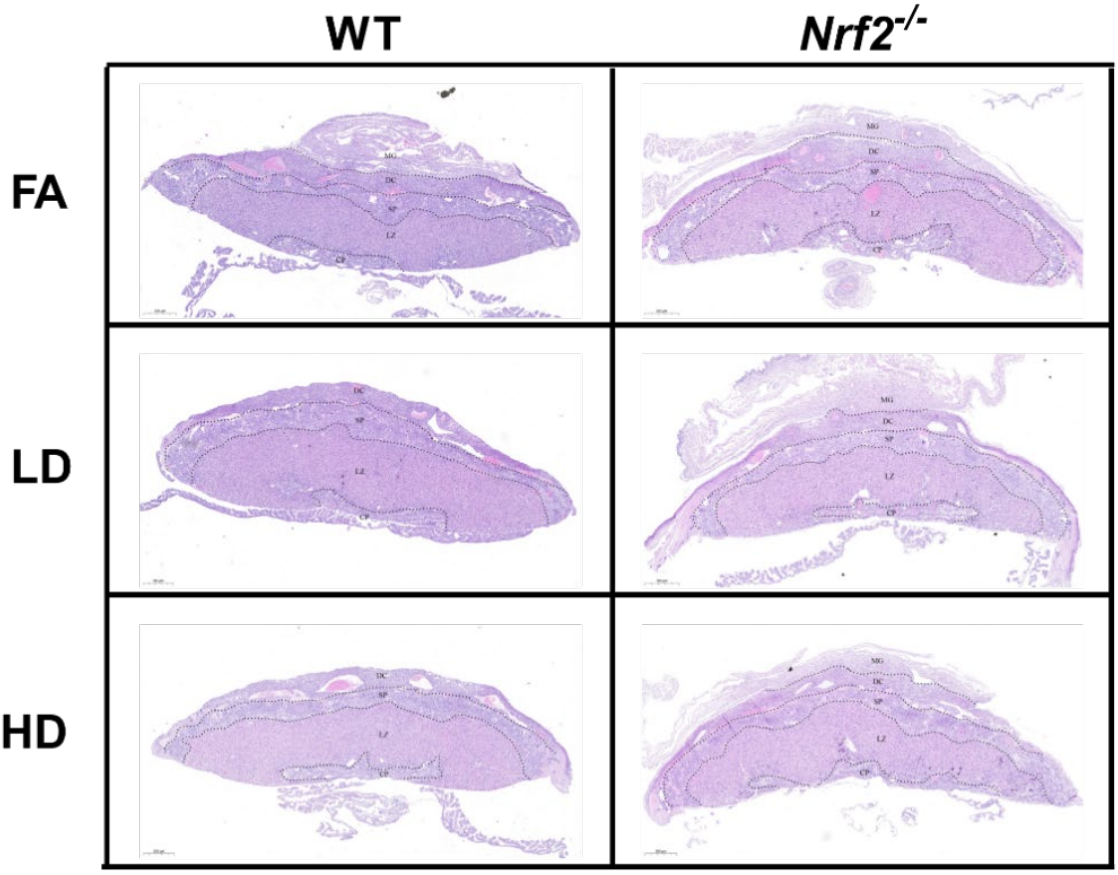

Figure 3.2 Placental histology.

Representative placental images collected from male offspring depicting wildtype (WT) and *Nrf2*$^{-/-}$ mice exposed to filtered air (FA) control, low dose (LD; 100 µg/m^3), and high

dose (HD; 500 µg/m^3). No gross histologic changes were observed across the different groups. Area measurements were made for decidua (DC), spongiotrophoblast (SP), and labyrinth zone (LZ) layers. Sample sizes for placenta from male offspring: WT FA (n = 7), WT LD (n = 11), WT HD (n = 13), *Nrf2*$^{-/-}$ FA (n = 10), *Nrf2*$^{-/-}$ LD (n = 9), *Nrf2*$^{-/-}$ HD (n = 8).

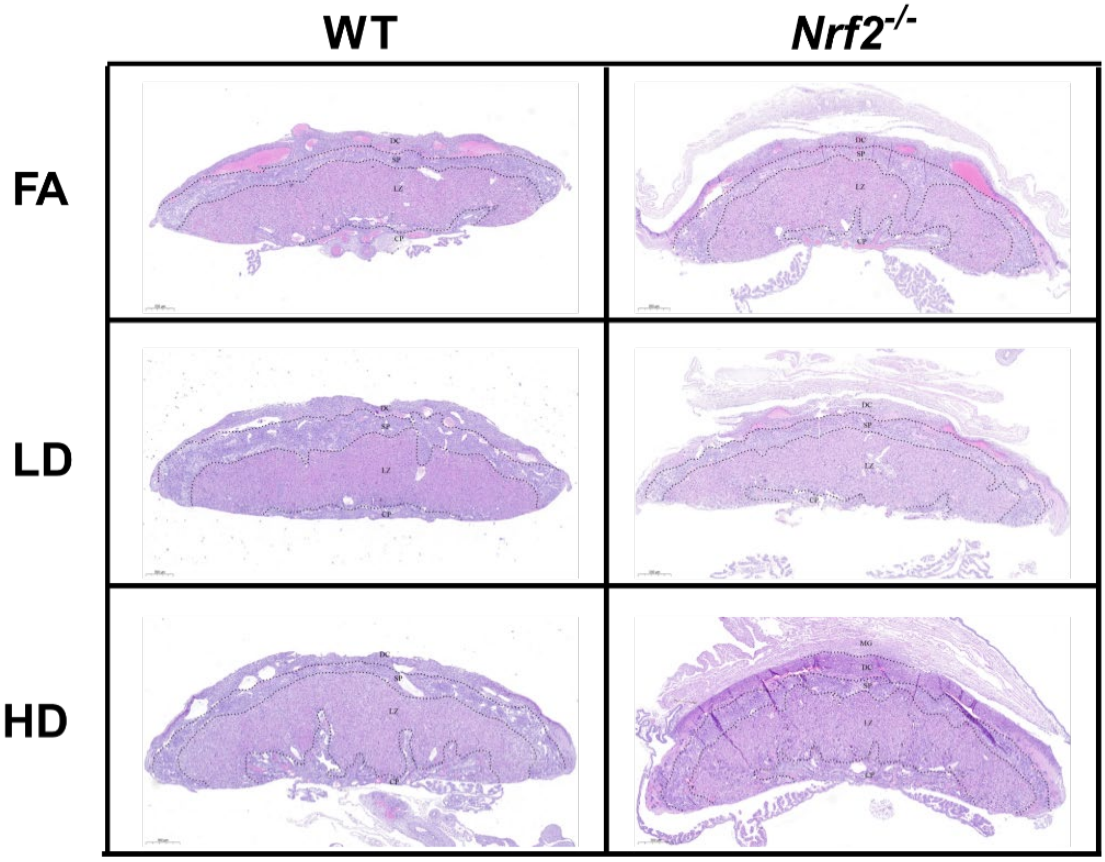

Figure 3.3 Placental histology.

Representative placental images collected from female offspring depicting wildtype (WT) and *Nrf2*$^{-/-}$ mice exposed to filtered air (FA) control, low dose (LD; 100 µg/m^3), and high dose (HD; 500 µg/m^3). No gross histologic changes were observed across the different

groups. Area measurements were made for decidua (DC), spongiotrophoblast (SP), and labyrinth zone (LZ) layers. Sample sizes for placenta from female offspring: WT FA (n = 8), WT LD (n = 12), WT HD (n = 12), *Nrf2*$^{-/-}$ FA (n = 5), *Nrf2*$^{-/-}$ LD (n = 8), *Nrf2*$^{-/-}$ HD (n = 6).

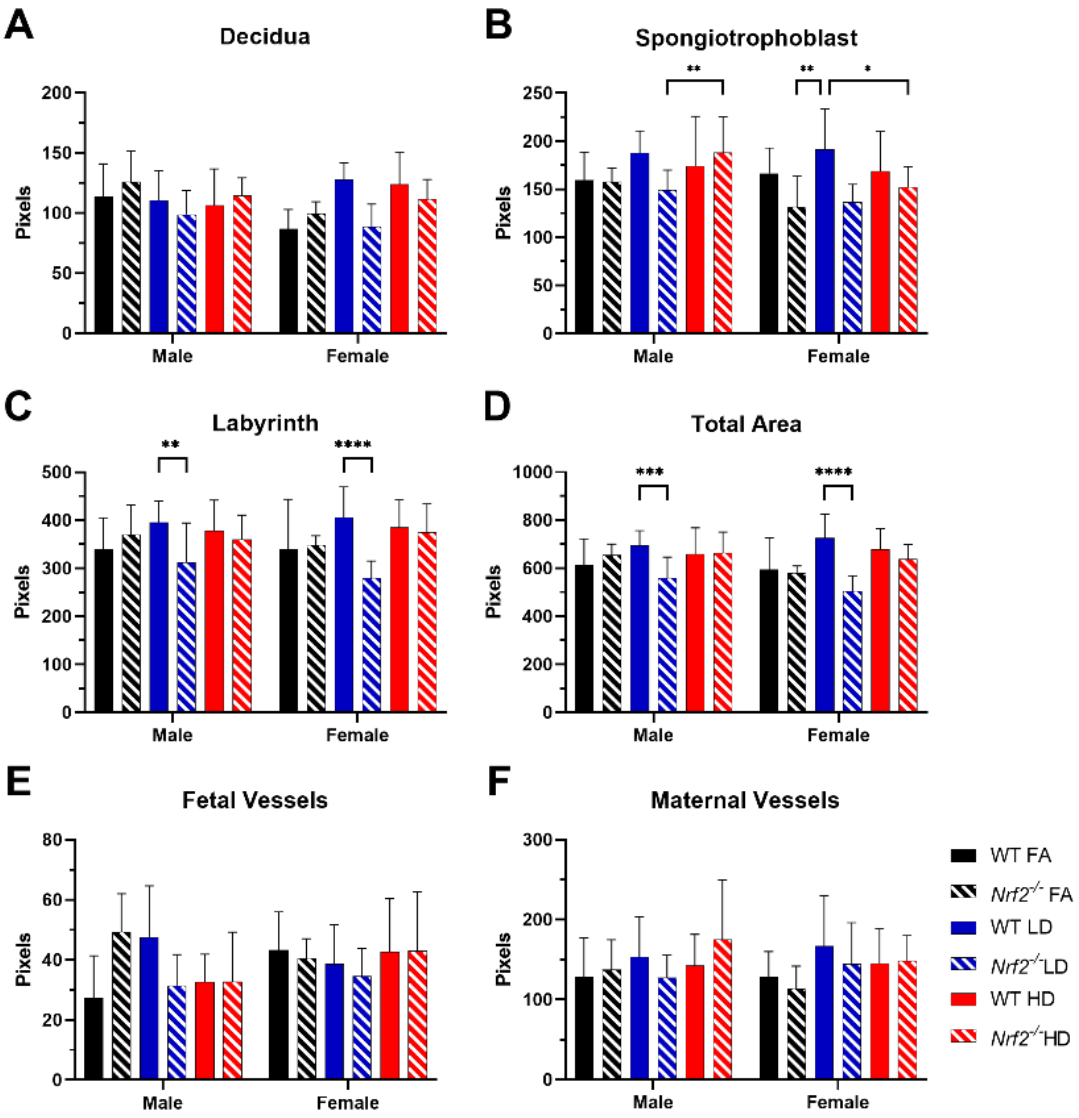

Figure 3.4 Placental morphology.

Comparisons of WT and *Nrf2*$^{-/-}$ placenta from pregnant mice exposed to filtered air (FA) control (black), low dose (LD) (blue), or high dose (HD) (red). Placenta area of the decidua (A), spongiotrophoblast (B), labyrinth zones (C) and total area (D) were quantified for each H&E-stained section. Fetal vessels (E) and maternal vessels (i.e., lacunae) (F) were measured in labyrinth zone images. Error bars represent SD. Data analyzed using one-way ANOVA with Tukey's multiple comparison test. (* $p < 0.05$; ** $p < 0.01$; *** $p < 0.001$; **** $p < 0.001$). Sample sizes shown in Figures 3.2 and 3.3.

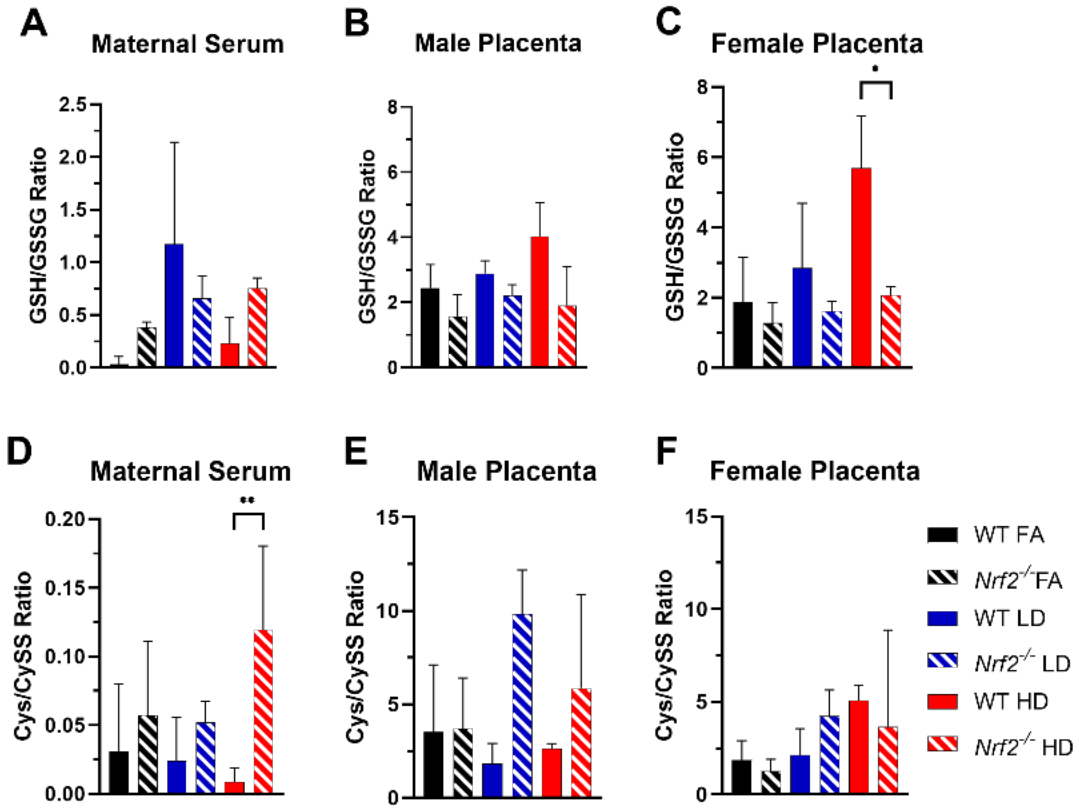

Figure 3.5 Oxidative stress biomarkers.

Glutathione/glutathione disulfide (GSH/GSSG) and cysteine/cystine (Cys/CySS) ratios with comparisons of WT and *Nrf2*$^{-/-}$ exposed to filtered air (FA) control (black), low dose (LD) (blue), or high dose (HD) (red) for maternal serum (A and D) and placenta homogenates from male (B and E) and female (C and F) offspring. Error bars represent SD. Data analyzed using one-way ANOVA with Tukey's multiple comparison test. (* $p < 0.05$; ** $p < 0.01$). Sample sizes for maternal serum: WT FA ($n = 5$), WT LD ($n = 6$), WT HD ($n = 5$), *Nrf2*$^{-/-}$ FA ($n = 3$), *Nrf2*$^{-/-}$ LD ($n = 3$), *Nrf2*$^{-/-}$ HD ($n = 5$). Sample sizes for placenta from male offspring: WT FA ($n = 6$), WT LD ($n = 11$), WT HD ($n = 6$), *Nrf2*$^{-/-}$ FA ($n = 7$), *Nrf2*$^{-/-}$ LD ($n = 7$), *Nrf2*$^{-/-}$ HD ($n = 15$). Sample sizes for placenta from female offspring: WT FA ($n = 10$), WT LD ($n = 13$), WT HD ($n = 12$), *Nrf2*$^{-/-}$ FA ($n = 8$), *Nrf2*$^{-/-}$ LD ($n = 4$), *Nrf2*$^{-/-}$ HD ($n = 14$).

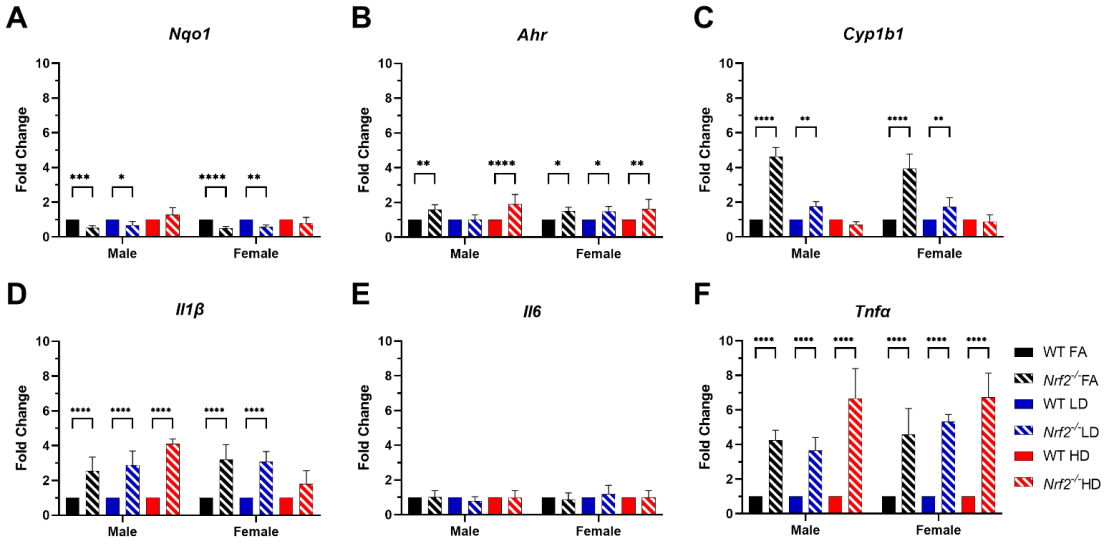

Figure 3.6 Placental gene expression data.

Fold change of *Nqo1* (A), *Ahr* (B), *Cyp1b1* (C), *Il1β* (D), *Il6* (E) and *Tnfα* (F). Error bars represent SD. Data analyzed using two-way ANOVA with Tukey's multiple comparison test. (* $p < 0.05$; ** $p < 0.01$; **** $p < 0.0001$). Male placenta homogenate numbers include WT FA ($n = 6$), WT LD ($n = 11$), WT HD ($n = 6$), *Nrf2*$^{-/-}$ FA ($n = 8$), *Nrf2*$^{-/-}$ LD ($n = 7$), and *Nrf2*$^{-/-}$ HD ($n = 15$). Female placenta homogenate numbers include WT FA ($n = 10$), WT LD ($n = 13$), WT HD ($n = 12$), *Nrf2*$^{-/-}$ FA ($n = 8$), *Nrf2*$^{-/-}$ LD ($n = 4$), and *Nrf2*$^{-/-}$ HD ($n = 14$).

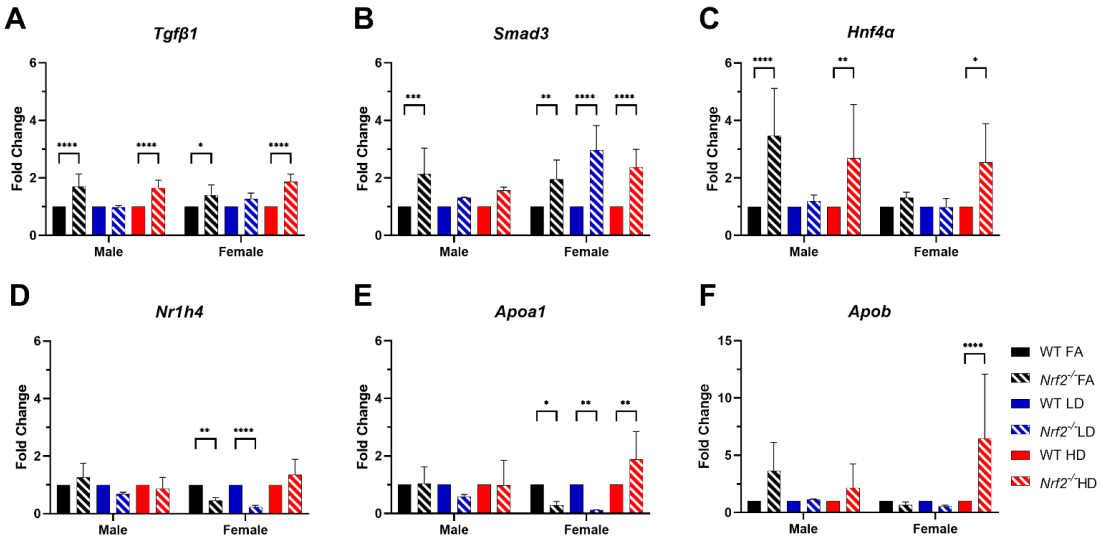

Figure 3.7 Placental gene expression data.

Placental gene expression. Fold change of *Tgfβ1* (**A**), *Smad3* (**B**), *Hnf4α* (**C**), *Nr1h4* (**D**), *Apoa1* (**E**), and *Apob* (**F**). Error bars represent SD. Data analyzed using two-way ANOVA with Tukey's multiple comparison test. (* $p < 0.05$; ** $p < 0.01$; *** $p < 0.001$; **** $p < 0.0001$). Sample sizes shown in Figure 3.6.

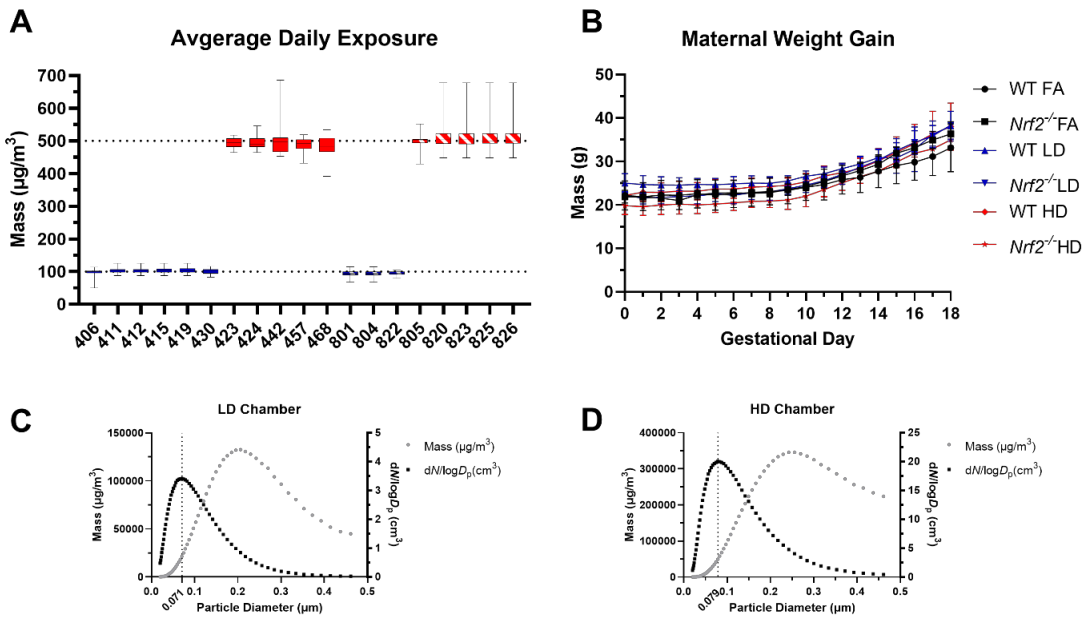

Figure 3.8 UFP characterization and average daily exposure.

(A) Individual dams shown by ID number for wildtype (WT) and *Nrf2*$^{-/-}$ pregnant mice with corresponding average daily PM mass concentrations ± SD measured within chambers from GD 0.5 to 18.5. (B) Average maternal weight gain mean ± SD across exposure groups. Groups include wildtype (WT) filtered air (FA) control (n= 6; black line with circle), WT low dose (LD) (n=6; blue line with square), WT high dose (HD) (n=5; red line with triangle), *Nrf2*$^{-/-}$ FA (n=3; black line with inverted triangle), *Nrf2*$^{-/-}$ LD (n=3; blue line with diamond), and *Nrf2*$^{-/-}$ HD (n=5; red line with circle). No significant differences were observed across groups. (C) Low dose (LD) PM size (black) and concentration (gray) distribution, indicating 0.071 µm (71 nm) as the peak particle

diameter. (D) High dose (HD) PM particle size (black) and concentration (gray) distribution, indicating 0.079 µm (79 nm) as the peak particle diameter.

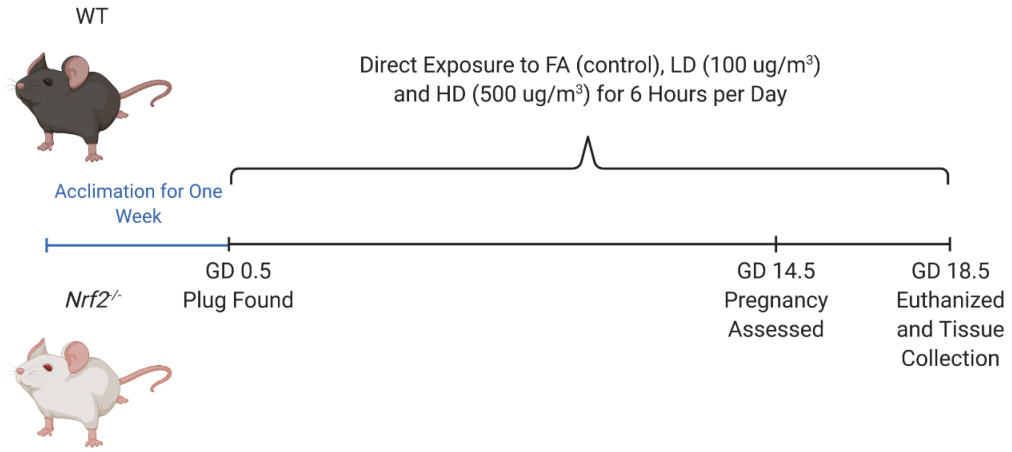

Figure 3.9 Illustration indicating exposure timeline.

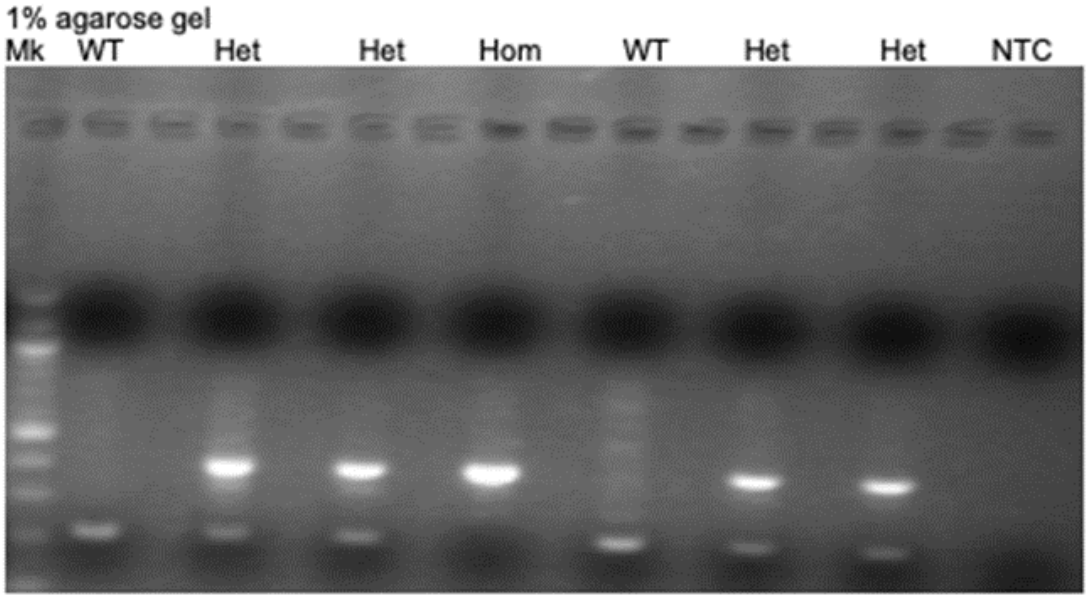

Figure 3.10 Genotypes of homozygous wildtype and *Nrf2*-deficient mice confirmed by PCR amplification of genomic DNA extracted from tail snips.

PCR amplification was carried out using established methods [399] by using three different primers, 5′-TGGACGGGACTATTGAAGGCTG-3′ (sense for both genotypes), 5′-CGCCTTTTCAGTAGATGGAGG-3′ (antisense for wild type), and 5′-GCGGATTGACCGTAATGGGATAGG-3′ (antisense for LacZ). Conditions were as follows, step 1 95°C 180 sec, step 2 95°C 30 sec, step 3 70°C 30 sec, step 4 72°C 30 sec, repeat steps 2-4 for 35 total cycles, followed by step 5 72°C 120 sec. Wild-type and mutant PCR products detected at 200-300 bp and 400 bp, respectively.

Table 3.1 Primer Sequences used in qRT-PCR of extracted RNA from pooled GD 18.5 sex- separated placentas.

Target	Forward Primer	Reverse Primer	NCBI Accession Number	Product Size (bp)
NQO1	TGGCCGAACACAAGAAGCTG	GCTACGAGCACTCTCTCAAACC	NM_008706	112
AhR	TGTGCAGAATCCCACATCCG	AATCAAGCGTGCATTGGACTG	NM_013464	114
CYP1b1	CAGTCTGGCGTTCGGTCAC	GCTGCGTTGGATCGAGGAA	NM_009994	197
IL-1β	GCCACCTTTTGACAGTGATGAG	AAGGTCCACGGGAAAGACAC	NM_008361	219
IL6	TCGTGGAAATGAGAAAAGAGTTGTG	GGTACTCCAGAAGACCAGAGG	NM_031168	177
TNFα	CCATGAGCACAGAAAGCATGATC	GCCATTTGGGAACTTCTCATCC	NM_013693	203
TGFβ1	CAAGGGCTACCATGCCAACT	GTACTGTGTGTCCAGGCTCCAA	NM_011577	67
SMAD3	CACGCAGAACGTGAACACC	GGCAGTAGATAACGTGAGGGA	NM_016769	101
HNF4α	GGTTTAGCCGACAATGTGTGG	TCCCGCTCATTTTGGACAGC	NM_008261	115
NR1H4	GCTTGATGTGCTACAAAAGCTG	CGTGGTGATGGTTGAATGTCC	NM_001163700	110
APOa1	GCTCAAGAGCAACCCTACCTT	GCTTTCTCGCCAAGTGTCTTC	NM_009692	75
APOb	AAGCACCTCCGAAAGTACGTG	CTCCAGCTCTACCTTACAGTTGA	NM_009693	111
GAPDH	TGTCAAGCTCATTTCCTGGTATGACA	GAGTTGGGATAGGGCCTCTCTT	NM_001289726	148

Table 3.2 Levels of individual redox species.

	Maternal Serum					
	WT FA	***Nrf2*** $^{-/-}$ **FA**	**WT LD**	***Nrf2*** $^{-/-}$ **LD**	**WT HD**	***Nrf2*** $^{-/-}$ **HD**
GSH	0.01 ± 0.03	0.58 ± 0.51	1.64 ± 1.87	1.14 ± 0.22	1.23 ± 1.78	1.25 ± 0.51
GSSG	0.73 ± 0.34	1.49 ± 1.30	1.68 ± 1.08	2.06 ± 0.46	4.92 ± 4.32	1.71 ± 0.77
Cys	0.33 ± 0.47	1.21 ±1.07	0.70 ± 1.22	1.39 ± 0.56	**0.12 ± 0.15**	**1.81 ± 0.29****
CySS	17.73 ± 9.63	15.55 ± 12.82	20.24 ± 8.91	25.47 ± 0.56	16.26 ± 2.64	17.64 ± 6.33
	Male Placenta					
	WT FA	***Nrf2*** $^{-/-}$ **FA**	**WT LD**	***Nrf2*** $^{-/-}$ **LD**	**WT HD**	***Nrf2*** $^{-/-}$ **HD**
GSH	2.39 ± 2.14	4.29 ± 3.70	**2.57 ± 1.22**	**10.22 ± 1.56****	1.94 ± 0.17	4.13 ± 3.54
GSSG	1.02 ± 0.79	2.51 ± 1.45	**0.86 ± 0.34**	**4.68 ± 0.75****	0.50 ± 0.13	1.91 ± 0.81
Cys	1.90 ± 1.28	1.78 ± 1.29	2.05 ± 1.26	5.00 ± 1.24	1.87 ± 0.29	2.53 ± 2.59
CySS	0.74 ± 9.63	0.49 ± 0.02	1.08 ± 0.25	0.51 ± 0.01	0.71 ± 0.08	0.36 ± 0.13
	Female Placenta					
	WT FA	***Nrf2*** $^{-/-}$ **FA**	**WT LD**	***Nrf2*** $^{-/-}$ **LD**	**WT HD**	***Nrf2*** $^{-/-}$ **HD**
GSH	2.33 ± 2.26	1.49 ± 1.04	3.68 ± 1.31	4.53 ± 2.69	3.13 ± 0.56	2.89 ± 4.53
GSSG	1.46 ± 0.99	1.36 ± 0.89	1.46 ± 0.40	2.77 ± 1.34	0.60 ± 0.30	1.39 ± 2.18
Cys	1.40 ± 1.60	0.60 ± 0.30	2.41 ± 1.73	1.63 ± 0.57	3.86 ± 0.61	1.35 ± 2.16
CySS	0.60 ± 0.42	0.47 ± 0.05	**1.18 ± 0.24**	**0.38 ± 0.02****	0.76 ± 0.07	0.24 ± 0.14

Oxidative stress biomarker averages ± SD depicting glutathione (GSH), glutathione disulfide (GSSG), cysteine (Cys), and cystine (CySS), values in maternal serum and placenta homogenates across exposure groups and genotype. Sample sizes shown in figure 3.2. Data analyzed using one-way ANOVA with Tukey's multiple comparison test. (*$p<0.05$; **$p<0.01$).

4. SULFORAPHANE AFFORDS MINIMAL PROTECTION AGAINST GESTATIONAL ULTRAFINE PARTICULATE MATTER EXPOSURE ON PLACENTAL BILE ACID PATHWAYS IN A C57BL/6N MURINE MODEL

4.1. Overview

Mounting evidence supports that particulate matter (PM) is associated with adverse birth and perinatal outcomes following prenatal exposure. Sulforaphane (SFN), a phytochemical found in cruciferous vegetables, has known antioxidant and anti-inflammatory properties through its activation of nuclear factor erythroid 2-related factor (NRF2) and antioxidant response element (ARE). Here we investigated if gestational SFN administration with daily UFP exposure rescues UFP driven lipid/bile acid signaling pathways within the placenta. Time-mated C57BL/6n mice were gestationally exposed for 6 hours daily in a dose response while given SFN supplementation or vehicle only post-UFP exposure. A significant increase was observed in crown to rump length in female offspring while UFP exposure or SFN administration did not impact other growth parameters. Oxidative stress biomarkers indicated no significant changes in redox species while maternal dam liver *Nqo1* gene expression increased due to SFN supplementation. Placental lipid metabolism pathways associated with UFP gestational exposure were minimally rescued with SFN supplementation. Our findings indicate the need for further investigation into the utility of SFN administration to counter UFP driven placenta toxicity.

4.2. Introduction

Air pollution, particularly ambient particulate matter (PM), represents a significant environmental health hazard [2]. PM is classified based on its size as either coarse (PM_{10}), fine ($PM_{2.5}$), or ultrafine ($PM_{0.1}$; UFP) [315, 317, 389]. UFPs can exist anywhere due to high traffic conditions and new particle formation through nucleation reactions [355, 393]. Mounting epidemiological evidence suggests that PM exposure leads to adverse pregnancy outcomes including preterm birth, low birth weight, and future deleterious health effects in offspring [291, 293, 294, 359, 390, 391]. Many studies only account for PM10 and/or PM2.5 exposure due to difficulty in measuring UFPs. While negligible in mass concentration, UFPs penetrate deep into the respiratory tract [360], even translocating into systemic circulation where they can reach fetal circulation [71, 73, 133]. Wick et al. determined size barrier capacity where 50, 80, and 240 nm fluorescently tagged particles crossed *ex vivo* human placenta but not 500 nm particles. Thus, UFPs are an important component potentially driving adverse pregnancy and neonatal outcomes [55, 316].

The placenta is a transient organ which serves as the interface between mother and fetus. The murine placenta is similar to humans in that it is classified as hemochorial, meaning maternal and fetal blood are in close contact allowing nutrient and waste exchange to occur [170, 172]. Proper fetal growth and development are dependent on nutrient availability from the placenta [162-164]. Placental dysfunction is regarded as an indicator of adverse perinatal outcomes [357]. Dysfunction within prenatal periods may affect developmental programming [276] and ultimately result in adverse perinatal outcomes [357]. Maternal and placental inflammation and oxidative stress have been

implicated as causative factors underlying deleterious effects on pregnancy-related outcomes due to PM [121]. Additionally, recent findings from our own gestational UFP exposure mouse models demonstrate altered placental lipid processing signaling pathways, placental morphology, and *Nrf2* related inflammatory cytokine signaling particularly in female offspring [394]. These initial studies indicate the potential hazards associated with UFPs and the placenta. While regulation of UFPs are lagging, safe and effective preventive interventions to protect against maternal-fetal outcomes are of crucial need.

Sulforaphane (SFN), is an isothiocyanate phytochemical predominantly found in cruciferous vegetables such as broccoli sprouts, bok choy, and cabbage [409]. This naturally occurring organosulfur compound has antioxidant and anti-inflammatory properties by activating nuclear factor erythroid 2-related factor 2 (NRF2) via antioxidant response element (ARE) [410, 411]. NRF2 is known as the master regulator of cellular antioxidants [98, 407]. Under physiological conditions, NRF2 is bound to Kelch-like ECH associated protein 1 (KEAP1)-Cullin3 (Cul3)-based E2 ubiquitin ligase complex which marks NRF2 for degradation [93, 106, 396]. Oxidative stress allows for the dissociation of KEAP1 with subsequent nuclear translocation and binding to the ARE by NRF2. SFN induces cysteine modifications on KEAP1 allowing for subsequent antioxidant and anti-inflammatory effects of NRF2 [412]. Given that most of the global population lacks access to targeted pharmaceuticals, foodstuffs containing bioavailable chemicals for disease prevention are a proposed potential strategy [413]. Therefore, in the present study, we investigated the potential protective effects of daily gestational SFN administration with

concurrent UFP exposure using our previously developed mouse model in which we identified adverse developmental effects [394].

4.3. Materials and Methods

4.3.1. Animals and Time Mating

All protocols and procedures were approved by the Institutional Animal Care and Use Committee of Texas A&M University #2019-0025. C57Bl/6n, wildtype (WT), mice were purchased from Jackson Laboratories and maintained in an AAALAC approved facility at Texas A&M Institute for Genomic Medicine (TIGM). C57Bl/6n were time-mated overnight, and pregnancy was established with the presence of a vaginal plug or sperm present via vaginal cytology confirmed under a microscope. All animals were house under standard conditions including a 12-hour light dark cycle, 22-24°C, and 40-60% humidity. Water and standard mouse chow (Teklad Global Diets) were provided *ad libitum*.

4.3.2. Gestational UFP Exposure and SFN Administration

To investigate the potential mitigating effects of SFN administration with UFP exposure, 8- to 10-week-old female mice were acclimated to a filtered air exposure chamber one week prior to exposure. Following acclimation period, time-mated pregnant females, termed gestational day (GD 0.5), were randomly assigned to three UFP exposure groups (filtered air or control, low dose or 100 $\mu g/m^3$, and high dose or 500 $\mu g/m^3$) with or without SFN administration: filtered air without SFN (FA-VEH); filtered air with SFN (FA-SFN); low dose without SFN (LD-VEH); low dose with SFN (LD-SFN); high dose without SFN (HD-VEH); and high dose with SFN (HD-SFN). Particle generation and

gestational exposure were performed as previously described [394]. UFP composition consisted of sulfates, nitrates, ammonium, chloride, and black carbon (diesel exhaust soot). Gestational UFP exposure occurred for 6-hours daily from GD 0.5 to 18.5 as illustrated in Figure 4.1.

Immediately post-UFP exposure, either dimethyl sulfoxide (DMSO; Sigma Aldrich Cat# D8418) vehicle alone or 600 ppm of SFN (Toronto Research Chemical Cat# 699115) dissolved in DMSO vehicle was administered via 1 gram of peanut butter (PB2 Organic Powered Peanut Butter) from GD 0.5 to 17.5. Following UFP exposure on GD 18.5, dams were euthanized with maternal tissue collection. Placental and fetal tissues were sex-separated and collected via dissection microscope and pooled per litter.

4.3.3. Sample Collection and Redox Processing

Post-euthanasia, maternal and fetal tissues were snap frozen in liquid nitrogen and stored at -80°C for further analysis. Additionally, maternal blood was collected for redox analysis via high performance liquid chromatography (HPLC) following Jones and Liang in 2009 [91] with slight modifications as previously described [414]. Briefly, whole blood was added to a borate buffer solution containing γ-glutamylglutamate (γ-GluGlut) as the internal standard. After centrifugation the supernatant was added to a new centrifuge tube containing a solution of perchloric and boric acid. Samples were snap-frozen until later processing could occur. Upon thawing, samples were centrifuged allowing for protein precipitation and removal. Post-centrifugation, samples were added to a potassium hydroxide and tetraborate solution to adjust the pH to 9.0. Then, dansyl chloride was added and samples were allowed to sit in the dark for 20-24 hours. Finally, chloroform was added

to form a perchlorate and chloroform layer. After centrifugation an upper aqueous layer was aliquot and frozen at -80°C until HPLC analysis.

4.3.4. HPLC Run Conditions and Redox Analysis

HPLC run and analysis conditions followed Jones and Liang [91] with slight modifications as previously described [414]. Briefly, previously derivatized samples were centrifuged and 35 µL volumes were injected into an UltiMate 3000 HPLC (Thermo Fisher Scientific) using a SUPELCOSIL™ LC-NH2 HPLC Column (Supelco 5 µm, 4.6 mm x 250 mm) at 35°C operating temperature. Additionally, fluorescence and excitation emission detection were set at 335.0 and 515.0, respectively. Flow rate was constant at 1 mL per minute where HPLC mobile phases included solvent A (80% v/v methanol/water) and solvent B (acetate-buffered methanol solution). Run conditions were as follows: 0-10 minutes of 80% solvent A and 20% solvent B; 10-30 minutes of 20% solvent A and 80% solvent B with a linear gradient change; 35-38 minutes of 80% solvent A and 20% solvent B with a linear gradient change and held until 42 minutes with total run time. Retention times of compounds of interest were as followed: cystine (CySS) from 9 to 9.5 minutes; cysteine (Cys) from 10 to 10.5 minutes; γ-GluGlut from 12 to 13 minutes; glutathione (GSH) from 19 to 19.5 minutes; and glutathione disulfide (GSSG) from 23.5 to 24 minutes.

4.3.5. RNA Isolation and qRT-PCR

Total RNA was extracted from pooled, sex-separated GD 18.5 placentas and maternal dam liver tissues using TRIzol reagent (Invitrogen, Thermo Fisher Scientific) as previously described [394]. Briefly, a Nanodrop Spectrophotometer/Fluorometer

(DeNovix DS-11 FX+ V3.35 software) was used to assess RNA purity and quality. Samples with ≥1.8 260/280 absorbance values were used and diluted to one µg/µL. One µg of total RNA was reverse transcribed (Qiagen QuantiTect® Reverse Transcription kit - Cat # 205311) into cDNA following manufacturer's instructions. Subsequently, 100 ng of cDNA was used in quantitative real-time PCR with Power SYBR™ Green PCR Master Mix (Applied Biosystems™ - Cat #4367659) on a Roche LightCycler® 96. qRT-PCR reaction conditions were as follows: 50°C for 2 min; 95°C for 10 min; and 45 cycles of 94°C for 15 sec, 60°C for 30 sec, and 72°C for 30 sec with *Gapdh* internal reference gene and $2^{-\Delta\Delta CT}$ analysis. Primer sequences are reported in Table 4.2.

4.3.6. Statistics

All statistical analyses were performed using GraphPad Prism (V9.3 software) and expressed as mean ± standard deviation (SD). Statistical significance was assessed using either a one-way analysis of variance (ANOVA) followed by Dunnett's multiple comparisons test or two-way ANOVA followed by Tukey's multiple comparison test. Significance was considered with $P<0.05$.

4.4. Results

4.4.1. Phenotypic and Perinatal Outcomes

UFP exposure did not demonstrate gross adverse toxicity as previously reported from our laboratory as indicated by fetal weight (Figure 4.2A) or placenta weight (Figure 4.2B). Interestingly, statistically significant increases in female HD-VEH crown to rump length (Figure 4.2C) were observed in comparison to female FA-VEH. SFN administration did not result in significant alteration to perinatal outcomes, but trends

towards increased fetal weight, placenta weight, and fetal crown to rump length (Figures 4.2A-C) were noted in comparison to FA-SFN.

4.4.2. Maternal Oxidative Stress

Figure 4.3A illustrates maternal dam liver *Nqo1* gene expression, indirectly demonstrating NRF2 activation due to SFN administration. A statistically significant increase was observed in FA-SFN compared with FA-VEH while a decrease was noted in LD-VEH compared to FA-VEH. Overall, groups administered peanut butter containing SFN demonstrated increased *Nqo1* maternal liver expression compared to their respective UFP-dosing vehicle group. Figure 4.3B demonstrates there were no significant differences in oxidative stress biomarkers, glutathione/glutathione disulfide (GSH/GSSG) and cysteine/cystine (Cys/CySS) ratios, in maternal serum across various groups.

4.4.3. qRT-PCR

Expression of several genes that were previously identified with RNA sequencing in relation to placenta UFP exposure were assessed using qRT-PCR. Figure 4A illustrates expression levels of *Nqo1* (Figure 4A) where male FA-VEH was significantly upregulated. We also evaluated *Tgfβ1* (Figure 4B) and downstream effector *Smad3* (Figure 4.4C) which was significantly increased in both male and female LD-SFN. Additionally, *Smad3* demonstrated significant increases in HD-VEH and HD-SFN for females only. The expression of *AhR* (Figure 4D) was significantly increased in male HD-SFN group only. Strikingly, *Cyp1b1* (Figure 4E) revealed increases in both male and female HD-SFN with additional female increases in FA-SFN, LD-SFN, and HD-VEH.

Continuing the evaluation of altered bile acid metabolism as previously reported [394], gene expression alterations were observed in *Hnf4α*, *Nr1h4* (Farnesoid X Receptor – FXR), *Apoa1*, and *Apob*. *Hnf4α* (Figure 4.5A) was significantly increased in both male and female HD-VEH in comparison to FA-VEH. Similarly, *Nr1h4*, *Apoa1*, and *Apob* (Figures 4.5B-D) all demonstrated significant increases in HD-VEH in female placentas only.

4.5. Discussion

Several adverse birth and perinatal outcomes are associated with gestational exposure to particulate matter [359]. Many effects include infant low birth weight, premature birth, and fetal growth restriction, all of which are indicators for infant morbidity and mortality [291, 294, 391]. Additionally, UFP-specific models have indicated adverse pregnancy and perinatal outcomes namely preterm birth and reduced fetal weights and lengths [316, 401]. We previously developed a gestational whole body inhalation exposure system which replicates urban UFP exposure utilizing either a low dose (LD, 100 $\mu g/m^3$) or high dose (HD, 500 $\mu g/m^3$). Sex- and dose-specific effects were identified on placental morphology where RNA sequencing recognized alterations in several molecular pathways predominantly lipid/bile acid metabolism [394]. SFN is a naturally occurring compound primarily found in cruciferous vegetables that has been investigated for years for its chemopreventive properties and ability to activate NRF2 antioxidant pathways [410, 415]. Therefore, in the present study, our objective was to determine if concomitant administration of SFN following daily gestational UFP exposure

could rescue altered gene expression levels in previously identified significantly altered genes.

We exposed time-mated pregnant C57Bl/6n mice to three doses (filtered air – FA, low dose – LD, or high dose – HD) while also administering 1 gram of peanut butter which either contained only DMSO (vehicle – VEH) or DMSO + SFN (600 PPM – SFN) from GD 0.5 to 18.5. While oral gavage is a more precise dosing method, we did not want to induce additional daily stress on the timed-mated mice that could impact pregnancy. Following gestational exposures, we observed no impact on growth parameters including fetal weight and placenta weight (Figure 4.2). Additionally, crown to rump length did not indicate an impact except for significantly increased female HD-VEH group. Supplementation of SFN did not indicate any effect either. In a similar gestational exposure model containing ammonium sulfate UFPs, rat offspring demonstrated reduced fetal weight and lengths [316]. Interestingly, our own previous model indicated trends of decreasing fetal crown to rump lengths with significant decreases in female LD group [394]. The lack of significance and even opposite trend requires further investigation.

To further assess the role of SFN administration and its potential ability to counter gestational UFP exposure, we evaluated several oxidative stress biomarkers. Oxidative stress pathways are implicated in adverse pregnancy outcomes [112]. NQO1 (NAD(P)H quinone dehydrogenase) is highly effective at detoxifying quinones through either NRF2 activation and/or activated as a component of AhR (aryl hydrocarbon receptor) in response to cellular stress including oxidative stress [416]. When assessing the maternal dam redox state, liver *Nqo1* expression (Figure 4.3A) was overall increased as expected from SFN

administration but significantly increased in FA-SFN compared to FA-VEH. *Nqo1* gene expression was modulated in both LD- and HD-VEH. Several disease pathologies are associated with redox disequilibrium due to environmental exposure [100, 101]. In a mouse model of diesel exhaust particle exposure, altered cysteine redox state was observed in house dust mite induced murine asthma [404]. In our model, we did not see any significant changes in redox species among the groups (Figure 4.3B and Table 4.1). The consistency in these findings suggest that the potential cellular damage that may occur by UFP exposure may be mediated by pathways other than oxidative stress, such as pro-inflammatory processes. Additional time point measures or utilizing various other GSH and/or Cys assays may better inform the redox state from our gestational SFN administration model.

Future analyses may shed light on the potential protective effects of SFN supplementation. First, identifying the SFN metabolites within the maternal serum could aide in better pharmacokinetic and pharmacodynamic dimensions underlying biological effects in the placenta. While cages, including bedding, were checked daily for peanut butter (vehicle or SFN) consumption, is may be possible that the dams may not have consumed the dose in entirety. Of the mice utilized in the study, all doses were marked as "consumed" following visual confirmation. Given our results, we anticipated large maternal *Nqo1* gene expression induction as well as increased GSH/GSSG and Cys/CySS ratios for available oxidative stress. Therefore, if SFN was not properly consumed and metabolites not found within the maternal serum and placental samples, it would indicate an issue with route of administration.

Additionally, future analyses may focus on chemical disposition of diesel exhaust particulate matter (DEPM) components to inform mitigation of placental effects. The DEPM mixture used was formulated as previously reported [394]. According to the certificate of analysis, the black carbon or diesel exhaust contained high levels of 1-nitropyrene. Therefore, the characterization of the compound may aid in determining maternal exposure and placental distribution. If incorrectly formulated, it may explain the lack of *AhR* gene expression as observed (Figure 4.4D). Considering that the expression of *Cyp1b1*, a gene downstream from *AhR*, does not correlate with *AhR* gene expression, alternative pathways for this difference needs to be explored. Additionally, further investigation needs to occur to determine if our route of administration is appropriate. We defaulted in diluting our SFN in DMSO according to manufacturer's instructions of 250 mg/mL then calculating the appropriate amount to achieve 600 PPM within 1 gram of peanut butter. However, after a cursory search, a previous paper identified that DMSO alters gene expression *in vitro* of several cellular processes including "metabolism of lipids and lipoproteins". According to the paper, human cardiac microtissues had the greatest differential gene expression alterations in the "metabolism" cluster. Utilizing DMSO as our solvent may dampened our ability to identify SFN as mitigating deleterious effects of gestational UFP exposure.

4.6. Conclusions

In summary, our study demonstrated that gestational administration of SFN concomitant with UFP exposure needs further investigation as to its potential therapeutic effects. While focusing on previously identified pathways of interests, SFN did not appear

to have the modulatory actions as anticipated. This could be due to any number of reasons such as compromised SFN product, interference of DMSO on lipid/bile acid metabolism pathways, route of SFN administration, appropriate dosing concentration, or other unknown actions. Regardless, additional investigation is needed given SFN's antioxidant effects and ease of dietary access to the compound.

4.7. Figures

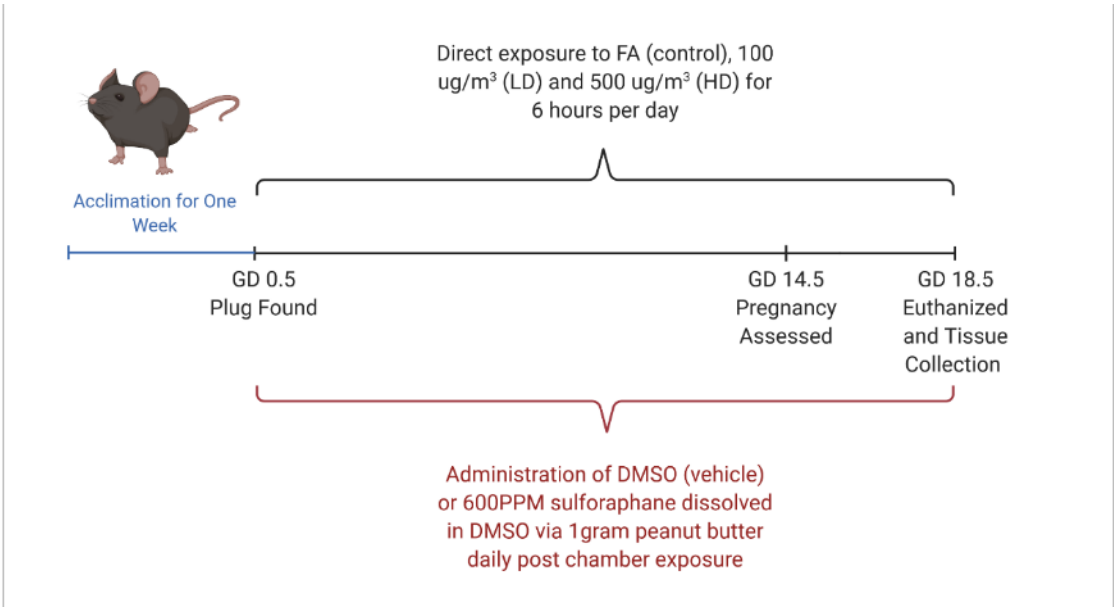

Figure 4.1 Illustration depicting exposure and ± SFN administration timeline.

Each dam had a one-week acclimation period without UFP within the exposure system prior to time-mating. Once pregnancy was assessed, dams were randomly assigned to an exposure group ± SFN administration until GD 185 as followed: filtered air without SFN (FA-VEH); filtered air with SFN (FA-SFN); low dose without SFN (LD-VEH); low

dose with SFN (LD-SFN); high dose without SFN (HD-VEH); and high dose with SFN (HD-SFN). Created with BioRender.com.

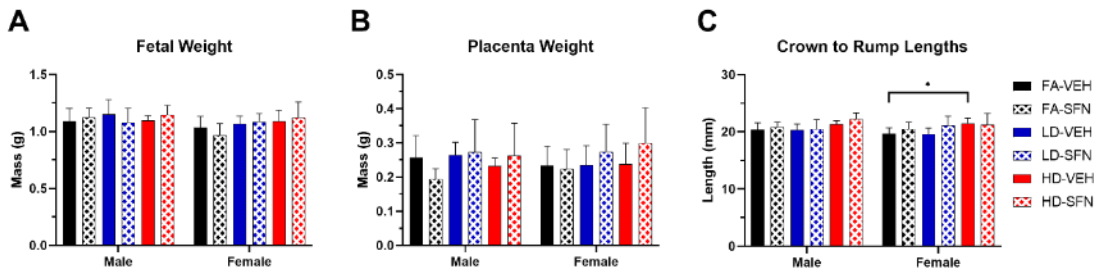

Figure 4.2 Fetal phenotypic and perinatal outcomes.

(A) Average sex-separated fetal weights at GD 18.5. (B) Average placenta weights by sex at GD 18.5. (C) Average crown to rump length at GD 18.5 show an increase in HD vs FA control in females. Offspring sample sizes include FA-VEH male (n=16), FA-SFN male (n=8), LD-VEH male (n=12), LD-SFN male (n=13), HD-VEH male (n=12), HD-SFN male (n=9), FA-VEH female (n=8), FA-SFN female (n=15), LD-VEH female (n=13), LD-SFN female (n=12), HD-VEH female (n=14), HD-SFN female (n=9). Data analyzed using two-way ANOVA with Tukey's multiple comparison test (* $p<0.05$).

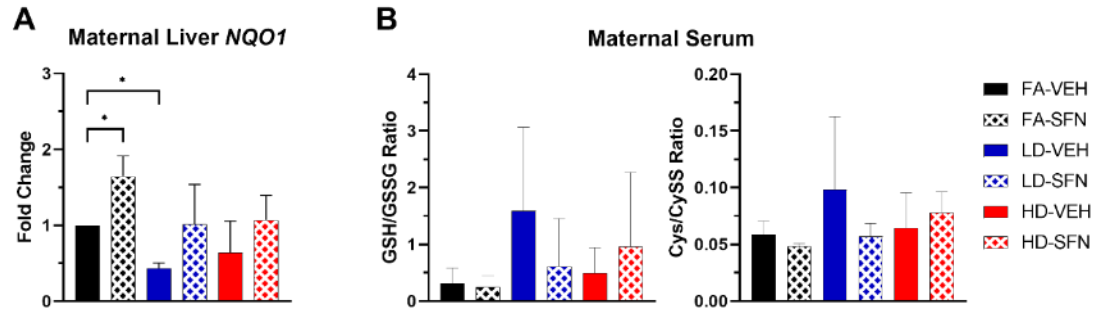

Figure 4.3 Maternal dam indicators of oxidative stress.

(A) qRT-PCR gene expression fold change of *Nqo1* in maternal dam liver. Significant differences are observed within FA-SFN and LD-VEH compared to FA-VEH. (B) Oxidative stress biomarkers illustrating glutathione/glutathione disulfide (GSH/GSSG) and cysteine/cystine (Cys/CySS) ratios. Error bars represent SD. All maternal dam groups contain a sample size of n=3. Data analyzed using one-way ANOVA with Dunnett's multiple comparison test. (*p<0.05).

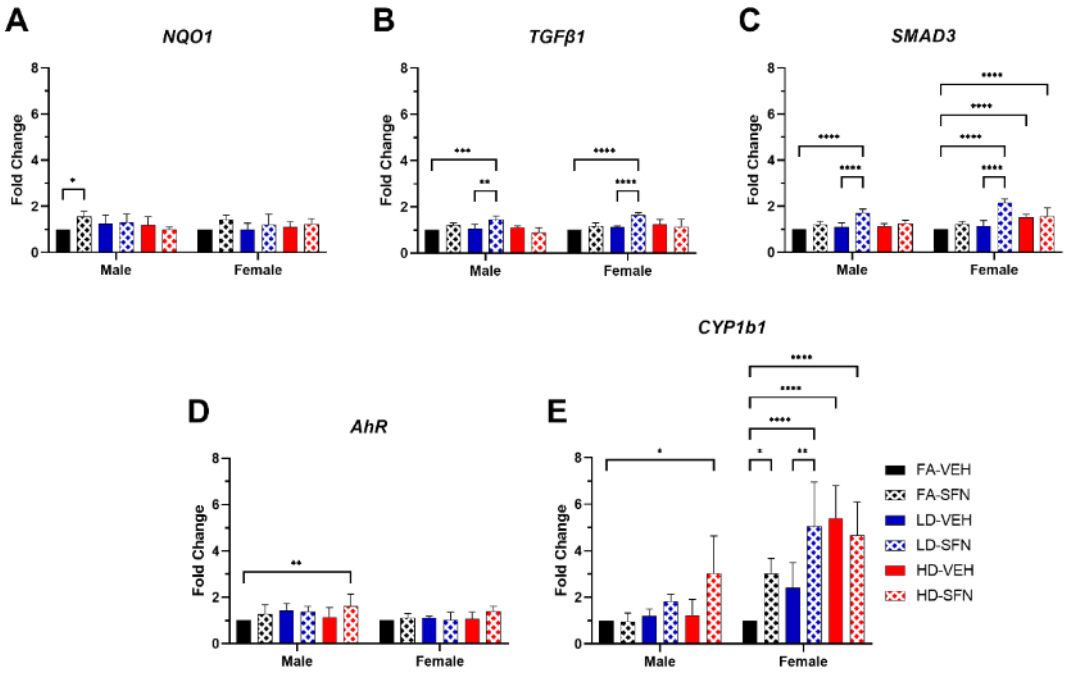

Figure 4.4 Sex-separated pooled placental gene expression data.

Fold change (A) *Nqo1*, (B) *Tgfβ1*, (C) *Smad3*, (D) *AhR*, and (E) *Cyp1b1*. Error bars represent SD. Data analyzed using two-way ANOVA with Tukey's multiple comparison test. (*P<0.05; ****P<0.0001). Sample sizes are shown in figure 4.2.

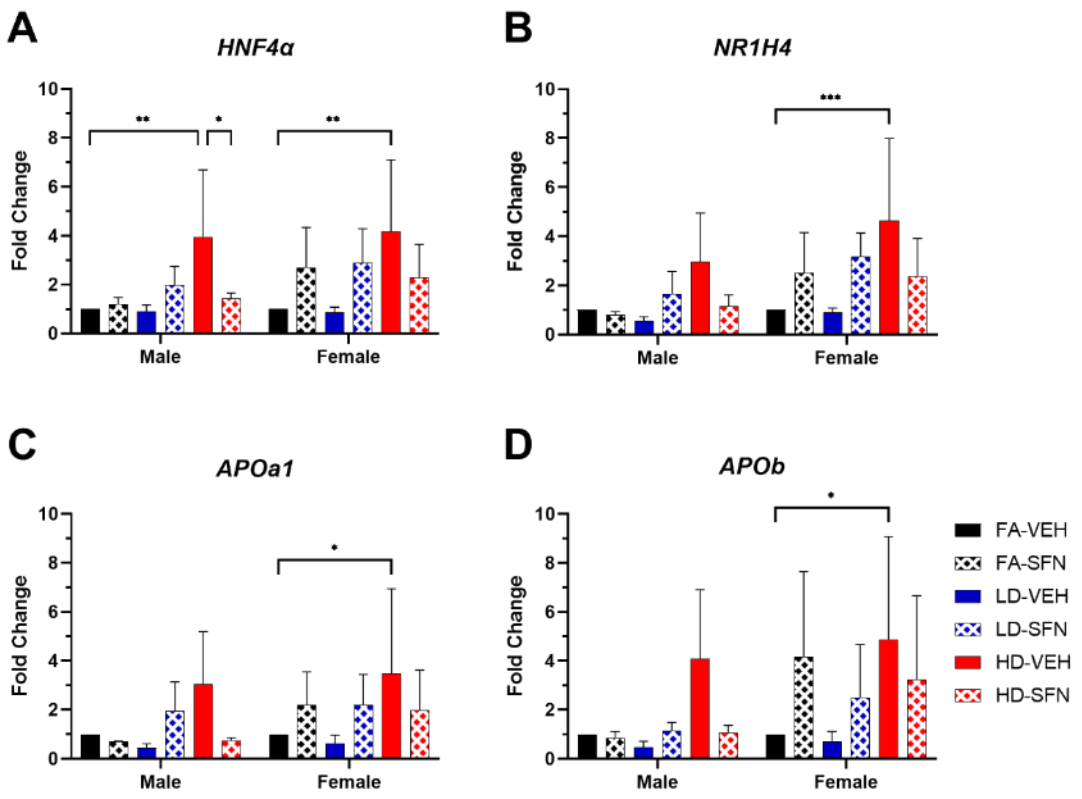

Figure 4.5 Sex-separated pooled placental gene expression data.

Fold change (A) *Hnf4α*, (B) *Nr1h4*, (C) *Apoa1*, (D) *Apob*. Error bars represent SD. Data analyzed using two-way ANOVA with Tukey's multiple comparison test. (*P<0.05; **P<0.01; ***P<0.001). Sample sizes are shown in figure 4.2.

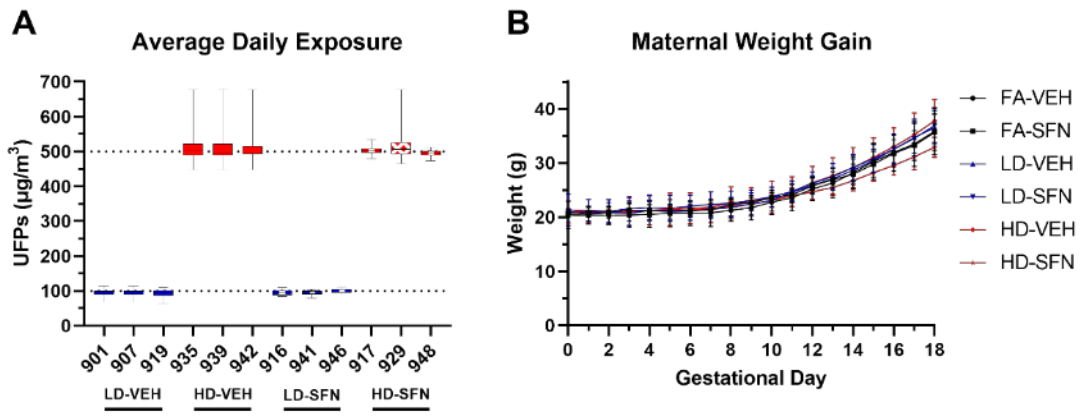

Figure 4.6 Maternal exposure data and weight gain.

(A) Individual dams indicated by ID number for LD-VEH, HD-VEH, LD-SFN, and HD-SFN with subsequent average daily UFP mass concentrations from GD 0.5 to 18.5. (B) Average maternal weight gain mean ± SD across all six exposure groups. No significant differences were observed across groups. Groups include filtered air without SFN (FA-VEH; n=3, black line with circle); filtered air with SFN (FA-SFN; n=3, black line with square); low dose without SFN (LD-VEH; n=3, blue line with upright triangle); low dose with SFN (LD-SFN; n=3, blue line with inverted triangle); high dose without SFN (HD-VEH; n=3, red line with diamond); and high dose with SFN (HD-SFN; n=3, red line with star).

Table 4.1 Maternal dam oxidative stress biomarker means ± SD in serum.

No significant differences were observed across groups. Biomarkers include glutathione (GSH), glutathione disulfide (GSSG), GSH/GSSG ratio, cysteine (Cys), cystine (CySS), and Cys/CySS ratio. All groups had an n=3. Data analyzed using two-way ANOVA with Tukey's multiple comparison test.

	Maternal Serum					
	FA-VEH	FA-SFN	LD-VEH	LD-SFN	HD-VEH	HD-SFN
GSH	0.4448 ± 0.29	0.9724 ± 0.33	1.1708 ± 0.82	0.3545 ± 0.47	4.0469 ± 5.21	0.6876 ± 0.38
GSSG	2.4118 ± 1.68	5.90056 ± 5.70	1.3662 ± 1.11	1.3174 ± 1.06	5.7569 ± 5.33	1.8007 ± 1.32
GSH/GSSG	0.3116 ± 0.27	0.2579 ± 0.19	1.5924 ± 1.47	0.6100 ± 0.85	0.4976 ± 0.44	0.9623 ± 1.31
Cys	0.6863 ± 0.14	0.4827 ± 0.09	1.1066 ± 0.42	0.6004 ± 0.19	0.7420 ± 0.26	0.9192 ± 0.30
CySS	12.1322 ± 3.87	10.0575 ± 2.31	12.7481 ± 4.96	11.0910 ± 5.50	11.9544 ± 1.77	11.6309 ± 2.11
Cys/CySS	0.0588 ± 0.01	0.0483 ± 0.00	0.0983 ± 0.06	0.0570 ± 0.01	0.0644 ± 0.03	0.0782 ± 0.02

Table 4.2 Primer sequences and product size utilized in qRT-PCR from maternal dam liver and pooled sex-separated GD 18.5 placentas.

Target	Forward Primer	Reverse Primer	NCBI Accession Number	Product Size (bp)
Nqo1	TGGCCGAACACAAGAAGCTG	GCTACGAGCACTCTCTCAAACC	NM_008706	112
Tgfβ1	CAAGGGCTACCATGCCAACT	GTACTGTGTGTCCAGGCTCCAA	NM_011577	67
Smad3	CACGCAGAACGTGAACACC	GGCAGTAGATAACGTGAGGGA	NM_016769	101
Ahr	TGTGCAGAATCCCACATCCG	AATCAAGCGTGCATTGGACTG	NM_013464	114
Cyp1b1	CAGTCTGGCGTTCGGTCAC	GCTGCGTTGGATCGAGGAA	NM_009994	197
Hnf4α	GGTTTAGCCGACAATGTGTGG	TCCCGCTCATTTTGGACAGC	NM_008261	115
Nr1h4	GCTTGATGTGCTACAAAAGCTG	CGTGGTGATGGTTGAATGTCC	NM_001163700	110
Apoa1	GCTCAAGAGCAACCCTACCTT	GCTTTCTCGCCAAGTGTCTTC	NM_009692	75
Apob	AAGCACCTCCGAAAGTACGTG	CTCCAGCTCTACCTTACAGTTGA	NM_009693	111
Gapdh	TGTCAAGCTCATTTCCTGGTATGACA	GAGTTGGGATAGGGCCTCTCTT	NM_001289726	148

5. CONCLUSIONS

5.1. Summary

The US EPA lists particulate matter as a constituent of air pollution and overall environmental exposure concern. However, there are not current guidelines established to regulate ultrafine particulate matter as there are for PM_{10} or $PM_{2.5}$. Additionally, UFPs are biologically plausible to result in increased toxicity due to their various physiochemical properties and concentration "hot spots". Furthermore, epidemiological data indicates adverse pregnancy and perinatal outcomes associated with particulate matter exposure. Therefore, these studies attempted to elucidate the cellular processes and potential mechanisms associated with UFP toxicity.

In the first aim, utilizing our murine whole body inhalation exposure model, low dose (100 $\mu g/m^3$) and high dose (500 $\mu g/m^3$) UFP levels were chosen to assess the exposure model, placenta and perinatal outcomes, and RNA sequencing for cellular pathway disruptions.

1. PM in both LD and HD chambers had a peak particle diameter of 49 and 66 nm size along with 101.40 ± 10.08 (mean ± SD) and 492.47 ± 33.14 $\mu g/m^3$ as average exposure dose concentrations respectively.
2. Gestational UFP exposures were not overtly toxic to pregnant dams. However, significant reductions in placental weight and fetal crown to rump length were observed in the LD female group. Additionally, average fetal weights and crown to rump length for both males and females indicated a decreasing trend. Finally,

increased decidua layer areas in female offspring were noted in both LD and HD groups.

3. RNA sequencing and pathway analysis clustering identified lipid transport and metabolism through farnesoid X receptor (FXR) as a primary cellular process of interest.

The second aim intended to evaluate the role of *Nrf2*, master regulator of cellular antioxidant defense, in response to UFP exposure. Knockout *Nrf2* mice were gestationally exposed in our previously defined model to assess its modulatory role.

1. *Nrf2*$^{-/-}$ demonstrated significant decreases in placental and fetal weight of females in the HD group with no histological alterations noted within the placenta.
2. GSH/GSSG ratio for female placenta was significantly increased for wildtype HD compared to HD-exposed *Nrf2*$^{-/-}$. Similarly, Cys/CySS ratio was significantly higher for wildtype than HD-exposed *Nrf2*$^{-/-}$.
3. Placental gene expression of several oxidative stress and inflammatory cytokines as well as bile acid metabolism pathways identified in aim 1 were assessed. In general, *Nrf2*$^{-/-}$demonstrated increased gene expression for *Nqo1, Ahr, Cyp1b1, Il1β, Tnfα, Tgfβ1, Smad3, and Apoa1* for female offspring. Overall, this indicates a direct impact on inflammatory cytokine signaling where lack of *Nrf2* exacerbates UFP exposure.

The third and final aim attempted to determine if dietary SFN administration offered protection from gestational UFP exposure. This proof of principle was designed to mitigate the adverse effects observed in aim 1.

1. Perinatal outcomes demonstrated, interestingly, significant increase in female crown to rump length within the HD-VEH group. Additionally, SFN administration demonstrated trends of increased fetal weight, placental weight, and fetal crown to rump length.
2. Maternal gene expression of *Nqo1* overall was increased from SFN administration, but oxidative stress biomarkers did not reveal significant differences across groups.

Overall, these studies provide evidence on the role of UFPs in adverse effects on placental development. Since pregnancy is a critical window of susceptibility, these data support protection for the most susceptible populations to prevent adverse maternal-fetal outcomes. The NRF2 antioxidant response pathway is known to play a critical role in oxidative stress response to PM. In our model, the lack of *Nrf2* enhances the pro-inflammatory effects of gestational PM exposure. However, administration of NRF2 activators during pregnancy warrants further investigation.

REFERENCES

1. Health Effects Institute. State of the Global Air 2020 2020 11/09/2020]; Available from: www.stateofglobalair.org.

2. U.S. Environmental Protection Agency. *Our Nation's Air - EPA Celebrates 50 Years!* [Web Page] 2021 [cited 2021 June 11, 2021]; Available from: https://gispub.epa.gov/air/trendsreport/2020/#home.

3. Loomis, D., et al., *The carcinogenicity of outdoor air pollution.* Lancet Oncol, 2013. **14**(13): p. 1262-3.

4. Kwon, H.S., M.H. Ryu, and C. Carlsten, *Ultrafine particles: unique physicochemical properties relevant to health and disease.* Exp Mol Med, 2020. **52**(3): p. 318-328.

5. Hofman, J., et al., *Ultrafine particles in four European urban environments: Results from a new continuous long-term monitoring network.* Atmospheric Environment, 2016. **136**: p. 68-81.

6. Peters, A., R. Rückerl, and J. Cyrys, *Lessons from air pollution epidemiology for studies of engineered nanomaterials.* J Occup Environ Med, 2011. **53**(6 Suppl): p. S8-s13.

7. Reche, C., et al., *New considerations for PM, Black Carbon and particle number concentration for air quality monitoring across different European cities.* Atmos. Chem. Phys., 2011. **11**(13): p. 6207-6227.

8. Spurny, K.R., *On the physics, chemistry and toxicology of ultrafine anthropogenic, atmospheric aerosols (UAAA): new advances.* Toxicology Letters, 1998. **96-97**: p. 253-261.

9. Kulmala, M., et al., *Formation and growth rates of ultrafine atmospheric particles: a review of observations.* Journal of Aerosol Science, 2004. **35**(2): p. 143-176.

10. Zhao, Y., F. Wang, and J. Zhao, *Size-Resolved Ultrafine Particle Deposition and Brownian Coagulation from Gasoline Vehicle Exhaust in an Environmental Test Chamber.* Environmental Science & Technology, 2015. **49**(20): p. 12153-12160.

11. Kumar, P., et al., *Chapter 15 - Ultrafine Particles Pollution and Measurements*, in *Comprehensive Analytical Chemistry*, M. de la Guardia and S. Armenta, Editors. 2016, Elsevier. p. 369-390.

12. Kumar, P., et al., *A review of factors impacting exposure to PM2.5, ultrafine particles and black carbon in Asian transport microenvironments.* Atmospheric Environment, 2018. **187**: p. 301-316.

13. Soppa, V.J., et al., *Effects of short-term exposure to fine and ultrafine particles from indoor sources on arterial stiffness – A randomized sham-controlled exposure study.* International Journal of Hygiene and Environmental Health, 2019. **222**(8): p. 1115-1132.

14. Nho, R., *Pathological effects of nano-sized particles on the respiratory system.* Nanomedicine: Nanotechnology, Biology and Medicine, 2020. **29**: p. 102242.

15. Bourdrel, T., et al., *Cardiovascular effects of air pollution.* Archives of Cardiovascular Diseases, 2017. **110**(11): p. 634-642.

16. Møller, K.L., et al., *Cardiovascular disease and long-term occupational exposure to ultrafine particles: A cohort study of airport workers.* International Journal of Hygiene and Environmental Health, 2020. **223**(1): p. 214-219.

17. Clifford, S., et al., *Effects of exposure to ambient ultrafine particles on respiratory health and systemic inflammation in children.* Environment International, 2018. **114**: p. 167-180.

18. Guo, L., et al., *Deposition of ambient ultrafine particles in the respiratory tract of children: A novel experimental method and its application.* Journal of Aerosol Science, 2020. **139**: p. 105465.

19. da Costa e Oliveira, J.R., et al., *Ultrafine particles and children's health: Literature review.* Paediatric Respiratory Reviews, 2019. **32**: p. 73-81.

20. Chen, R., et al., *Beyond PM2.5: The role of ultrafine particles on adverse health effects of air pollution.* Biochim Biophys Acta, 2016. **1860**(12): p. 2844-55.

21. Gao, R. and N. Sang, *Quasi-ultrafine particles promote cell metastasis via HMGB1-mediated cancer cell adhesion.* Environmental Pollution, 2020. **256**: p. 113390.

22. Pourret, O. and A. Hursthouse, *It's Time to Replace the Term "Heavy Metals" with "Potentially Toxic Elements" When Reporting Environmental Research.* International Journal of Environmental Research and Public Health, 2019. **16**(22).

23. Zhang, L., et al., *Size distribution of particulate polycyclic aromatic hydrocarbons in fresh combustion smoke and ambient air: A review.* Journal of Environmental Sciences, 2020. **88**: p. 370-384.

24. Santibáñez-Andrade, M., et al., *Air pollution and genomic instability: The role of particulate matter in lung carcinogenesis.* Environmental Pollution, 2017. **229**: p. 412-422.

25. Billet, S., et al., *Chemical characterization of fine and ultrafine PM, direct and indirect genotoxicity of PM and their organic extracts on pulmonary cells.* Journal of Environmental Sciences, 2018. **71**: p. 168-178.

26. Shukla, A., et al., *Air pollution associated epigenetic modifications: Transgenerational inheritance and underlying molecular mechanisms.* Science of The Total Environment, 2019. **656**: p. 760-777.

27. Chu, B., et al., *Atmospheric new particle formation in China.* Atmos. Chem. Phys., 2019. **19**(1): p. 115-138.

28. Dalmora, A.C., et al., *Nanoparticulate mineral matter from basalt dust wastes.* Chemosphere, 2016. **144**: p. 2013-2017.

29. Dias, C.L., et al., *Nanominerals and ultrafine particles from coal fires from Santa Catarina, South Brazil.* International Journal of Coal Geology, 2014. **122**: p. 50-60.

30. Moreno-Ríos, A.L., L.P. Tejeda-Benítez, and C.F. Bustillo-Lecompte, *Sources, characteristics, toxicity, and control of ultrafine particles: An overview.* Geoscience Frontiers, 2022. **13**(1): p. 101-147.

31. Keuken, M.P., et al., *Total and size-resolved particle number and black carbon concentrations near an industrial area.* Atmospheric Environment, 2015. **122**: p. 196-205.

32. Braun, M., et al., *Particulate Matter Emissions of Four Different Cigarette Types of One Popular Brand: Influence of Tobacco Strength and Additives.* Int J Environ Res Public Health, 2019. **16**(2).

33. Zhang, Q., et al., *Measurement of ultrafine particles and other air pollutants emitted by cooking activities.* Int J Environ Res Public Health, 2010. **7**(4): p. 1744-59.

34. Jones, A.M. and R.M. Harrison, *Emission of ultrafine particles from the incineration of municipal solid waste: A review.* Atmospheric Environment, 2016. **140**: p. 519-528.

35. Mishra, R.K., et al., *Urban roadside monitoring and prediction of CO, NO2 and SO2 dispersion from on-road vehicles in megacity Delhi.* Transportation Research Part D: Transport and Environment, 2016. **46**: p. 157-165.

36. Abramesko, V. and L. Tartakovsky, *Ultrafine particle air pollution inside diesel-propelled passenger trains.* Environmental Pollution, 2017. **226**: p. 288-296.

37. de Oliveira Galvão, M.F., et al., *Biomass burning particles in the Brazilian Amazon region: Mutagenic effects of nitro and oxy-PAHs and assessment of health risks.* Environmental Pollution, 2018. **233**: p. 960-970.

38. Kelly, F.J. and J.C. Fussell, *Size, source and chemical composition as determinants of toxicity attributable to ambient particulate matter.* Atmospheric Environment, 2012. **60**: p. 504-526.

39. Buzea, C., I.I. Pacheco, and K. Robbie, *Nanomaterials and nanoparticles: Sources and toxicity.* Biointerphases, 2007. **2**(4): p. MR17-MR71.

40. Schneider, I.L., et al., *Atmospheric particle number concentration and size distribution in a traffic–impacted area.* Atmospheric Pollution Research, 2015. **6**(5): p. 877-885.

41. Simkhovich, B.Z., M.T. Kleinman, and R.A. Kloner, *Air Pollution and Cardiovascular Injury: Epidemiology, Toxicology, and Mechanisms.* Journal of the American College of Cardiology, 2008. **52**(9): p. 719-726.

42. Chen, R., et al., *Beyond PM2.5: The role of ultrafine particles on adverse health effects of air pollution.* Biochimica et Biophysica Acta (BBA) - General Subjects, 2016. **1860**(12): p. 2844-2855.

43. Corsini, E., et al., *Insights on wood combustion generated proinflammatory ultrafine particles (UFP).* Toxicology Letters, 2017. **266**: p. 74-84.

44. Sydbom, A., et al., *Health effects of diesel exhaust emissions.* European Respiratory Journal, 2001. **17**(4): p. 733.

45. Agudelo-Castañeda, D.M., et al., *Cluster analysis of urban ultrafine particles size distributions.* Atmospheric Pollution Research, 2019. **10**(1): p. 45-52.

46. Lü, S., et al., *Size distribution of chemical elements and their source apportionment in ambient coarse, fine, and ultrafine particles in Shanghai urban summer atmosphere.* Journal of Environmental Sciences, 2012. **24**(5): p. 882-890.

47. Lu, S., et al., *Mineralogical characterization of ambient fine/ultrafine particles emitted from Xuanwei C1 coal combustion.* Atmospheric Research, 2016. **169**: p. 17-23.

48. Health Effects Institute. *Understanding the health effects of ambient ultrafine particles*. 2013, January; Available from: https://www.healtheffects.org/publication/understanding-health-effects-ambient-ultrafine-particles.

49. *Some non-heterocyclic polycyclic aromatic hydrocarbons and some related exposures.* IARC Monogr Eval Carcinog Risks Hum, 2010. **92**: p. 1-853.

50. Zhang, Y., et al., *Biological impact of environmental polycyclic aromatic hydrocarbons (ePAHs) as endocrine disruptors.* Environmental Pollution, 2016. **213**: p. 809-824.

51. Abbas, I., et al., *Polycyclic aromatic hydrocarbon derivatives in airborne particulate matter: sources, analysis and toxicity.* Environmental Chemistry Letters, 2018. **16**(2): p. 439-475.

52. Song, H., et al., *Seasonal variation, sources and health risk assessment of polycyclic aromatic hydrocarbons in different particle fractions of PM2.5 in Beijing, China.* Atmospheric Pollution Research, 2019. **10**(1): p. 105-114.

53. Morawska, L., et al., *Ambient nano and ultrafine particles from motor vehicle emissions: Characteristics, ambient processing and implications on human exposure.* Atmospheric Environment, 2008. **42**(35): p. 8113-8138.

54. Kumar, P., et al., *A review of the characteristics of nanoparticles in the urban atmosphere and the prospects for developing regulatory controls.* Atmospheric Environment, 2010. **44**(39): p. 5035-5052.

55. Rychlik, K.A., et al., *In utero ultrafine particulate matter exposure causes offspring pulmonary immunosuppression.* Proc Natl Acad Sci U S A, 2019. **116**(9): p. 3443-3448.

56. Kim, H.-L., et al., *MEMS-based particle detection system for measuring airborne ultrafine particles.* Sensors and Actuators A: Physical, 2018. **283**: p. 235-244.

57. Miller, M.R., C.A. Shaw, and J.P. Langrish, *From particles to patients: oxidative stress and the cardiovascular effects of air pollution.* Future Cardiology, 2012. **8**(4): p. 577-602.

58. Gao, D., et al., *Ambient particulate matter oxidative potential: Chemical determinants, associated health effects, and strategies for risk management.* Free Radical Biology and Medicine, 2020. **151**: p. 7-25.

59. Agudelo-Castañeda, D.M., et al., *Exposure to polycyclic aromatic hydrocarbons in atmospheric PM1.0 of urban environments: Carcinogenic and mutagenic*

respiratory health risk by age groups. Environmental Pollution, 2017. **224**: p. 158-170.

60. Yang, B., et al., *Effects of fine air particulates on gene expression in non-small-cell lung cancer.* Advances in Medical Sciences, 2017. **62**(2): p. 295-301.

61. Yang, L., et al., *Biomarkers of the health outcomes associated with ambient particulate matter exposure.* Science of The Total Environment, 2017. **579**: p. 1446-1459.

62. Martins, V., et al., *Chemical characterisation of particulate matter in urban transport modes.* Journal of Environmental Sciences, 2021. **100**: p. 51-61.

63. Geiser, M. and W.G. Kreyling, *Deposition and biokinetics of inhaled nanoparticles.* Part Fibre Toxicol, 2010. **7**: p. 2.

64. Ionescu, C.M., *The Human Respiratory System*, in *The Human Respiratory System*. 2013.

65. *Human respiratory tract model for radiological protection. A report of a Task Group of the International Commission on Radiological Protection.* Ann ICRP, 1994. **24**(1-3): p. 1-482.

66. Kreyling, W.G., M. Semmler-Behnke, and W. Möller, *Health implications of nanoparticles.* Journal of Nanoparticle Research, 2006. **8**(5): p. 543-562.

67. Kreyling, W.G., M. Semmler-Behnke, and W. Möller, *Ultrafine particle-lung interactions: does size matter?* J Aerosol Med, 2006. **19**(1): p. 74-83.

68. Oberdörster, G., E. Oberdörster, and J. Oberdörster, *Nanotoxicology: An Emerging Discipline Evolving from Studies of Ultrafine Particles.* Environmental Health Perspectives, 2005. **113**(7): p. 823-839.

69. Möller, W., et al., *Deposition, retention, and translocation of ultrafine particles from the central airways and lung periphery.* Am J Respir Crit Care Med, 2008. **177**(4): p. 426-32.

70. Schürch, S., et al., *Surfactant displaces particles toward the epithelium in airways and alveoli.* Respir Physiol, 1990. **80**(1): p. 17-32.

71. Bové, H., et al., *Ambient black carbon particles reach the fetal side of human placenta.* Nat Commun, 2019. **10**(1): p. 3866.

72. Wick, P., et al., *Barrier capacity of human placenta for nanosized materials.* Environ Health Perspect, 2010. **118**(3): p. 432-6.

73. Valentino, S.A., et al., *Maternal exposure to diluted diesel engine exhaust alters placental function and induces intergenerational effects in rabbits.* Part Fibre Toxicol, 2016. **13**(1): p. 39.

74. Veras, M.M., et al., *Particulate urban air pollution affects the functional morphology of mouse placenta.* Biol Reprod, 2008. **79**(3): p. 578-84.

75. Paul, E., et al., *Pulmonary exposure to metallic nanomaterials during pregnancy irreversibly impairs lung development of the offspring.* Nanotoxicology, 2017. **11**(4): p. 484-495.

76. Muoth, C., et al., *Nanoparticle transport across the placental barrier: pushing the field forward!* Nanomedicine (Lond), 2016. **11**(8): p. 941-57.

77. Chen, X.-C., et al., *Characteristics and toxicological effects of commuter exposure to black carbon and metal components of fine particles (PM2.5) in Hong Kong.* Science of The Total Environment, 2020. **742**: p. 140501.

78. Saikia, B.K., et al., *Ambient nanoparticles/nanominerals and hazardous elements from coal combustion activity: Implications on energy challenges and health hazards.* Geoscience Frontiers, 2018. **9**(3): p. 863-875.

79. Chen, Q.Y., T. DesMarais, and M. Costa, *Metals and Mechanisms of Carcinogenesis.* Annu Rev Pharmacol Toxicol, 2019. **59**: p. 537-554.

80. Platel, A., et al., *Study of in vitro and in vivo genotoxic effects of air pollution fine (PM2.5-0.18) and quasi-ultrafine (PM0.18) particles on lung models.* Science of The Total Environment, 2020. **711**: p. 134666.

81. Wei, H., et al., *Role of oxidative stress and DNA hydroxymethylation in the neurotoxicity of fine particulate matter.* Toxicology, 2017. **380**: p. 94-103.

82. Topinka, J., et al., *Ultrafine particles are not major carriers of carcinogenic PAHs and their genotoxicity in size-segregated aerosols.* Mutation Research/Genetic Toxicology and Environmental Mutagenesis, 2013. **754**(1): p. 1-6.

83. Paunescu, A.-C., et al., *Associations of black carbon with lung function and airway inflammation in schoolchildren.* Environment International, 2019. **131**: p. 104984.

84. Bhargava, A., et al., *Exposure to ultrafine particulate matter induces NF-κβ mediated epigenetic modifications.* Environmental Pollution, 2019. **252**: p. 39-50.

85. Saenen, N.D., et al., *Air pollution-induced placental alterations: an interplay of oxidative stress, epigenetics, and the aging phenotype?* Clin Epigenetics, 2019. **11**(1): p. 124.

86. Yan, Q., et al., *Maternal serum metabolome and traffic-related air pollution exposure in pregnancy.* Environ Int, 2019. **130**: p. 104872.

87. Finkel, T., *Signal transduction by reactive oxygen species.* J Cell Biol, 2011. **194**(1): p. 7-15.

88. Ma, Q., *Role of nrf2 in oxidative stress and toxicity.* Annu Rev Pharmacol Toxicol, 2013. **53**: p. 401-26.

89. Ma, Q., *Transcriptional responses to oxidative stress: Pathological and toxicological implications.* Pharmacology & Therapeutics, 2010. **125**(3): p. 376-393.

90. Finkel, T., *Signal Transduction by Mitochondrial Oxidants*.* Journal of Biological Chemistry, 2012. **287**(7): p. 4434-4440.

91. Jones, D.P. and Y. Liang, *Measuring the poise of thiol/disulfide couples in vivo.* Free Radic Biol Med, 2009. **47**(10): p. 1329-38.

92. Moi, P., et al., *Isolation of NF-E2-related factor 2 (Nrf2), a NF-E2-like basic leucine zipper transcriptional activator that binds to the tandem NF-E2/AP1 repeat of the beta-globin locus control region.* Proc Natl Acad Sci U S A, 1994. **91**(21): p. 9926-30.

93. Tonelli, C., I.I.C. Chio, and D.A. Tuveson, *Transcriptional Regulation by Nrf2.* Antioxid Redox Signal, 2018. **29**(17): p. 1727-1745.

94. Zeng, R., et al., *The long non-coding RNA MALAT1 activates Nrf2 signaling to protect human umbilical vein endothelial cells from hydrogen peroxide.* Biochemical and Biophysical Research Communications, 2018. **495**(4): p. 2532-2538.

95. Chen, J., et al., *Long noncoding RNA MALAT1 regulates generation of reactive oxygen species and the insulin responses in male mice.* Biochem Pharmacol, 2018. **152**: p. 94-103.

96. Ma, Q. and X. He, *Molecular basis of electrophilic and oxidative defense: promises and perils of Nrf2.* Pharmacol Rev, 2012. **64**(4): p. 1055-81.

97. Dinkova-Kostova, A.T., J.W. Fahey, and P. Talalay, *Chemical Structures of Inducers of Nicotinamide Quinone Oxidoreductase 1 (NQO1)*, in *Methods in Enzymology*. 2004, Academic Press. p. 423-448.

98. Dinkova-Kostova, A.T., et al., *KEAP1 and done? Targeting the NRF2 pathway with sulforaphane.* Trends in Food Science & Technology, 2017. **69**: p. 257-269.

99. Fahey, J.W., et al., *Protection of humans by plant glucosinolates: efficiency of conversion of glucosinolates to isothiocyanates by the gastrointestinal microflora.* Cancer Prev Res (Phila), 2012. **5**(4): p. 603-11.

100. Jones, D.P., *Redefining oxidative stress.* Antioxid Redox Signal, 2006. **8**(9-10): p. 1865-79.

101. Jones, D.P., *Radical-free biology of oxidative stress.* Am J Physiol Cell Physiol, 2008. **295**(4): p. C849-68.

102. Li, N., et al., *Ultrafine particulate pollutants induce oxidative stress and mitochondrial damage.* Environ Health Perspect, 2003. **111**(4): p. 455-60.

103. Pardo, M., et al., *Nrf2 protects against diverse PM2.5 components-induced mitochondrial oxidative damage in lung cells.* Sci Total Environ, 2019. **669**: p. 303-313.

104. Stejskalova, L. and P. Pavek, *The function of cytochrome P450 1A1 enzyme (CYP1A1) and aryl hydrocarbon receptor (AhR) in the placenta.* Curr Pharm Biotechnol, 2011. **12**(5): p. 715-30.

105. Shin, S., et al., *NRF2 modulates aryl hydrocarbon receptor signaling: influence on adipogenesis.* Mol Cell Biol, 2007. **27**(20): p. 7188-97.

106. Kensler, T.W., N. Wakabayashi, and S. Biswal, *Cell survival responses to environmental stresses via the Keap1-Nrf2-ARE pathway.* Annu Rev Pharmacol Toxicol, 2007. **47**: p. 89-116.

107. Kabe, Y., et al., *Redox regulation of NF-kappaB activation: distinct redox regulation between the cytoplasm and the nucleus.* Antioxid Redox Signal, 2005. **7**(3-4): p. 395-403.

108. Wakabayashi, N., et al., *When NRF2 talks, who's listening?* Antioxid Redox Signal, 2010. **13**(11): p. 1649-63.

109. Wardyn, J.D., A.H. Ponsford, and C.M. Sanderson, *Dissecting molecular cross-talk between Nrf2 and NF-kappaB response pathways.* Biochem Soc Trans, 2015. **43**(4): p. 621-6.

110. Risom, L., P. Møller, and S. Loft, *Oxidative stress-induced DNA damage by particulate air pollution.* Mutat Res, 2005. **592**(1-2): p. 119-37.

111. Ambroz, A., et al., *Impact of air pollution on oxidative DNA damage and lipid peroxidation in mothers and their newborns.* Int J Hyg Environ Health, 2016. **219**(6): p. 545-56.

112. Nagiah, S., et al., *Oxidative stress and air pollution exposure during pregnancy: A molecular assessment.* Hum Exp Toxicol, 2015. **34**(8): p. 838-47.

113. Ren, C., et al., *Lipid and endothelium-related genes, ambient particulate matter, and heart rate variability--the VA Normative Aging Study.* J Epidemiol Community Health, 2010. **64**(1): p. 49-56.

114. Hogervorst, J.G.F., et al., *Prenatal particulate air pollution exposure and cord blood homocysteine in newborns: Results from the ENVIRONAGE birth cohort.* Environ Res, 2019. **168**: p. 507-513.

115. Saenen, N.D., et al., *Placental Nitrosative Stress and Exposure to Ambient Air Pollution During Gestation: A Population Study.* Am J Epidemiol, 2016. **184**(6): p. 442-9.

116. Rosa, M.J., et al., *Identifying sensitive windows for prenatal particulate air pollution exposure and mitochondrial DNA content in cord blood.* Environ Int, 2017. **98**: p. 198-203.

117. Brunst, K.J., et al., *Prenatal particulate matter exposure and mitochondrial dysfunction at the maternal-fetal interface: Effect modification by maternal lifetime trauma and child sex.* Environ Int, 2018. **112**: p. 49-58.

118. Grevendonk, L., et al., *Mitochondrial oxidative DNA damage and exposure to particulate air pollution in mother-newborn pairs.* Environ Health, 2016. **15**: p. 10.

119. Martens, D.S., et al., *Prenatal Air Pollution and Newborns' Predisposition to Accelerated Biological Aging.* JAMA Pediatr, 2017. **171**(12): p. 1160-1167.

120. Rosa, M.J., et al., *Association between prenatal particulate air pollution exposure and telomere length in cord blood: Effect modification by fetal sex.* Environ Res, 2019. **172**: p. 495-501.

121. Erickson, A.C. and L. Arbour, *The shared pathoetiological effects of particulate air pollution and the social environment on fetal-placental development.* J Environ Public Health, 2014. **2014**: p. 901017.

122. Vadillo-Ortega, F., et al., *Air pollution, inflammation and preterm birth: a potential mechanistic link.* Med Hypotheses, 2014. **82**(2): p. 219-24.

123. Mihu, D., et al., *C-reactive protein, marker for evaluation of systemic inflammatory response in preeclampsia.* Rev Med Chir Soc Med Nat Iasi, 2008. **112**(4): p. 1019-25.

124. Lee, P.C., et al., *Particulate air pollution exposure and C-reactive protein during early pregnancy.* Epidemiology, 2011. **22**(4): p. 524-31.

125. Fedulov, A.V., et al., *Pulmonary exposure to particles during pregnancy causes increased neonatal asthma susceptibility.* Am J Respir Cell Mol Biol, 2008. **38**(1): p. 57-67.

126. Morales-Rubio, R.A., et al., *In utero exposure to ultrafine particles promotes placental stress-induced programming of renin-angiotensin system-related elements in the offspring results in altered blood pressure in adult mice.* Part Fibre Toxicol, 2019. **16**(1): p. 7.

127. Sharkhuu, T., et al., *Effects of prenatal diesel exhaust inhalation on pulmonary inflammation and development of specific immune responses.* Toxicol Lett, 2010. **196**(1): p. 12-20.

128. Fujimoto, A., et al., *Diesel exhaust affects immunological action in the placentas of mice.* Environ Toxicol, 2005. **20**(4): p. 431-40.

129. Ye, Z., et al., *In Utero Exposure to Fine Particulate Matter Causes Hypertension Due to Impaired Renal Dopamine D1 Receptor in Offspring.* Cell Physiol Biochem, 2018. **46**(1): p. 148-159.

130. de Melo, J.O., et al., *Inhalation of fine particulate matter during pregnancy increased IL-4 cytokine levels in the fetal portion of the placenta.* Toxicol Lett, 2015. **232**(2): p. 475-80.

131. Liu, W., et al., *The Influence of Quercetin on Maternal Immunity, Oxidative Stress, and Inflammation in Mice with Exposure of Fine Particulate Matter during Gestation.* Int J Environ Res Public Health, 2017. **14**(6).

132. Liu, Y., et al., *Effect of Fine Particulate Matter (PM2.5) on Rat Placenta Pathology and Perinatal Outcomes.* Med Sci Monit, 2016. **22**: p. 3274-80.

133. Veras, M.M., et al., *The effects of particulate ambient air pollution on the murine umbilical cord and its vessels: a quantitative morphological and immunohistochemical study.* Reprod Toxicol, 2012. **34**(4): p. 598-606.

134. Wang, P., et al., *Maternal exposure to combustion generated PM inhibits pulmonary Th1 maturation and concomitantly enhances postnatal asthma development in offspring.* Part Fibre Toxicol, 2013. **10**: p. 29.

135. Jirtle, R.L. and M.K. Skinner, *Environmental epigenomics and disease susceptibility.* Nature reviews genetics, 2007. **8**(4): p. 253.

136. Hamm, C.A. and F.F. Costa, *Epigenomes as therapeutic targets.* Pharmacology & Therapeutics, 2015. **151**: p. 72-86.

137. Waddington, C.H., *Organisers and genes.* Organisers and genes., 1940.

138. Ferrari, L., M. Carugno, and V. Bollati, *Particulate matter exposure shapes DNA methylation through the lifespan.* Clin Epigenetics, 2019. **11**(1): p. 129.

139. Vaiserman, A., *Epidemiologic evidence for association between adverse environmental exposures in early life and epigenetic variation: a potential link to disease susceptibility?* Clinical epigenetics, 2015. **7**(1): p. 96.

140. Janssen, B.G., et al., *Placental DNA hypomethylation in association with particulate air pollution in early life.* Particle and fibre toxicology, 2013. **10**(1): p. 22.

141. Fraga, M.F. and M. Esteller, *Epigenetics and aging: the targets and the marks.* Trends in genetics, 2007. **23**(8): p. 413-418.

142. Wilson, A.S., B.E. Power, and P.L. Molloy, *DNA hypomethylation and human diseases.* Biochimica et Biophysica Acta (BBA)-Reviews on Cancer, 2007. **1775**(1): p. 138-162.

143. Reichetzeder, C., et al., *Increased global placental DNA methylation levels are associated with gestational diabetes.* Clinical epigenetics, 2016. **8**(1): p. 82.

144. Jin, S., et al., *Global DNA hypermethylation in down syndrome placenta.* PLoS genetics, 2013. **9**(6): p. e1003515.

145. Kingsley, S.L., et al., *Maternal residential proximity to major roadways, birth weight, and placental DNA methylation.* Environ Int, 2016. **92-93**: p. 43-9.

146. Maghbooli, Z., et al., *Air pollution during pregnancy and placental adaptation in the levels of global DNA methylation.* PloS one, 2018. **13**(7): p. e0199772.

147. Saenen, N.D., et al., *Lower placental leptin promoter methylation in association with fine particulate matter air pollution during pregnancy and placental*

nitrosative stress at birth in the ENVIR ON AGE cohort. Environmental health perspectives, 2016. **125**(2): p. 262-268.

148. Zhou, G., et al., *Prenatal ambient air pollution exposure and SOD2 promoter methylation in maternal and cord blood.* Ecotoxicol Environ Saf, 2019. **181**: p. 428-434.

149. Breton, C.V., et al., *Particulate matter, the newborn methylome, and cardio-respiratory health outcomes in childhood.* Environ Epigenet, 2016. **2**(2): p. dvw005.

150. Yang, A.S., et al., *A simple method for estimating global DNA methylation using bisulfite PCR of repetitive DNA elements.* Nucleic acids research, 2004. **32**(3): p. e38-e38.

151. Neven, K.Y., et al., *Placental promoter methylation of DNA repair genes and prenatal exposure to particulate air pollution: an ENVIRONAGE cohort study.* The Lancet Planetary Health, 2018. **2**(4): p. e174-e183.

152. Alvarado-Cruz, I., et al., *Increased methylation of repetitive elements and DNA repair genes is associated with higher DNA oxidation in children in an urbanized, industrial environment.* Mutation Research/Genetic Toxicology and Environmental Mutagenesis, 2017. **813**: p. 27-36.

153. Wallace, D.C., *Mitochondrial DNA mutations in disease and aging.* Environmental and molecular mutagenesis, 2010. **51**(5): p. 440-450.

154. Janssen, B.G., et al., *Placental mitochondrial methylation and exposure to airborne particulate matter in the early life environment: an ENVIR ON AGE birth cohort study.* Epigenetics, 2015. **10**(6): p. 536-544.

155. Nana-Sinkam, S.P., et al., *Integrating the MicroRNome into the study of lung disease.* American journal of respiratory and critical care medicine, 2009. **179**(1): p. 4-10.

156. Erson, A. and E. Petty, *MicroRNAs in development and disease.* Clinical genetics, 2008. **74**(4): p. 296-306.

157. Alvarez-Garcia, I. and E.A. Miska, *MicroRNA functions in animal development and human disease.* Development, 2005. **132**(21): p. 4653-4662.

158. Tsamou, M., et al., *Air pollution-induced placental epigenetic alterations in early life: a candidate miRNA approach.* Epigenetics, 2018. **13**(2): p. 135-146.

159. Bollati, V., et al., *Exposure to metal-rich particulate matter modifies the expression of candidate microRNAs in peripheral blood leukocytes.* Environmental health perspectives, 2010. **118**(6): p. 763-768.

160. Bourdon, J.A., et al., *Carbon black nanoparticle intratracheal installation results in large and sustained changes in the expression of miR-135b in mouse lung.* Environmental and molecular mutagenesis, 2012. **53**(6): p. 462-468.

161. Amoroso, E.C., *The evolution of viviparity.* Proc R Soc Med, 1968. **61**(11 Pt 2): p. 1188-1200.

162. Watson, E.D. and J.C. Cross, *Development of structures and transport functions in the mouse placenta.* Physiology (Bethesda), 2005. **20**: p. 180-93.

163. Cross, J.C., D.G. Simmons, and E.D. Watson, *Chorioallantoic morphogenesis and formation of the placental villous tree.* Ann N Y Acad Sci, 2003. **995**: p. 84-93.

164. Soares, M.J., K.M. Varberg, and K. Iqbal, *Hemochorial placentation: development, function, and adaptations†.* Biology of Reproduction, 2018. **99**(1): p. 196-211.

165. Gundling, W.E., Jr. and D.E. Wildman, *A review of inter- and intraspecific variation in the eutherian placenta.* Philos Trans R Soc Lond B Biol Sci, 2015. **370**(1663): p. 20140072.

166. Benirschke, K. and P. Kaufmann, *Placental Types*, in *Pathology of the Human Placenta*, K. Benirschke and P. Kaufmann, Editors. 2000, Springer New York: New York, NY. p. 29-41.

167. Roberts, R.M., J.A. Green, and L.C. Schulz, *The evolution of the placenta.* Reproduction, 2016. **152**(5): p. R179-R189.

168. Carter, A.M., *Animal Models of Human Placentation – A Review.* Placenta, 2007. **28**: p. S41-S47.

169. Carter, A.M., *Evolution of the Placenta and Fetal Membranes Seen in the Light of Molecular Phylogenetics.* Placenta, 2001. **22**(10): p. 800-807.

170. Georgiades, P., A.C. Ferguson-Smith, and G.J. Burton, *Comparative Developmental Anatomy of the Murine and Human Definitive Placentae.* Placenta, 2002. **23**(1): p. 3-19.

171. Rossant, J. and J.C. Cross, *Placental development: Lessons from mouse mutants.* Nature Reviews Genetics, 2001. **2**(7): p. 538-548.

172. Adamson, S.L., et al., *Interactions between Trophoblast Cells and the Maternal and Fetal Circulation in the Mouse Placenta.* Developmental Biology, 2002. **250**(2): p. 358-373.

173. Monk, J.M., et al., *Induction of murine spiral artery modification by recombinant human interferon-gamma.* Placenta, 2005. **26**(10): p. 835-838.

174. Moffett, A. and C. Loke, *Immunology of placentation in eutherian mammals.* Nature Reviews Immunology, 2006. **6**(8): p. 584-594.

175. Malassiné, A., J.L. Frendo, and D. Evain-Brion, *A comparison of placental development and endocrine functions between the human and mouse model.* Human Reproduction Update, 2003. **9**(6): p. 531-539.

176. Soares, M.J., et al., *Rat placentation: An experimental model for investigating the hemochorial maternal-fetal interface.* Placenta, 2012. **33**(4): p. 233-243.

177. Hill, P.M. and M. Young, *Net placental transfer of free amino acids against varying concentrations.* J Physiol, 1973. **235**(2): p. 409-22.

178. Jansson, T. and E. Persson, *Placental Transfer of Glucose and Amino Acids in Intrauterine Growth Retardation: Studies with Substrate Analogs in the Awake Guinea Pig.* Pediatric Research, 1990. **28**(3): p. 203-208.

179. Enders, A.C., *A comparative study of the fine structure of the trophoblast in several hemochorial placentas.* American Journal of Anatomy, 1965. **116**(1): p. 29-67.

180. Rodrigues, R.F., et al., *The subplacenta of the red-rumped agouti (Dasyprocta leporina L).* Reproductive Biology and Endocrinology, 2006. **4**(1): p. 31.

181. Clausen, H.V., L.G. Larsen, and A.M. Carter, *Vascular Reactivity of the Preplacental Vasculature in Guinea Pigs.* Placenta, 2003. **24**(6): p. 686-697.

182. Gallaher, B.W., et al., *Periconceptual undernutrition resets plasma IGFBP levels and alters the response of IGFBP-1, IGFBP-3 and IGF-1 to subsequent maternal undernutrition in fetal sheep.* Progress in Growth Factor Research, 1995. **6**(2): p. 189-195.

183. Morrison, J.L., *Sheep models of intrauterine growth restriction: fetal adaptations and consequences.* Clin Exp Pharmacol Physiol, 2008. **35**(7): p. 730-43.

184. Carter, A.M. and A. Mess, *Evolution of the Placenta in Eutherian Mammals.* Placenta, 2007. **28**(4): p. 259-262.

185. Fazleabas, A.T., et al., *A Modified Baboon Model for Endometriosis.* Annals of the New York Academy of Sciences, 2002. **955**(1): p. 308-317.

186. Schramm, R.D. and B.D. Bavister, *A macaque model for studying mechanisms controlling oocyte development and maturation in human and non-human primates.* Human Reproduction, 1999. **14**(10): p. 2544-2555.

187. Blankenship, T.N. and A.C. Enders, *Modification of uterine vasculature during pregnancy in macaques.* Microscopy Research and Technique, 2003. **60**(4): p. 390-401.

188. Ramsey, E.M. and M.W. Donner, *Placental Vasculature and Circulation in Primates*, in *Placental Vascularization and Blood Flow: Basic Research and Clinical Applications*, P. Kaufmann and R.K. Miller, Editors. 1988, Springer US: Boston, MA. p. 217-233.

189. de Rijk, E.P.C.T. and E. Van Esch, *The Macaque Placenta: A Mini-Review*. 2008, Taylor & Francis: Great Britain. p. 108S.

190. Enders, A.C., *Transition from lacunar to villous stage of implantation in the macaque, including establishment of the trophoblastic shell.* Acta Anat (Basel), 1995. **152**(3): p. 151-69.

191. Enders, A.C., K.C. Lantz, and S. Schlafke, *Preference of Invasive Cytotrophoblast for Maternal Vessels in Early Implantation in the Macaque.* Cells Tissues Organs, 1996. **155**(3): p. 145-162.

192. Pijnenborg, R., et al., *Evaluation of trophoblast invasion in placental bed biopsies of the baboon, with immunohistochemical localisation of cytokeratin, fibronectin, and laminin.* Journal of Medical Primatology, 1996. **25**(4): p. 272-281.

193. Pijnenborg, R., L. Vercruysse, and M. Hanssens, *The Uterine Spiral Arteries In Human Pregnancy: Facts and Controversies.* Placenta, 2006. **27**(9): p. 939-958.

194. Coan, P.M., et al., *Adaptations in placental nutrient transfer capacity to meet fetal growth demands depend on placental size in mice.* The Journal of Physiology, 2008. **586**(18): p. 4567-4576.

195. Soares, M.J., *The prolactin and growth hormone families: Pregnancy-specific hormones/cytokines at the maternal-fetal interface.* Reproductive Biology and Endocrinology, 2004. **2**(1): p. 51.

196. Simmons, D.G., A.L. Fortier, and J.C. Cross, *Diverse subtypes and developmental origins of trophoblast giant cells in the mouse placenta.* Dev Biol, 2007. **304**(2): p. 567-78.

197. Simmons, D.G., et al., *Spatial and temporal expression of the 23 murine Prolactin/Placental Lactogen-related genes is not associated with their position in the locus.* BMC Genomics, 2008. **9**(1): p. 352.

198. Coan, P.M., et al., *Origin and characteristics of glycogen cells in the developing murine placenta.* Developmental Dynamics, 2006. **235**(12): p. 3280-3294.

199. Metz, J., D. Heinrich, and W.G. Forssmann, *Gap junctions in hemodichorial and hemotrichorial placentae.* Cell and Tissue Research, 1976. **171**(3): p. 305-315.

200. Coan, P.M., A.C. Ferguson-Smith, and G.J. Burton, *Ultrastructural changes in the interhaemal membrane and junctional zone of the murine chorioallantoic placenta across gestation.* Journal of Anatomy, 2005. **207**(6): p. 783-796.

201. Cross, J.C., Z. Werb, and S.J. Fisher, *Implantation and the placenta: key pieces of the development puzzle.* Science, 1994. **266**(5190): p. 1508-18.

202. Latos, P.A. and M. Hemberger, *From the stem of the placental tree: trophoblast stem cells and their progeny.* Development, 2016. **143**(20): p. 3650-3660.

203. Woods, L., V. Perez-Garcia, and M. Hemberger, *Regulation of Placental Development and Its Impact on Fetal Growth—New Insights From Mouse Models.* Frontiers in Endocrinology, 2018. **9**: p. 570.

204. Copp, A.J., *Interaction between inner cell mass and trophectoderm of the mouse blastocyst. II. The fate of the polar trophectoderm.* J Embryol Exp Morphol, 1979. **51**: p. 109-20.

205. Hemberger, M., *Health during pregnancy and beyond: Fetal trophoblast cells as chief co-ordinators of intrauterine growth and reproductive success.* Annals of Medicine, 2012. **44**(4): p. 325-337.

206. Soares, M.J., K. Iqbal, and K. Kozai, *Hypoxia and Placental Development.* Birth Defects Res, 2017. **109**(17): p. 1309-1329.

207. Parr, M.B., H.N. Tung, and E.L. Parr, *The ultrastructure of the rat primary decidual zone.* Am J Anat, 1986. **176**(4): p. 423-36.

208. Burton, G.J., A.L. Fowden, and K.L. Thornburg, *Placental Origins of Chronic Disease.* Physiological Reviews, 2016. **96**(4): p. 1509-1565.

209. Simmons, D.G., et al., *Early patterning of the chorion leads to the trilaminar trophoblast cell structure in the placental labyrinth.* Development, 2008. **135**(12): p. 2083-2091.

210. Anson-Cartwright, L., et al., *The glial cells missing-1 protein is essential for branching morphogenesis in the chorioallantoic placenta.* Nature Genetics, 2000. **25**(3): p. 311-314.

211. Pardi, G., A.M. Marconi, and I. Cetin, *Placental-fetal Interrelationship in IUGR Fetuses—A Review.* Placenta, 2002. **23**: p. S136-S141.

212. Hu, D. and J.C. Cross, *Ablation of Tpbpa-positive trophoblast precursors leads to defects in maternal spiral artery remodeling in the mouse placenta.* Developmental Biology, 2011. **358**(1): p. 231-239.

213. Ain, R., L.N. Canham, and M.J. Soares, *Gestation stage-dependent intrauterine trophoblast cell invasion in the rat and mouse: novel endocrine phenotype and regulation.* Developmental Biology, 2003. **260**(1): p. 176-190.

214. Salafia, C.M., et al., *Placental surface shape, function, and effects of maternal and fetal vascular pathology.* Placenta, 2010. **31**(11): p. 958-962.

215. Burton, G.J. and E. Jauniaux, *Sonographic, stereological and Doppler flow velocimetric assessments of placental maturity.* BJOG: An International Journal of Obstetrics & Gynaecology, 1995. **102**(10): p. 818-825.

216. Carter, A.M., A.C. Enders, and R. Pijnenborg, *The role of invasive trophoblast in implantation and placentation of primates.* Philosophical Transactions of the Royal Society B: Biological Sciences, 2015. **370**(1663): p. 20140070.

217. Huppertz, B., *The anatomy of the normal placenta.* Journal of Clinical Pathology, 2008. **61**(12): p. 1296.

218. Burton, G.J., M. Scioscia, and T.W. Rademacher, *Endometrial secretions: creating a stimulatory microenvironment within the human early placenta and implications for the aetiopathogenesis of preeclampsia.* Journal of Reproductive Immunology, 2011. **89**(2): p. 118-125.

219. Burton, G.J., et al., *Uterine Glands Provide Histiotrophic Nutrition for the Human Fetus during the First Trimester of Pregnancy.* The Journal of Clinical Endocrinology & Metabolism, 2002. **87**(6): p. 2954-2959.

220. Pötgens, A.J.G., et al., *Mechanisms of Syncytial Fusion: A Review.* Placenta, 2002. **23**: p. S107-S113.

221. Pötgens, A.J.G., et al., *Syncytin: the major regulator of trophoblast fusion? Recent developments and hypotheses on its action.* Human Reproduction Update, 2004. **10**(6): p. 487-496.

222. Huppertz, B., et al., *Villous cytotrophoblast regulation of the syncytial apoptotic cascade in the human placenta.* Histochemistry and Cell Biology, 1998. **110**(5): p. 495-508.

223. Huppertz, B., et al., *Oxygen as modulator of trophoblast invasion.* Journal of Anatomy, 2009. **215**(1): p. 14-20.

224. Zhou, Y., et al., *Human cytotrophoblasts adopt a vascular phenotype as they differentiate. A strategy for successful endovascular invasion?* The Journal of Clinical Investigation, 1997. **99**(9): p. 2139-2151.

225. Ashton, S.V., et al., *Uterine spiral artery remodeling involves endothelial apoptosis induced by extravillous trophoblasts through Fas/FasL interactions.* Arterioscler Thromb Vasc Biol, 2005. **25**(1): p. 102-8.

226. Burton, G.J., J. Hempstock, and E. Jauniaux, *Oxygen, early embryonic metabolism and free radical-mediated embryopathies.* Reproductive BioMedicine Online, 2003. **6**(1): p. 84-96.

227. Haram, K., et al., *Early development of the human placenta and pregnancy complications.* The Journal of Maternal-Fetal & Neonatal Medicine, 2020. **33**(20): p. 3538-3545.

228. Kingdom, J., et al., *Development of the placental villous tree and its consequences for fetal growth.* European Journal of Obstetrics & Gynecology and Reproductive Biology, 2000. **92**(1): p. 35-43.

229. Brosens, I., et al., *The "Great Obstetrical Syndromes" are associated with disorders of deep placentation.* American Journal of Obstetrics and Gynecology, 2011. **204**(3): p. 193-201.

230. Mayhew, T.M., *Fetoplacental Angiogenesis During Gestation is Biphasic, Longitudinal and Occurs by Proliferation and Remodelling of Vascular Endothelial Cells.* Placenta, 2002. **23**(10): p. 742-750.

231. Wilkening, R.B. and G. Meschia, *Current topic: comparative physiology of placental oxygen transport.* Placenta, 1992. **13**(1): p. 1-15.

232. Day, P.E., et al., *What factors determine placental glucose transfer kinetics?* Placenta, 2013. **34**(10): p. 953-8.

233. Illsley, N.P., *Glucose transporters in the human placenta.* Placenta, 2000. **21**(1): p. 14-22.

234. Nagai, A., et al., *Cellular expression of the monocarboxylate transporter (MCT) family in the placenta of mice.* Placenta, 2010. **31**(2): p. 126-33.

235. Cleal, J.K. and R.M. Lewis, *The mechanisms and regulation of placental amino acid transport to the human foetus.* J Neuroendocrinol, 2008. **20**(4): p. 419-26.

236. Kulkarni, S.R., et al., *Maternal lipids are as important as glucose for fetal growth: findings from the Pune Maternal Nutrition Study.* Diabetes Care, 2013. **36**(9): p. 2706-13.

237. Woollett, L.A., *Review: Transport of maternal cholesterol to the fetal circulation.* Placenta, 2011. **32**: p. S218-S221.

238. Wittmaack, F.M., et al., *Localization and regulation of the human very low density lipoprotein/apolipoprotein-E receptor: trophoblast expression predicts a role for the receptor in placental lipid transport.* Endocrinology, 1995. **136**(1): p. 340-8.

239. Ethier-Chiasson, M., et al., *Influence of maternal lipid profile on placental protein expression of LDLr and SR-BI.* Biochemical and Biophysical Research Communications, 2007. **359**(1): p. 8-14.

240. Alsat, E. and A. Malassiné, *High density lipoprotein interaction with human placenta: Biochemical and ultrastructural characterization of binding to microvillous receptor and lack of internalization.* Molecular and Cellular Endocrinology, 1991. **77**(1): p. 97-108.

241. Murata, M., et al., *Decreased very-low-density lipoprotein and low-density lipoprotein receptor messenger ribonucleic acid expression in placentas from preeclamptic pregnancies.* Am J Obstet Gynecol, 1996. **175**(6): p. 1551-6.

242. Wadsack, C., et al., *Intrauterine growth restriction is associated with alterations in placental lipoprotein receptors and maternal lipoprotein composition.* American Journal of Physiology-Endocrinology and Metabolism, 2007. **292**(2): p. E476-E484.

243. Gauster, M., et al., *Dysregulation of placental endothelial lipase and lipoprotein lipase in intrauterine growth-restricted pregnancies.* J Clin Endocrinol Metab, 2007. **92**(6): p. 2256-63.

244. Duttaroy, A.K., *Transport of fatty acids across the human placenta: a review.* Prog Lipid Res, 2009. **48**(1): p. 52-61.

245. Schneider, H. and R.K. Miller, *Receptor-mediated uptake and transport of macromolecules in the human placenta.* Int J Dev Biol, 2010. **54**(2-3): p. 367-75.

246. Lambot, N., et al., *Evidence for a clathrin-mediated recycling of albumin in human term placenta.* Biol Reprod, 2006. **75**(1): p. 90-7.

247. Beckman, D.A., J.B. Lloyd, and R.L. Brent, *Quantitative studies on the mechanisms of amino acid supply to rat embryos during organogenesis.* Reprod Toxicol, 1998. **12**(2): p. 197-200.

248. Napso, T., et al., *The Role of Placental Hormones in Mediating Maternal Adaptations to Support Pregnancy and Lactation.* Front Physiol, 2018. **9**: p. 1091.

249. Wiemers, D.O., et al., *The Mouse Prolactin Gene Family Locus.* Endocrinology, 2003. **144**(1): p. 313-325.

250. Linzer, D.I.H. and S.J. Fisher, *The Placenta and the Prolactin Family of Hormones: Regulation of the Physiology of Pregnancy.* Molecular Endocrinology, 1999. **13**(6): p. 837-840.

251. Soares, M.J., T. Konno, and S.M.K. Alam, *The prolactin family: effectors of pregnancy-dependent adaptations.* Trends in Endocrinology & Metabolism, 2007. **18**(3): p. 114-121.

252. Weinhaus, A.J., L.E. Stout, and R.L. Sorenson, *Glucokinase, hexokinase, glucose transporter 2, and glucose metabolism in islets during pregnancy and prolactin-treated islets in vitro: mechanisms for long term up-regulation of islets.* Endocrinology, 1996. **137**(5): p. 1640-1649.

253. Bridges, R.S., et al., *Central Lactogenic Regulation of Maternal Behavior in Rats: Steroid Dependence, Hormone Specificity, and Behavioral Potencies of Rat Prolactin and Rat Placental Lactogen I*.* Endocrinology, 1997. **138**(2): p. 756-763.

254. Costa, M.A., *The endocrine function of human placenta: an overview.* Reproductive BioMedicine Online, 2016. **32**(1): p. 14-43.

255. Edey, L.F., et al., *Progesterone, the maternal immune system and the onset of parturition in the mouse†.* Biology of Reproduction, 2018. **98**(3): p. 376-395.

256. Qi, X., et al., *Decreased cord blood estradiol levels in related to mothers with gestational diabetes.* Medicine, 2017. **96**(21): p. e6962-e6962.

257. Açıkgöz, S., et al., *Levels of oxidized LDL, estrogens, and progesterone in placenta tissues and serum paraoxonase activity in preeclampsia.* Mediators Inflamm, 2013. **2013**: p. 862982.

258. Leturque, A., et al., *Pregnancy-induced insulin resistance in the rat: assessment by glucose clamp technique.* American Journal of Physiology-Endocrinology and Metabolism, 1984. **246**(1): p. E25-E31.

259. Ahmed-Sorour, H. and C.J. Bailey, *Role of ovarian hormones in the long-term control of glucose homeostasis. Interaction with insulin, glucagon and epinephrine.* Horm Res, 1980. **13**(6): p. 396-403.

260. Stelmańska, E. and E. Sucajtys-Szulc, *Enhanced food intake by progesterone-treated female rats is related to changes in neuropeptide genes expression in hypothalamus.* Endokrynol Pol, 2014. **65**(1): p. 46-56.

261. Fungfuang, W., et al., *Effects of estrogen on food intake, serum leptin levels and leptin mRNA expression in adipose tissue of female rats.* Lab Anim Res, 2013. **29**(3): p. 168-73.

262. Fang, X., S. Wong, and B.F. Mitchell, *Effects of RU486 on Estrogen, Progesterone, Oxytocin, and Their Receptors in the Rat Uterus during Late Gestation*.* Endocrinology, 1997. **138**(7): p. 2763-2768.

263. Kota, S.K., et al., *Endocrinology of parturition.* Indian J Endocrinol Metab, 2013. **17**(1): p. 50-9.

264. Chandran, S., et al., *Transcriptomic effects of estradiol treatment on cultured human uterine smooth muscle cells.* Molecular and Cellular Endocrinology, 2014. **393**(1): p. 16-23.

265. Lee, H.J., et al., *Progesterone drives mammary secretory differentiation via RankL-mediated induction of Elf5 in luminal progenitor cells.* Development, 2013. **140**(7): p. 1397-1401.

266. Ribeiro, A.C., et al., *siRNA silencing of estrogen receptor-α expression specifically in medial preoptic area neurons abolishes maternal care in female mice.* Proceedings of the National Academy of Sciences, 2012. **109**(40): p. 16324.

267. Soliman, A., et al., *Placental melatonin system is present throughout pregnancy and regulates villous trophoblast differentiation.* Journal of Pineal Research, 2015. **59**(1): p. 38-46.

268. Wu, H.-H., S. Choi, and P. Levitt, *Differential patterning of genes involved in serotonin metabolism and transport in extra-embryonic tissues of the mouse.* Placenta, 2016. **42**: p. 74-83.

269. de Pedro, M.A., et al., *Circadian Kisspeptin expression in human term placenta.* Placenta, 2015. **36**(11): p. 1337-1339.

270. Bajoria, R. and M. Babawale, *Ontogeny of Endogenous Secretion of Immunoreactive-Thyrotropin Releasing Hormone by the Human Placenta.* The Journal of Clinical Endocrinology & Metabolism, 1998. **83**(11): p. 4148-4155.

271. van Gelder, M.M.H.J., et al., *Teratogenic mechanisms of medical drugs.* Human Reproduction Update, 2010. **16**(4): p. 378-394.

272. Robbins, J.R., et al., *Placental syncytiotrophoblast constitutes a major barrier to vertical transmission of Listeria monocytogenes.* PLoS Pathog, 2010. **6**(1): p. e1000732.

273. Aye, I.L. and J.A. Keelan, *Placental ABC transporters, cellular toxicity and stress in pregnancy.* Chem Biol Interact, 2013. **203**(2): p. 456-66.

274. Vähäkangas, K. and P. Myllynen, *Drug transporters in the human blood-placental barrier.* Br J Pharmacol, 2009. **158**(3): p. 665-78.

275. Myllynen, P., M. Pasanen, and O. Pelkonen, *Human placenta: a human organ for developmental toxicology research and biomonitoring.* Placenta, 2005. **26**(5): p. 361-71.

276. McMillen, I.C. and J.S. Robinson, *Developmental Origins of the Metabolic Syndrome: Prediction, Plasticity, and Programming.* Physiological Reviews, 2005. **85**(2): p. 571-633.

277. Barker, D.J. and K.L. Thornburg, *The obstetric origins of health for a lifetime.* Clin Obstet Gynecol, 2013. **56**(3): p. 511-9.

278. Barker, D.J.P., et al., *WEIGHT IN INFANCY AND DEATH FROM ISCHAEMIC HEART DISEASE.* The Lancet, 1989. **334**(8663): p. 577-580.

279. Rich-Edwards, J.W., et al., *Birth weight and risk of cardiovascular disease in a cohort of women followed up since 1976.* BMJ, 1997. **315**(7105): p. 396.

280. Fan, Z., et al., *Relationship between birth size and coronary heart disease in China.* Annals of Medicine, 2010. **42**(8): p. 596-602.

281. Leon, D.A., et al., *Reduced fetal growth rate and increased risk of death from ischaemic heart disease: cohort study of 15 000 Swedish men and women born 1915-29.* BMJ, 1998. **317**(7153): p. 241.

282. Bagby, S.P., *Maternal Nutrition, Low Nephron Number, and Hypertension in Later Life: Pathways of Nutritional Programming.* The Journal of Nutrition, 2007. **137**(4): p. 1066-1072.

283. Limesand, S.W., et al., *Diminished β-cell replication contributes to reduced β-cell mass in fetal sheep with intrauterine growth restriction.* American Journal of Physiology-Regulatory, Integrative and Comparative Physiology, 2005. **288**(5): p. R1297-R1305.

284. Botting, K.J., et al., *Chronic Hypoxemia in Late Gestation Decreases Cardiomyocyte Number but Does Not Change Expression of Hypoxia-Responsive Genes.* Journal of the American Heart Association, 2014. **3**(4): p. e000531.

285. de Rooij, S.R., et al., *Prenatal undernutrition and cognitive function in late adulthood.* Proceedings of the National Academy of Sciences, 2010. **107**(39): p. 16881.

286. Gentili, S., J.L. Morrison, and I.C. McMillen, *Intrauterine Growth Restriction and Differential Patterns of Hepatic Growth and Expression of IGF1, PCK2, and HSDL1 mRNA in the Sheep Fetus in Late Gestation1.* Biology of Reproduction, 2009. **80**(6): p. 1121-1127.

287. Maritz, G.S., et al., *Effects of fetal growth restriction on lung development before and after birth: A morphometric analysis.* Pediatric Pulmonology, 2001. **32**(3): p. 201-210.

288. Giussani, D.A., et al. *Heart Disease Link to Fetal Hypoxia and Oxidative Stress*. in *Advances in Fetal and Neonatal Physiology*. 2014. New York, NY: Springer New York.

289. Cottrell, E.C., et al., *Reconciling the nutritional and glucocorticoid hypotheses of fetal programming.* The FASEB Journal, 2012. **26**(5): p. 1866-1874.

290. Kamai, E.M., T.F. McElrath, and K.K. Ferguson, *Fetal growth in environmental epidemiology: mechanisms, limitations, and a review of associations with biomarkers of non-persistent chemical exposures during pregnancy.* Environmental Health, 2019. **18**(1): p. 43.

291. Stieb, D.M., et al., *Ambient air pollution, birth weight and preterm birth: a systematic review and meta-analysis.* Environ Res, 2012. **117**: p. 100-11.

292. Zhu, X., et al., *Maternal exposure to fine particulate matter (PM2.5) and pregnancy outcomes: a meta-analysis.* Environ Sci Pollut Res Int, 2015. **22**(5): p. 3383-96.

293. Lamichhane, D.K., et al., *A meta-analysis of exposure to particulate matter and adverse birth outcomes.* Environ Health Toxicol, 2015. **30**: p. e2015011.

294. Sun, X., et al., *The associations between birth weight and exposure to fine particulate matter (PM2.5) and its chemical constituents during pregnancy: A meta-analysis.* Environ Pollut, 2016. **211**: p. 38-47.

295. DeFranco, E., et al., *Exposure to airborne particulate matter during pregnancy is associated with preterm birth: a population-based cohort study.* Environ Health, 2016. **15**: p. 6.

296. Percy, Z., et al., *Trimester specific PM2.5 exposure and fetal growth in Ohio, 2007-2010.* Environ Res, 2019. **171**: p. 111-118.

297. Rich, D.Q., et al., *Differences in Birth Weight Associated with the 2008 Beijing Olympics Air Pollution Reduction: Results from a Natural Experiment.* Environ Health Perspect, 2015. **123**(9): p. 880-7.

298. DeFranco, E., et al., *Air pollution and stillbirth risk: exposure to airborne particulate matter during pregnancy is associated with fetal death.* PLoS One, 2015. **10**(3): p. e0120594.

299. Siddika, N., et al., *Prenatal ambient air pollution exposure and the risk of stillbirth: systematic review and meta-analysis of the empirical evidence.* Occup Environ Med, 2016. **73**(9): p. 573-81.

300. Chen, L.C. and M. Lippmann, *Inhalation toxicology methods: the generation and characterization of exposure atmospheres and inhalational exposures.* Curr Protoc Toxicol, 2015. **63**: p. 24 4 1-24 4 23.

301. Mauad, T., et al., *Chronic exposure to ambient levels of urban particles affects mouse lung development.* Am J Respir Crit Care Med, 2008. **178**(7): p. 721-8.

302. Wei, Y., et al., *Chronic exposure to air pollution particles increases the risk of obesity and metabolic syndrome: findings from a natural experiment in Beijing.* Faseb j, 2016. **30**(6): p. 2115-22.

303. Allen, J.L., et al., *Developmental exposure to concentrated ambient particles and preference for immediate reward in mice.* Environ Health Perspect, 2013. **121**(1): p. 32-8.

304. Allen, J.L., et al., *Developmental exposure to concentrated ambient ultrafine particulate matter air pollution in mice results in persistent and sex-dependent behavioral neurotoxicity and glial activation.* Toxicol Sci, 2014. **140**(1): p. 160-78.

305. Allen, J.L., et al., *Early postnatal exposure to ultrafine particulate matter air pollution: persistent ventriculomegaly, neurochemical disruption, and glial activation preferentially in male mice.* Environ Health Perspect, 2014. **122**(9): p. 939-45.

306. Allen, J.L., et al., *Developmental neurotoxicity of inhaled ambient ultrafine particle air pollution: Parallels with neuropathological and behavioral features of autism and other neurodevelopmental disorders.* Neurotoxicology, 2017. **59**: p. 140-154.

307. Cory-Slechta, D.A., et al., *Developmental exposure to low level ambient ultrafine particle air pollution and cognitive dysfunction.* Neurotoxicology, 2018. **69**: p. 217-231.

308. Sobolewski, M., et al., *Developmental exposures to ultrafine particle air pollution reduces early testosterone levels and adult male social novelty preference: Risk for children's sex-biased neurobehavioral disorders.* Neurotoxicology, 2018. **68**: p. 203-211.

309. Klocke, C., et al., *Neuropathological Consequences of Gestational Exposure to Concentrated Ambient Fine and Ultrafine Particles in the Mouse.* Toxicol Sci, 2017. **156**(2): p. 492-508.

310. Klocke, C., et al., *Enhanced cerebellar myelination with concomitant iron elevation and ultrastructural irregularities following prenatal exposure to ambient particulate matter in the mouse.* Inhal Toxicol, 2018. **30**(9-10): p. 381-396.

311. Church, J.S., et al., *Perinatal exposure to concentrated ambient particulates results in autism-like behavioral deficits in adult mice.* Neurotoxicology, 2018. **65**: p. 231-240.

312. Gorr, M.W., et al., *Early life exposure to air pollution induces adult cardiac dysfunction.* Am J Physiol Heart Circ Physiol, 2014. **307**(9): p. H1353-60.

313. Tanwar, V., et al., *In Utero Particulate Matter Exposure Produces Heart Failure, Electrical Remodeling, and Epigenetic Changes at Adulthood.* J Am Heart Assoc, 2017. **6**(4).

314. Chen, M., et al., *Programming of mouse obesity by maternal exposure to concentrated ambient fine particles.* Part Fibre Toxicol, 2017. **14**(1): p. 20.

315. Zhang, R., et al., *Formation of urban fine particulate matter.* Chem Rev, 2015. **115**(10): p. 3803-55.

316. Wu, G., et al., *Adverse organogenesis and predisposed long-term metabolic syndrome from prenatal exposure to fine particulate matter.* Proc Natl Acad Sci U S A, 2019. **116**(24): p. 11590-11595.

317. Guo, S., et al., *Elucidating severe urban haze formation in China.* Proc Natl Acad Sci U S A, 2014. **111**(49): p. 17373-8.

318. dela Cruz, A.L., et al., *Detection of environmentally persistent free radicals at a superfund wood treating site.* Environ Sci Technol, 2011. **45**(15): p. 6356-65.

319. Vejerano, E.P., et al., *Environmentally Persistent Free Radicals: Insights on a New Class of Pollutants.* Environ Sci Technol, 2018. **52**(5): p. 2468-2481.

320. Thevenot, P.T., et al., *Radical-containing ultrafine particulate matter initiates epithelial-to-mesenchymal transitions in airway epithelial cells.* Am J Respir Cell Mol Biol, 2013. **48**(2): p. 188-97.

321. Saravia, J., et al., *Early-life exposure to combustion-derived particulate matter causes pulmonary immunosuppression.* Mucosal Immunol, 2014. **7**(3): p. 694-704.

322. Lee, G.I., et al., *Exposure to combustion generated environmentally persistent free radicals enhances severity of influenza virus infection.* Part Fibre Toxicol, 2014. **11**: p. 57.

323. Stephenson, E.J., et al., *Exposure to environmentally persistent free radicals during gestation lowers energy expenditure and impairs skeletal muscle mitochondrial function in adult mice.* Am J Physiol Endocrinol Metab, 2016. **310**(11): p. E1003-15.

324. Jaligama, S., et al., *Regulatory T cells and IL10 suppress pulmonary host defense during early-life exposure to radical containing combustion derived ultrafine particulate matter.* Respir Res, 2017. **18**(1): p. 15.

325. Davis, D.A., et al., *Prenatal exposure to urban air nanoparticles in mice causes altered neuronal differentiation and depression-like responses.* PLoS One, 2013. **8**(5): p. e64128.

326. Woodward, N.C., et al., *Exposure to Nanoscale Particulate Matter from Gestation to Adulthood Impairs Metabolic Homeostasis in Mice.* Sci Rep, 2019. **9**(1): p. 1816.

327. Hougaard, K.S., et al., *Effects of prenatal exposure to diesel exhaust particles on postnatal development, behavior, genotoxicity and inflammation in mice.* Part Fibre Toxicol, 2008. **5**: p. 3.

328. Hamada, K., et al., *Exposure of pregnant mice to an air pollutant aerosol increases asthma susceptibility in offspring.* J Toxicol Environ Health A, 2007. **70**(8): p. 688-95.

329. Corson, L., et al., *Prenatal allergen and diesel exhaust exposure and their effects on allergy in adult offspring mice.* Allergy Asthma Clin Immunol, 2010. **6**(1): p. 7.

330. Ema, M., et al., *Developmental toxicity of diesel exhaust: a review of studies in experimental animals.* Reprod Toxicol, 2013. **42**: p. 1-17.

331. Yokota, S., et al., *Social Isolation-Induced Territorial Aggression in Male Offspring Is Enhanced by Exposure to Diesel Exhaust during Pregnancy.* PLoS One, 2016. **11**(2): p. e0149737.

332. Chang, Y.C., T.B. Cole, and L.G. Costa, *Prenatal and early-life diesel exhaust exposure causes autism-like behavioral changes in mice.* Part Fibre Toxicol, 2018. **15**(1): p. 18.

333. Weldy, C.S., et al., *In utero and early life exposure to diesel exhaust air pollution increases adult susceptibility to heart failure in mice.* Part Fibre Toxicol, 2013. **10**(1): p. 59.

334. Harrigan, J., et al., *In Utero Exposure of Hyperlipidemic Mice to Diesel Exhaust: Lack of Effects on Atherosclerosis in Adult Offspring Fed a Regular Chow Diet.* Cardiovasc Toxicol, 2017. **17**(4): p. 417-425.

335. Manners, S., et al., *A mouse model links asthma susceptibility to prenatal exposure to diesel exhaust.* J Allergy Clin Immunol, 2014. **134**(1): p. 63-72.

336. Hong, X., et al., *Maternal exposure to airborne particulate matter causes postnatal immunological dysfunction in mice offspring.* Toxicology, 2013. **306**: p. 59-67.

337. Chen, M., et al., *Prenatal exposure to diesel exhaust PM2.5 causes offspring beta cell dysfunction in adulthood.* Am J Physiol Endocrinol Metab, 2018. **315**(1): p. E72-E80.

338. Chen, M., et al., *Prenatal and postnatal mothering by diesel exhaust PM2.5-exposed dams differentially program mouse energy metabolism.* Part Fibre Toxicol, 2017. **14**(1): p. 3.

339. Miranda, R.A., et al., *Particulate Matter Exposure During Perinatal Life Results in Impaired Glucose Metabolism in Adult Male Rat Offspring.* Cell Physiol Biochem, 2018. **49**(1): p. 395-405.

340. Tang, W., et al., *Expression of HMGB1 in maternal exposure to fine particulate air pollution induces lung injury in rat offspring assessed with micro-CT.* Chem Biol Interact, 2018. **280**: p. 64-69.

341. Costa, D.L., et al., *Comparative pulmonary toxicological assessment of oil combustion particles following inhalation or instillation exposure.* Toxicol Sci, 2006. **91**(1): p. 237-46.

342. Shang, Y. and Q. Sun, *Particulate air pollution: major research methods and applications in animal models.* Environ Dis, 2018. **3**(3): p. 57-62.

343. Fleisch, A.F., et al., *Prenatal exposure to traffic pollution: associations with reduced fetal growth and rapid infant weight gain.* Epidemiology, 2015. **26**(1): p. 43-50.

344. Tsukue, N., H. Tsubone, and A.K. Suzuki, *Diesel exhaust affects the abnormal delivery in pregnant mice and the growth of their young.* Inhal Toxicol, 2002. **14**(6): p. 635-51.

345. Jedrychowski, W., et al., *Estimated risk for altered fetal growth resulting from exposure to fine particles during pregnancy: an epidemiologic prospective cohort study in Poland.* Environ Health Perspect, 2004. **112**(14): p. 1398-402.

346. Glinianaia, S.V., et al., *Particulate air pollution and fetal health: a systematic review of the epidemiologic evidence.* Epidemiology, 2004. **15**(1): p. 36-45.

347. Srám, R.J., et al., *Ambient air pollution and pregnancy outcomes: a review of the literature.* Environ Health Perspect, 2005. **113**(4): p. 375-82.

348. Li, N., et al., *A work group report on ultrafine particles (American Academy of Allergy, Asthma & Immunology): Why ambient ultrafine and engineered nanoparticles should receive special attention for possible adverse health outcomes in human subjects.* Journal of Allergy and Clinical Immunology, 2016. **138**(2): p. 386-396.

349. Hanson, M.A. and P.D. Gluckman, *Developmental origins of health and disease: new insights.* Basic Clin Pharmacol Toxicol, 2008. **102**(2): p. 90-3.

350. Godfrey, K.M. and D.J. Barker, *Fetal programming and adult health.* Public Health Nutr, 2001. **4**(2b): p. 611-24.

351. Barker, D.J., *Fetal nutrition and cardiovascular disease in later life.* Br Med Bull, 1997. **53**(1): p. 96-108.

352. Landrigan, P.J., et al., *The Lancet Commission on pollution and health.* Lancet, 2018. **391**(10119): p. 462-512.

353. Health Effects Institute, *State of Global Air 2019*. 2019, Health Effects Institute: Boston, MA.

354. Levy, M.E., et al., *Measurements of submicron aerosols in Houston, Texas during the 2009 SHARP field campaign.* Journal of Geophysical Research-Atmospheres, 2013. **118**(18): p. 10518-10534.

355. Guo, S., et al., *Remarkable nucleation and growth of ultrafine particles from vehicular exhaust.* Proceedings of the National Academy of Sciences, 2020. **117**(7): p. 3427.

356. Liu, S., et al., *Association between maternal exposure to ambient air pollutants during pregnancy and fetal growth restriction.* J Expo Sci Environ Epidemiol, 2007. **17**(5): p. 426-32.

357. Dunlop, K., et al., *Altered fetal skeletal muscle nutrient metabolism following an adverse in utero environment and the modulation of later life insulin sensitivity.* Nutrients, 2015. **7**(2): p. 1202-16.

358. Åsvold, B.O., et al., *Angiogenic factors in maternal circulation and the risk of severe fetal growth restriction.* American journal of epidemiology, 2011. **173**(6): p. 630-639.

359. Johnson, N.M., et al., *Air pollution and children's health-a review of adverse effects associated with prenatal exposure from fine to ultrafine particulate matter.* Environ Health Prev Med, 2021. **26**(1): p. 72.

360. Zhang, R., N.M. Johnson, and Y. Li, *Establishing the exposure-outcome relation between airborne particulate matter and children's health.* Thorax, 2021.

361. Xue, H., et al., *Effects of coating of dicarboxylic acids on the mass-mobility relationship of soot particles.* Environ Sci Technol, 2009. **43**(8): p. 2787-92.

362. Xue, H., et al., *Effects of dicarboxylic acid coating on the optical properties of soot.* Phys Chem Chem Phys, 2009. **11**(36): p. 7869-75.

363. Zhao, F., et al., *Hydrogen sulfide alleviates placental injury induced by maternal cigarette smoke exposure during pregnancy in rats.* Nitric Oxide, 2018. **74**: p. 102-111.

364. Dobin, A., et al., *STAR: ultrafast universal RNA-seq aligner.* Bioinformatics, 2013. **29**(1): p. 15-21.

365. Liao, Y., G.K. Smyth, and W. Shi, *featureCounts: an efficient general purpose program for assigning sequence reads to genomic features.* Bioinformatics, 2014. **30**(7): p. 923-30.

366. Love, M.I., W. Huber, and S. Anders, *Moderated estimation of fold change and dispersion for RNA-seq data with DESeq2.* Genome Biol, 2014. **15**(12): p. 550.

367. Jiménez-Marín, Á., et al., *Biological pathway analysis by ArrayUnlock and Ingenuity Pathway Analysis.* BMC Proc, 2009. **3 Suppl 4**(Suppl 4): p. S6.

368. Mustapha, T.A., et al., *Gestational exposure to particulate air pollution exacerbates the growth phenotypes induced by preconception paternal alcohol use: a multiplex model of exposure.* Environmental Epigenetics, 2020. **6**(1).

369. Kajantie, E., et al., *In preeclampsia, the placenta grows slowly along its minor axis.* Int J Dev Biol, 2010. **54**(2-3): p. 469-73.

370. Barker, D.J., et al., *Foetal and childhood growth and asthma in adult life.* Acta Paediatr, 2013. **102**(7): p. 732-8.

371. Barker, D.J., et al., *The intrauterine origins of Hodgkin's lymphoma.* Cancer Epidemiol, 2013. **37**(3): p. 321-3.

372. Barker, D.J., et al., *The placental origins of sudden cardiac death.* Int J Epidemiol, 2012. **41**(5): p. 1394-9.

373. Eriksson, J.G., et al., *Mother's body size and placental size predict coronary heart disease in men.* Eur Heart J, 2011. **32**(18): p. 2297-303.

374. Wang, Y.-D., et al., *FXR: a metabolic regulator and cell protector.* Cell Research, 2008. **18**(11): p. 1087-1095.

375. Wente, W., et al., *Activation of Liver X Receptors and Retinoid X Receptors Induces Growth Arrest and Apoptosis in Insulin-Secreting Cells.* Endocrinology, 2007. **148**(4): p. 1843-1849.

376. Harmon, C.M., S. McGonigal, and J.C. Larkin, *Impairment of trophoblast survival and differentiation by LXR ligands is prevented by cholesterol but not ABCA1 silencing.* Placenta, 2018. **69**: p. 50-56.

377. Lu, H., F.J. Gonzalez, and C. Klaassen, *Alterations in hepatic mRNA expression of phase II enzymes and xenobiotic transporters after targeted disruption of hepatocyte nuclear factor 4 alpha.* Toxicol Sci, 2010. **118**(2): p. 380-90.

378. Stanger, B.Z., *HNF4A and Diabetes.* Diabetes, 2008. **57**(6): p. 1461.

379. Yin, L., et al., *Hepatic hepatocyte nuclear factor 4α is essential for maintaining triglyceride and cholesterol homeostasis.* Arterioscler Thromb Vasc Biol, 2011. **31**(2): p. 328-36.

380. Chen, W.S., et al., *Disruption of the HNF-4 gene, expressed in visceral endoderm, leads to cell death in embryonic ectoderm and impaired gastrulation of mouse embryos.* Genes Dev, 1994. **8**(20): p. 2466-77.

381. Hayhurst, G.P., et al., *Hepatocyte nuclear factor 4alpha (nuclear receptor 2A1) is essential for maintenance of hepatic gene expression and lipid homeostasis.* Mol Cell Biol, 2001. **21**(4): p. 1393-403.

382. Lu, H., *Crosstalk of HNF4α with extracellular and intracellular signaling pathways in the regulation of hepatic metabolism of drugs and lipids.* Acta Pharm Sin B, 2016. **6**(5): p. 393-408.

383. Shapiro, M.D. and S. Fazio, *Apolipoprotein B-containing lipoproteins and atherosclerotic cardiovascular disease.* F1000Res, 2017. **6**: p. 134.

384. Contini, C., et al., *Lipoprotein turnover and possible remnant accumulation in preeclampsia: insights from the Freiburg Preeclampsia H.E.L.P.-apheresis study.* Lipids Health Dis, 2018. **17**(1): p. 49.

385. Rosenfeld, C.S., *Sex-Specific Placental Responses in Fetal Development.* Endocrinology, 2015. **156**(10): p. 3422-34.

386. Tarrade, A., et al., *Sexual dimorphism of the feto-placental phenotype in response to a high fat and control maternal diets in a rabbit model.* PLoS One, 2013. **8**(12): p. e83458.

387. Braun, A.E., et al., *"Females Are Not Just 'Protected' Males": Sex-Specific Vulnerabilities in Placenta and Brain after Prenatal Immune Disruption.* eNeuro, 2019. **6**(6).

388. Saoi, M., et al., *Placental Metabolomics for Assessment of Sex-specific Differences in Fetal Development During Normal Gestation.* Sci Rep, 2020. **10**(1): p. 9399.

389. Kim, K.-H., E. Kabir, and S. Kabir, *A review on the human health impact of airborne particulate matter.* Environment International, 2015. **74**: p. 136-143.

390. Jacobs, M., et al., *The association between ambient air pollution and selected adverse pregnancy outcomes in China: A systematic review.* Science of The Total Environment, 2017. **579**: p. 1179-1192.

391. Uwak, I., et al., *Application of the navigation guide systematic review methodology to evaluate prenatal exposure to particulate matter air pollution and infant birth weight.* Environ Int, 2021. **148**: p. 106378.

392. van den Hooven, E.H., et al., *Air pollution exposure and markers of placental growth and function: the generation R study.* Environ Health Perspect, 2012. **120**(12): p. 1753-9.

393. Zhang, R.Y., et al., *Nucleation and Growth of Nanoparticles in the Atmosphere.* Chemical Reviews, 2012. **112**(3): p. 1957-2011.

394. Behlen, J.C., et al., *Gestational Exposure to Ultrafine Particles Reveals Sex- and Dose-Specific Changes in Offspring Birth Outcomes, Placental Morphology, and Gene Networks.* Toxicol Sci, 2021.

395. Yang, S.I., et al., *Prenatal Particulate Matter/Tobacco Smoke Increases Infants' Respiratory Infections: COCOA Study.* Allergy Asthma Immunol Res, 2015. **7**(6): p. 573-82.

396. Cullinan, S.B., et al., *The Keap1-BTB protein is an adaptor that bridges Nrf2 to a Cul3-based E3 ligase: oxidative stress sensing by a Cul3-Keap1 ligase.* Mol Cell Biol, 2004. **24**(19): p. 8477-86.

397. Tebay, L.E., et al., *Mechanisms of activation of the transcription factor Nrf2 by redox stressors, nutrient cues, and energy status and the pathways through which it attenuates degenerative disease.* Free Radic Biol Med, 2015. **88**(Pt B): p. 108-146.

398. Li, Y.J., T. Kawada, and A. Azuma, *Nrf2 is a protective factor against oxidative stresses induced by diesel exhaust particle in allergic asthma.* Oxid Med Cell Longev, 2013. **2013**: p. 323607.

399. Itoh, K., et al., *An Nrf2/Small Maf Heterodimer Mediates the Induction of Phase II Detoxifying Enzyme Genes through Antioxidant Response Elements.*

Biochemical and Biophysical Research Communications, 1997. **236**(2): p. 313-322.

400. Nobles, C.J., et al., *Ambient air pollution and fetal growth restriction: Physician diagnosis of fetal growth restriction versus population-based small-for-gestational age.* Sci Total Environ, 2019. **650**(Pt 2): p. 2641-2647.

401. Chen, M., et al., *Prenatal and postnatal mothering by diesel exhaust PM(2.5)-exposed dams differentially program mouse energy metabolism.* Part Fibre Toxicol, 2017. **14**(1): p. 3.

402. Tantengco, O.A.G., et al., *The role of nuclear factor erythroid 2–related factor 2 (NRF2) in normal and pathological pregnancy: A systematic review.* American Journal of Reproductive Immunology, 2021. **n/a**(n/a).

403. Kweider, N., et al., *The effects of Nrf2 deletion on placental morphology and exchange capacity in the mouse.* J Matern Fetal Neonatal Med, 2017. **30**(17): p. 2068-2073.

404. Lee, G.B., et al., *Diesel exhaust particles induce cysteine oxidation and s-glutathionylation in house dust mite induced murine asthma.* PLoS One, 2013. **8**(3): p. e60632.

405. Braekke, K., et al., *Homocysteine, cysteine, and related metabolites in maternal and fetal plasma in preeclampsia.* Pediatr Res, 2007. **62**(3): p. 319-24.

406. El-Khairy, L., et al., *Plasma total cysteine, pregnancy complications, and adverse pregnancy outcomes: the Hordaland Homocysteine Study.* Am J Clin Nutr, 2003. **77**(2): p. 467-72.

407. Ahmed, S.M., et al., *Nrf2 signaling pathway: Pivotal roles in inflammation.* Biochim Biophys Acta Mol Basis Dis, 2017. **1863**(2): p. 585-597.

408. Lacher, S.E., et al., *Beyond antioxidant genes in the ancient Nrf2 regulatory network.* Free Radic Biol Med, 2015. **88**(Pt B): p. 452-465.

409. Fahey, J.W., Y. Zhang, and P. Talalay, *Broccoli sprouts: an exceptionally rich source of inducers of enzymes that protect against chemical carcinogens.* Proc Natl Acad Sci U S A, 1997. **94**(19): p. 10367-72.

410. Zhang, Y., et al., *A major inducer of anticarcinogenic protective enzymes from broccoli: isolation and elucidation of structure.* Proceedings of the National Academy of Sciences, 1992. **89**(6): p. 2399.

411. Riedl, M.A., A. Saxon, and D. Diaz-Sanchez, *Oral sulforaphane increases Phase II antioxidant enzymes in the human upper airway.* Clinical Immunology, 2009. **130**(3): p. 244-251.

412. Zhang Donna, D. and M. Hannink, *Distinct Cysteine Residues in Keap1 Are Required for Keap1-Dependent Ubiquitination of Nrf2 and for Stabilization of Nrf2 by Chemopreventive Agents and Oxidative Stress.* Molecular and Cellular Biology, 2003. **23**(22): p. 8137-8151.

413. Fahey, J.W., P. Talalay, and T.W. Kensler, *Notes from the Field: "Green" Chemoprevention as Frugal Medicine.* Cancer Prevention Research, 2012. **5**(2): p. 179.

414. Behlen, J.C., et al., *NRF2-Dependent Placental Effects Vary by Sex and Dose following Gestational Exposure to Ultrafine Particles.* Antioxidants, 2022. **11**(2).

415. Zhang, Y., et al., *Anticarcinogenic activities of sulforaphane and structurally related synthetic norbornyl isothiocyanates.* Proceedings of the National Academy of Sciences, 1994. **91**(8): p. 3147.

416. Ross, D. and D. Siegel, *The diverse functionality of NQO1 and its roles in redox control.* Redox Biology, 2021. **41**: p. 101950.